

Southern Methodist University

SMU Scholar

---

Electrical Engineering Theses and Dissertations

Electrical Engineering

---

Fall 2018

## Standing-Wave Dielectric Array Antennas

Ayman Althuwayb

*Southern Methodist University*, [aalthuwayb@smu.edu](mailto:aalthuwayb@smu.edu)

Follow this and additional works at: [https://scholar.smu.edu/engineering\\_electrical\\_etds](https://scholar.smu.edu/engineering_electrical_etds)



Part of the [Electromagnetics and Photonics Commons](#)

---

### Recommended Citation

Althuwayb, Ayman, "Standing-Wave Dielectric Array Antennas" (2018). *Electrical Engineering Theses and Dissertations*. 21.

[https://scholar.smu.edu/engineering\\_electrical\\_etds/21](https://scholar.smu.edu/engineering_electrical_etds/21)

This Dissertation is brought to you for free and open access by the Electrical Engineering at SMU Scholar. It has been accepted for inclusion in Electrical Engineering Theses and Dissertations by an authorized administrator of SMU Scholar. For more information, please visit <http://digitalrepository.smu.edu>.



STANDING-WAVE DIELECTRIC  
ARRAY ANTENNAS

Approved by:

---

Prof. Choon Lee  
Associate Professor of Electrical Engineering

---

Prof. Jerome Butler  
Distinguished Professor of Electrical Engineering

---

Prof. Duncan MacFarlane  
Professor of Electrical Engineering

---

Prof. Jianhui Wang  
Associate Professor of Electrical Engineering

---

Prof. David Willis  
Associate Professor of Mechanical Engineering

STANDING-WAVE DIELECTRIC  
ARRAY ANTENNAS

A Dissertation Presented to the Graduate Faculty of

Bobby B. Lyle School of Engineering

Southern Methodist University

in

Partial Fulfillment of the Requirements

for the degree of

Doctor of Philosophy

with a

Major in Electrical Engineering

By

Ayman Althuwayb

M.S., Electrical Engineering, California State University Fullerton, 2014

B.S., Electrical Engineering, Aljouf University, 2011

December 15, 2018

Copyright (2018)

Ayman Althuwayb

All Rights Reserved

## ACKNOWLEDGMENTS

I would like to first and foremost convey my deepest gratitude to my dissertation advisor Professor Choon Lee, whose extremely professional propositions and accurate guidance have greatly assisted me to succeed in my research. Any time I get lost in perplexities and complexities, his farsighted and experience based suggestions have always motivated me to dig into the issues deeper seeking for all potential rationalistic options before concluding results. My preliminary results that were based on youthful analyzing strategy were promptly corrected while core issues were intentionally steered to be focused on. His strategy and resourcefulness have escalated my potential to realize, evaluate and defeat the imminent errors at all research stages. Without his paramount guidance and support, this work would not have been possible due to my youthful impatience and wavering trajectory.

I would like also to express my sincere gratitude to the Saudi government represented by Aljouf University for providing the opportunity to pursue my Ph.D. degree at one of the reputable universities. I am deeply grateful to my generous country for taking responsibility of all my study expenses.

My gratitude is extended to Dr. Jerome Butler, Dr. Ping Gui, Dr. Duncan MacFarlane, Dr. Jianhui Wang, and Dr. David Willis for their willingness to serve as supervisory and examination committee members to monitor my research process at its

all stages. Your valuable comments and insightful suggestions have been highly appreciated. Each of you has ultimately contributed to this presented dissertation.

My sincere thanks go to Dr. Luis-Enrique García-Muñoz and Mr. Kerlos Atia from Charles III University of Madrid, Spain. Their assistance in the fabrication and measurements is duly recognized and highly appreciated.

I also would like to express my special gratefulness to my fellow Dr. Yang Fan for all the support he has provided since the beginning of my study journey. He trained me how to appropriately operate the lab equipment and to use the simulation software. We spent numerous hours at the library preparing for the written qualifying examination. His brilliant techniques to approach technical problems were extremely helpful. I wish him all the best in his personal and career life.

Lastly and most importantly, I'm greatly indebted to my parents and siblings for all the love, honest prayers, invaluable support, and persistent encouragement. Special profound thanks go to my devoted and affectionate spouse Razan for supplying my life with true love and happiness. She carried every responsibility and suffered all the bitterness to take care of our household affairs and to appropriately raise our wonderful kid. Without her endless support and numerous sacrifices, I never would have made it this far. My heartfelt thanks to all of you!

Ayman Althuwayb  
Southern Methodist University  
October 2018

Althuwayb, Ayman Abdulhadi

M.S.E.E., California State University Fullerton, 2014  
B.S.E.E., Aljouf University, 2011

Standing-wave Dielectric  
Array Antennas

Advisor: Professor Choon Lee

Doctor of Philosophy conferred December 15, 2018

Dissertation completed October 25, 2018

Due to the evolutions in wireless communication systems, antenna engineers have been confronting a number of challenges regarding improving the performance of antennas, miniaturizing the size as well as considering the fabrication simplicity. Although dielectric resonator antennas typically suffer from exhibiting low gain, they have been thoroughly under investigating as they are being excellent candidates to be utilized to fulfill contemporary communication systems requirements and specifications, especially at high-frequency ranges. The reason behind this solicitude is because they have several advantageous features, including but not limited to the simplicity of the used excitation mechanism and fabrication easiness.

One of the well-known methods to improve the gain is by arraying additional individual DRAs. However, one major obstacle evokes when designing the array to operate at a higher frequency. Spurious radiations from the feeding network are considerable and unfavorably influence the overall array performance. Moreover, it is mandatory to have several quarter-wavelength transmission lines and power dividers which, in turns, lead to high configuration complexity.

The substantial intention of this dissertation is to explore dielectric resonator array antenna designs where the concept of standing waves is utilized. In contradictory to



corporate-fed traveling-wave array antennas designs, the need to utilize microstrip discontinuities such as quarter-wave transformers or power dividers is eliminated while having a single feeding port to excite the entire array structure. Consequently, undesired spurious coupling and radiations can be exceedingly minimized especially when operating at very high-frequency bands.

The dissertation proposes two novel dielectric array configurations based on the concept of standing-wave. In the first configuration, vertical and horizontal low-profile dielectric bridges have been employed to connect 3x3 dielectric array elements. The top surface of each bridge is covered by a metallic patch to prevent unfavorable radiations coming out of the bridges. The array structure is fed using a single coupling aperture resides symmetrically underneath the center element only. When exciting waves are coupled to the center element, these waves can be transferred to other array elements via the introduced dielectric bridges. Therefore, the entire structure resonates at the resonant frequency as a whole. The proposed design provides a realized gain of about 15 dBi at the boresight. The return loss is about -20 dB possessing about 35.7% useful impedance bandwidth. The experimental results show excellent agreement with those obtained by simulation.

The second proposed configuration consists of four dielectric resonator antennas forming a linear array. On the top surface of the substrate and between the array elements, there are three metallic patches which are employed to excite the array elements. These patches are slightly extended under the slabs to allow sufficient coupling. Under each dielectric slab, there is one metallic patch reside symmetrically at the center to enhance the wave coupling in both directions toward the array elements. The

single feeding coaxial probe is attached to the center patch, and its location was optimized to provide excellent impedance matching. The maximum observed gain is 15 dBi at the boresight. The array structure is well matched and the return loss is measured to be -45 dB.

The validity and versatility of both designs are realized and illustrated. One powerful advantageous feature is that the feeding network was extremely simplified to a single port to excite the entire array structure. Another advantage is that both designs were partially fabricated using 3D printing technology. Therefore, it can be said that the proposed configurations are easy to fabricate since the complexity of designing feeding networks was obviated.

## TABLE OF CONTENTS

LIST OF FIGURES .....	xii
LIST OF TABLES .....	xvi
CHAPTER	
1. INTRODUCTION .....	1
1.1 History of Antenna and Overview .....	1
1.2 Problem Statement .....	3
1.3 Dissertation Contribution.....	5
1.4 Dissertation Overview .....	6
2. INTRODUCTION ON DIELECTRIC RESONATOR ANTENNA.....	8
2.1 History of DRA.....	8
2.2 Structure of DRA .....	9
2.3 Excitation Techniques of DRA.....	12
2.3.1 Microstrip Transmission Line Feeding.....	12
2.3.2 Coaxial Probe Feeding.....	13
2.3.3 Aperture Coupling Feeding.....	14
2.4 Applications of DRAs.....	15
2.4.1 RADAR and Surveillance Applications .....	15
2.4.2 GNSS and GPS Applications.....	16
2.4.3 Tomography and Biomedical Applications .....	16

3. RECTANGULAR DIELECTRIC RESONATOR ANTENNA CHARACTERIZATION .....	18
3.1 Overview of Analyzing Models.....	18
3.2 Field Distribution .....	20
3.3 Radiation Characteristics .....	22
3.4 Resonant Frequency and Higher-order Modes .....	24
4. ARRAY ANTENNAS AND STANDING WAVES.....	28
4.1 History of Array Antenna and Its Development.....	28
4.2 General Concept of Array Antenna .....	31
4.2.1 Multidimensional Array Antennas.....	36
4.3 Dielectric Resonator Antenna Arrays.....	36
4.4 Standing-wave Arrays.....	39
4.4.1 Corporate Feed Drawbacks.....	43
4.5 Antenna Gain .....	43
4.5.1 Matched Gain.....	44
4.5.2 Realized Gain.....	45
4.6 Electrically Large High-gain Array Antennas .....	45
5. STANDING WAVE DIELECTRIC ARRAY ANTENNAS .....	47
5.1 Motivations .....	47
5.2 Previous Work .....	49
5.3 Design, Analysis, Fabrication, and Measurement of Planar Standing-wave Dielectric Array Antennas .....	54
5.3.1 Single Element Design .....	54
5.3.2 Three Elements Linear Array Design (Parallel to the Feeding Line).....	58

5.3.3 Three Elements Linear Array Design (Orthogonal to the Feeding Line).....	64
5.3.4 Final 3x3 Planar Dielectric Array Antennas Design .....	69
5.3.5 Fabrication Tolerance and Design Sensitivity .....	76
5.3.6 Fabrication and Measurements Results, and Discussion .....	77
5.3.7 Summary of the Design Steps and Results.....	81
5.4 Design, Analysis, and Simulation of Linear Standing-wave Dielectric Array Antennas .....	83
5.4.1 Single Element Design.....	83
5.4.2 Two-Element Linear Array Design .....	87
5.4.3 Four-Element Linear Array Design .....	92
5.4.4 Field Distribution In the Standing-wave Linear Array.....	97
5.4.5 Summary of the Design Procedure .....	100
6. CONCLUSION AND FUTURE WORK .....	102
6.1 Conclusion .....	102
6.2 Future Prospects.....	104
APPENDIX	
A. COMSOL DESIGN PROCEDURE AND RESULTS POST-PROCESSING OF THE PLANAR ARRAY ANTENNA .....	106
B. COMSOL DESIGN PROCEDURE AND RESULTS POST-PROCESSING OF THE LINEAR ARRAY ANTENNA .....	140
REFERENCES .....	169

## LIST OF FIGURES

Figure	page
2.1 General Structure of DRA .....	10
2.2 Examples of Various DRA Geometries.....	10
2.3 3D view of conventional (a) and conformal (b) microstrip line feeding.....	13
2.4 3D view of coaxial probe penetrating (a) or adjacent to (b) the DRA.....	14
2.5 3D view (a) and cross-sectional view (b) of an aperture-fed rectangular DRA ....	15
3.1 Normalized frequency of a rectangular dielectric resonator antenna [17].....	25
3.2 E-field (lines) and H-field (dots and crosses) of (a) $TE_{111}^x$ , (b) $TE_{113}^x$ , and (c) $TE_{115}^x$ modes inside a grounded rectangular DRA [34].....	27
4.1 Braun's three-element array [38].....	30
4.2 (a) Inspection Approach, (b) Array factor plot, and (c) 3D array factor plot .....	32
4.3 Geometry for pattern calculation using rays.....	33
4.4 Illustration of (a) slot, (b) probe and (c) microstrip coupling corporate feed arrangements of DRA array.....	40
4.5 Inline series feeding method.....	41
4.6 Standing wave pattern as a function of time.....	42
5.1 Cylindrical dielectric resonator array antenna [56] .....	49
5.2 Rectangular dielectric resonator array antenna [58].....	50
5.3 Four-element rectangular dielectric resonator array antenna [59].....	51

5.4	Geometry of coaxial probe-fed embedded DRA array inside a pyramidal hard horn [61].....	52
5.5	Prototype of 16-element DRA array with perforated connecting rods [62] .....	52
5.6	Proposed single rectangular dielectric resonator antenna.....	54
5.7	Return loss S11 vs frequency of the single rectangular dielectric antenna.....	55
5.8	Input impedance on Smith chart of the single rectangular dielectric antenna .....	55
5.9	Realized gain vs Frequency at TE <sub>115</sub> mode .....	56
5.10	3D radiation pattern of the single rectangular dielectric antenna at f = 5.3 GHz ..	56
5.11	2D far electric fields in both x-z and y-z planes at f=5.3 GHz .....	57
5.12	Field distribution inside the slab at the resonance frequency .....	57
5.13	Top, front, side, and 3D views of the proposed linear array antennas.....	58
5.14	Return loss S11 vs frequency of three-element linear array antennas .....	60
5.15	Input impedance on Smith chart of three-element linear array antennas.....	61
5.16	Realized gain vs Frequency of parallel three-element linear array.....	61
5.17	3D radiation pattern of parallel three-element array antennas at f = 5.6 GHz.....	62
5.18	2D far fields in both x-z and y-z planes at f=5.6 GHz.....	63
5.19	Field distribution inside the array structure at the resonance frequency .....	63
5.20	Top, front, side, and 3D views of the proposed linear array antennas.....	64
5.21	Return loss S11 vs frequency of orthogonal three-element linear array antennas.	66
5.22	Input impedance on Smith chart of three-element linear array antennas.....	66
5.23	Realized gain vs Frequency of orthogonal three-element linear array .....	67
5.24	The 3D radiation pattern of orthogonal three-element array antennas at f = 5.6 GHz.....	68
5.25	The 2D far fields in both x-z and y-z planes at f=5.6 GHz.....	68

5.26	Top, front, and side views of the proposed 2D planar array antennas.....	69
5.27	3D view of the proposed planar array antennas.....	70
5.28	Effect of the vertical spacing (Width of the vertical bridges ( $W_{vb}$ )) on the array gain.....	71
5.29	Effect of the horizontal spacing (Length of the horizontal bridges ( $L_{hb}$ )) on the array gain .....	72
5.30	Effect of the length of resonators number 3 ( $L_{r3}$ ) on the array gain.....	73
5.31	Effect of the width of resonators number 2 ( $W_{r2}$ ) on the array gain .....	73
5.32	The 3D radiation pattern of the proposed 3x3 planar array antennas at $f = 5.6$ GHz.....	74
5.33	2D far fields in both x-z and y-z planes at $f=5.6$ GHz.....	75
5.34	Field distribution within the proposed planar array structure.....	76
5.35	Fabrication tolerance and the sensitivity effect on the gain of the planar array ....	76
5.36	Fabricated 3x3 planar dielectric array antennas.....	77
5.37	3D printing the proposed 3x3 planar dielectric array prototype.....	78
5.38	Testing the proposed 3x3 planar dielectric array prototype.....	78
5.39	Return loss S11 vs frequency of the proposed planar array.....	79
5.40	Realized gain vs frequency of the proposed planar array.....	80
5.41	E- and H- plane radiation patterns of the proposed planar array .....	80
5.42	Proposed single rectangular dielectric resonator antenna.....	83
5.43	Return loss S11 vs frequency of the single rectangular dielectric antenna.....	84
5.44	Realized gain vs Frequency of the single rectangular dielectric antenna .....	85
5.45	The 3D radiation pattern of the single rectangular dielectric antenna at $f = 3.9$ GHz.....	85
5.46	2D far electric fields in both x-z and y-z planes at $f = 3.9$ GHz.....	86



5.47	Field distribution inside the cavity at the resonant frequency 3.9 GHz.....	86
5.48	Top view of the proposed two-element linear array antennas .....	87
5.49	3D view of the proposed two-element linear array antennas.....	88
5.50	Return loss S11 vs frequency of two-element linear array antenna.....	89
5.51	Realized gain vs frequency of two-element linear array antenna .....	89
5.52	The 3D radiation pattern of two-element linear array antennas at $f = 3.85$ GHz.....	90
5.53	2D far fields in both x-z and y-z planes at $f=3.85$ GHz.....	91
5.54	Field distribution inside the array structure at the resonance frequency .....	91
5.55	(a) Top and (b) 3D view of the proposed four-element linear array antennas.....	92
5.56	Return loss S11 vs frequency of the four-element linear array antenna .....	94
5.57	Realized gain vs frequency of the four-element linear array antenna .....	94
5.58	Cross- and Co-polar radiation pattern of four-element linear array antenna .....	95
5.59	3D radiation pattern of the four-element linear array .....	95
5.60	3D radiation pattern of the four-element linear array without vias .....	96
5.61	Field distribution inside the array structure at the resonance frequency .....	97
5.62	Array factor of four equally-spaced isotropic sources.....	98
5.63	Radiation pattern of antenna element (Element factor).....	98
5.64	Calculated and simulated radiation pattern of 4-element standing-wave dielectric resonator array antenna .....	99

## LIST OF TABLES

Table	page
5.1 Summary of linear DRA array examples.....	53
5.2 Summary of planar DRA array examples.....	53
5.3 Summary of design parameters and performance results of the planar array.....	82
5.4 Summary of design parameters and performance results of the linear array.....	99

*In affectionate dedication to the most caring individuals*

*my parents Abdulhadi and Aysha*

*and my lovely spouse Razan*

# Chapter 1

## INTRODUCTION

### 1.1 History of Antenna and Overview

"[T]he antenna is so to speak the mouth or ear of the radio station," this is how Fleming recognized the paramount nature of antennas back in 1909 [1]. An antenna can be defined as a device that is capable of converting electrical current and voltage confined in a structure into propagating electromagnetic radio waves and vice versa. The *IEEE Standard Definitions of Terms for Antennas* defines the antenna or aerial as "a means for radiating or receiving radio waves." [2]

That is to say, the antenna is the intermediate entity between an open environment and a guiding device. The guiding device or transmission line can be any medium to guide the electromagnetic energy such as a coaxial cable or a hollow tube like a waveguide. This guiding device is utilized to transfer electromagnetic energy from the transmitting source to the antenna; in this case, the antenna can be referred to as a transmitting antenna. Furthermore, it can be utilized to transport the electromagnetic energy from the antenna to the receiver; and here it can be referred to as a receiving antenna.

In a historical note on antenna design trends, the first conducted electromagnetic waves propagation can be dated back to 1886 when a professor at the Technical Institute

in Karlsruhe named Heinrich Rudolph Hertz successfully built an apparatus that now would be characterized as a sophisticated wireless radio system. The system consisted of an end-loaded half-wave dipole as a transmitter and a resonant square loop antenna as a receiver. He was able to detect a spark in the closely located loop antenna after being generated at the center of the dipole. For more than a decade, this achievement was nothing but an inquisitive idea. Until during a summer vacation in Alep, an idea twinkled in Guglielmo Marconi's head after reading a description of Hertz laboratory experiment. He questioned himself if these Hertzian waves could be utilized to send and receive messages. In mid-December 1901, Marconi effectively received the first transatlantic radio message. It was nothing but the Morse-code of the letter 'S'. This achievement was perhaps the most substantial event in the first era of wireless communications [3], [4]. Since then, antennas have been fundamentally existed in communication applications, with most employment in wireless radio communication systems.

For tens of years, non-discounted evolvments have been carried out in all orientations. Improvement in various disciplines including but not limited to signal processing and antenna theories have all participated in the pervasiveness of sophisticated wireless communication systems nowadays. Although enormous ameliorations have been witnessed on antenna since

the days of Marconi, The need to have very high data rates as well as strong and adequate network coverages has recently skyrocketed, which, in turns, has dramatically increased the demand to have enough spectrum that can tolerate the increased number of cellphone users and shared data amount. To meet this demand, industry engineers and scientists

have started to work on improving antennas specifications such as large bandwidth, high gain, small size, and good temperature stability to be utilized in designing radio frequency communication systems suitable for very high-frequency applications. In fact, different antenna solutions that are well known to have a small size and low profile and cost have been proposed for very high-frequency applications. However, unless well-developed design solutions based on the integration of adequate dielectric super/substrates or lensing structures are applied, these antennas normally will suffer from reduced radiation efficiency and narrow impedance bandwidth due to the effect of lossy materials. On the other hand, dielectric resonator antennas (DRAs) are considered to be promising candidates to substitute these radiating elements, especially for applications at high frequency due to the fact that DRAs lack the existence of metal surfaces and therefore do not suffer much from conduction losses. Also, DRAs are well known to have high radiation efficiency when excited properly [5].

## **1.2 Problem Statement**

Due to the numerous evolutions in wireless communication systems, antenna engineers have been confronting number of challenges regarding improving the performance of the antenna, miniaturizing its size as well as considering the fabrication simplicity. Although DRAs typically suffer from providing low gain [6], they have been thoroughly under investigating as they are being excellent candidates that can be utilized to fulfill contemporary communication systems requirements and specifications operating at high-frequency ranges. The reason behind this solicitude is only because of the fact that they have several advantageous features, including but not limited to the simplicity of the used excitation mechanism and fabrication easiness.

On the other hand, according to antenna theories, as the operating frequency increases, the size of the antenna decreases. Therefore, according to Friis equation, the captured or transmitted power is reduced as the size of the antenna shrinks. However, to avoid this specific obstacle, it is strongly preferred to have a relatively high gain to maintain the received/transmitted power amount within an acceptable range when increasing the operational frequency.

Recently, different gain enhancement techniques have been proposed in the literature. For instance, introducing thin air gap between the dielectric slab and the ground plane [7], stackable layered of various dielectric materials with different relative permittivity [8], and integration of additional objects that surround the dielectric slab as a surface mounted short horn [9] or lens [10]. Although these enhancement methods have been proven to produce considerably high gain, to an extent, they suffer from certain drawbacks, such as not being versatile, design complexity, or cost ineffectiveness. More analytical study will be presented in the following chapters. One of the well-known methods to improve the gain is by arraying additional individual DRAs. The main obstacle evokes when designing the array to operate at high frequency. Spurious radiations from the feeding network are considerable and unfavorably influence the overall array performance [11]. Moreover, it is mandatory to have several quarter-wavelength transmission lines and power divider which, in turns, leads to high configuration complexity; unless the array is designed with single feeding port and the concept of standing waves takes place which was accomplished in this dissertation.

### **1.3 Dissertation Contribution**

The objective of this dissertation is to explore and investigate dilemmas that are associated with designing improved gain dielectric resonator antenna, specifically arrays, for contemporaneous communication systems and providing versatile solutions. High gain DRA is extremely desired for certain applications that require a point to point communication.

This dissertation successfully achieved two novel prototypes for dielectric resonator array antenna based on two different feeding mechanism making advantage of standing wave concept. The first design is effectively applicable for the one-dimensional linear array. It is based on coupling electromagnetic waves from microstrip patches into the dielectric slabs using single coaxial probe as feeding port. The other design can beneficially be utilized in both linear and planner arrays. This design is based on aperture coupling for the feeding with bridges in both vertical and horizontal directions connecting the array elements.

This part illustrates the essential contributions of this dissertation, highlighting two major scopes. These scopes are the process of the simulation investigation and the process of fabrication and implementation of the two proposed prototypes. These contributions can be listed as follows:

- Design, implementation, and measurement of an improved gain standing wave dielectric resonator array antenna for linear array applications.



- Design, implementation, and measurement of an improved gain standing wave dielectric resonator array antenna for both linear and planar array applications.
- Make advantage of using modern masterful technology for the fabrication procedure such as 3D printing technology.

#### **1.4 Dissertation Overview**

This dissertation demonstrates the design and implementation of enhanced gain dielectric resonator array antenna for one- and two-dimensional arrays. It also provides Matlab code to characterize single element dielectric resonator antenna.

Chapter 2 provides general information about dielectric resonator antenna. Historical overview on DRA will be provided. Essential components of a DRA and its excitation techniques are also illustrated. Finally, a list of DRA applications is provided.

Chapter 3 describes number of numerical models that are typically applied to characterize DRA. Methods for predicting the resonance frequency are reviewed. Calculating the Quality factor and estimating the input impedance will take place in this chapter.

Chapter 4 provides a review of the general concept of array antenna in terms of basic definitions and theories. A dedicated part on DRA array is provided as well. Then, a detailed comparison of the concept of traveling waves versus standing waves is highlighted. Lastly, the parameter gain will be defined with indicating the difference between realized and matched gain.

Chapter 5 includes two main sections. The first part demonstrates the design and fabrication of one- and two-dimensional high gain dielectric resonator array antenna. Experimental results of this prototype are included. The second part is about the design and implementation of the high gain linear dielectric resonator array antenna. The design procedure and simulations results are also presented. At the beginning of this chapter, the motivations that lead to this accomplishment are demonstrated along with a review of previous work that is presented in the literature.

Chapter 6 concludes this dissertation by illustrating the advantage of the proposed solutions. Future work insight and suggestions to further improve the proposed prototypes are given.

## Chapter 2

### INTRODUCTION ON DIELECTRIC RESONATOR ANTENNA

#### 2.1 History of DRA

Decades ago and due to the fact that dielectric resonators have high-quality factor and are made of materials having high relative permittivity ( $\epsilon_r$ ), dielectric resonators have been exceedingly utilized in microwave circuits for various applications such as filters, oscillators, amplifiers, or tuners [12] and treated as an energy storage elements rather than radiators. This idea of dealing with dielectric resonators had to wait a long time until the year 1983. At that time, it was proposed by Long and his research group that cylindrical dielectric resonator can be used as a radiating antenna [13]. It was observed that at very high-frequency range such as millimeter wave range, the only loss for a DRA comes from imperfect dielectric material which in effect very trivial. With an adequate feeding mechanism for the sake of exciting the appropriate mode, these dielectric resonators become efficacious radiators. Contrariwise, in antennas that fundamentally have metallic structures and surfaces the conducting loss turns out to be severe and therefore the efficiency of the antennas is reduced drastically. Long and his crew had made further investigation on DRA having various geometries [14] and [15] and due to their contributory work, the foundation for further investigations of DRAs was established.

The early work on examining and studying dielectric resonator antenna was predominantly accomplished by three research groups: one was led by Kishk, Glisson, and Junker, one by Leung and Luk, and lastly by Mongia [16]. This work was carried out between 1986 and 1997, roughly. The scope of these treatises was considerably concentrated on characterizing unpretentious shapes in terms of inspecting different feeding techniques, examining number of operating modes, and providing simple and straightforward equations based on certain numerical techniques to predict the resonance frequency, evaluate the input impedance and Quality factor, and lastly to determine the radiation patterns of dielectric resonator antennas. Ever since dielectric resonator antennas have become the subject of unquenched and intensive research exploring and discussing further functional aspects. Antenna researchers have begun investigating DRAs with regard to several areas, including but not limited to circular polarization, gain enhancement methodologies, multi- and wideband, and miniaturization mechanisms.

## **2.2 Structure of DRA**

A dielectric resonator antenna typically consists of four essential components: a dielectric element, a ground plane, a substrate, and a feeding network. The radiating dielectric slab is mounted on top of the ground plane whereas the dielectric substrate resides underneath the ground plane, as shown in Figure 2.1.

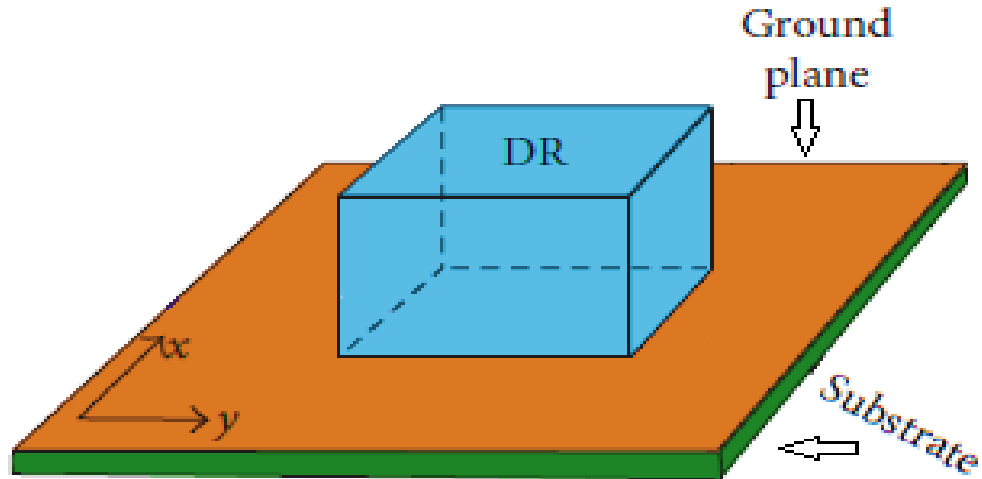


Figure 2.1: General Structure of DRA

The dielectric resonator slab generally is made out of a dielectric material such as quartz or ceramic with a comparatively high dielectric constant of the range 3 and above. The slab can have any geometrical shape a person may think of. However, the most common shapes are rectangular, cylindrical, and semispherical. Furthermore, it can be a low-profile circular disk, low-profile triangular, or a spherical-cap as illustrated in Figure 2.2.

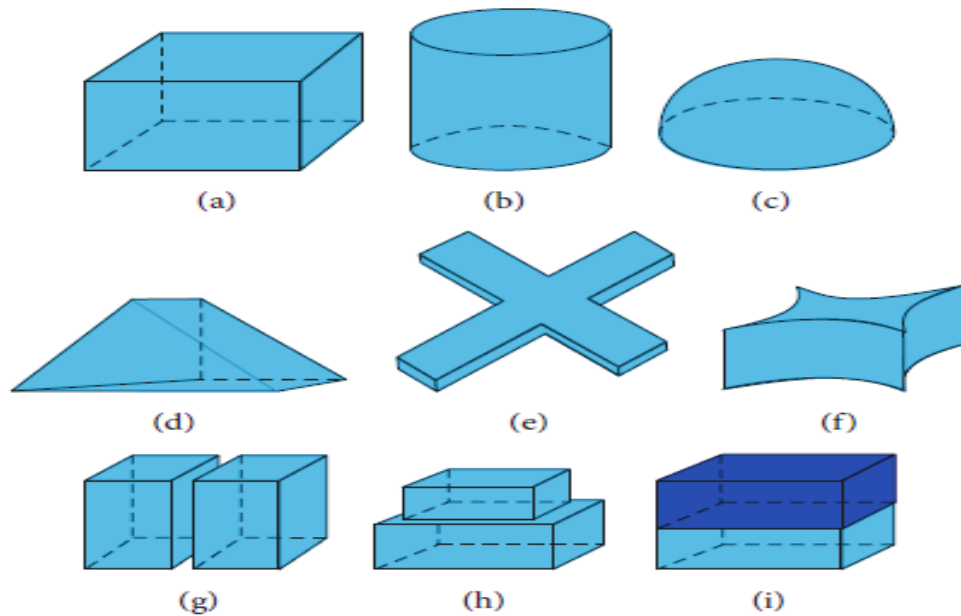


Figure 2.2: Examples of Various DRA Geometries

The substrate is usually very thin and its thickness  $h \ll \lambda_0$  where  $\lambda_0$  is the wavelength in the free space. Indeed, there is a variety of materials that can be utilized to design substrates of diverse thicknesses such as Roger and Arlon. The relative permittivity of the substrate  $\epsilon_{rs}$  can range from 2 to more than 10. It has been witnessed that the substrate dielectric constant drastically influences the input impedance. Leung has observed that for an aperture coupled dielectric antenna, higher  $\epsilon_{rs}$  leads to a stronger coupling. This is as the result of the fact that increasing  $\epsilon_{rs}$  will reduce the effective wavelength in the slot and consequently lengthen the slot from the electrical point of view [17].

The ground plane is typically a flat metallic surface made out of copper or any other strong conductive material. Its fundamental function is to separate the radiating element from the feeding network which, in turn, facilitates in minimizing back lobe radiation. In fact, the ground plane is not necessarily to be flat since utilizing soft corrugated ground plane has been studied and its ramifications were presented in [18] and [19]. Generating nearly identical radiation patterns in E- and H-planes was effectively accomplished. This achievement relies on the fact that symmetric rotationally corrugated ground plane provides rotationally symmetric boundary conditions which are solely due to the polarization independent reflection coefficients of the soft surface. It was also proven that the sidelobes radiations and the cross polarization are substantially evolved. It is to say that the circular soft corrugations can be efficiently utilized to enhance the radiation patterns of any antennas seated on ground planes. The ground plane thickness plays a relatively considerable role on the resonance frequency, useful bandwidth, and front-to-back radiation ratio. Leung and his research crew have demonstrated in [20] that

for an aperture-coupled hemispherical dielectric resonator antenna, as the ground plane thickness increases the resonance frequency and the bandwidth decreases, as well as the front-to-back radiation ratio. Furthermore, it was suggested to consider a thick ground plane as a mechanical support for antennas fabricated with the thin substrate.

### **2.3 Excitation Techniques of DRA**

To excite a dielectric resonator antenna, there are several feeding techniques that can be utilized which indeed one of the attractive advantages that dielectric resonator antennas possess. Some of these methods depend on directly deliver the RF power to the dielectric resonator slab using a conducting object such as a microstrip line or a coaxial probe. This method is known as a contacting excitation method. Other methods depend on transferring the power from the feeding network to the radiator through a coupling aperture without any direct contact between them. This technique is called non-contacting excitation method. The most used feeding methods are microstrip transmission line, coaxial probe, coplanar waveguide, and aperture coupling.

#### **2.3.1 Microstrip Transmission Line Feeding**

As shown in Figure 2.3, in this feeding mechanism the dielectric resonator is mounted straight on top of a printed microstrip line. The first time this method proposed to excite a dielectric resonator antenna was reported back in 1988 [21]. It was proven that the coupling intensity of this method depends mainly on the overlapping distance  $x$ . In other words for preciseness, more coupling between the feeding line and the dielectric resonator occurs when the overlapping distance is marginally shorter than one-quarter of the wavelength in the dielectric resonator  $\epsilon_{rd}$ . This feeding method suffers from one

major disadvantage. Since the feeding line is not separated from the radiating element, spurious undesired radiations can be generated and thus negatively impact the radiation performance. Furthermore, even with negligible transmission line thickness, an unfavorable air gap between the substrate and the radiating slab is generated.

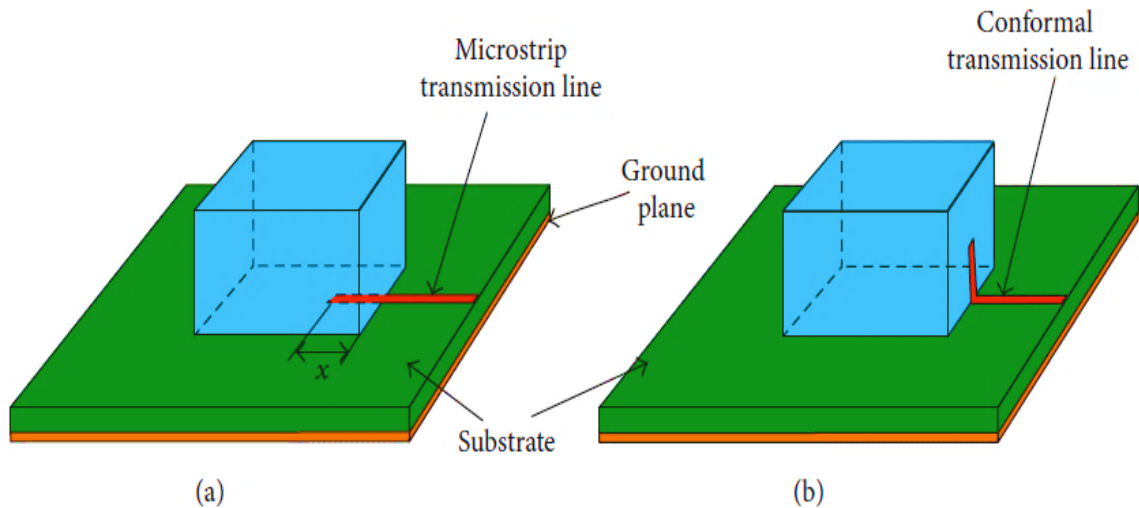


Figure 2.3: 3D view of conventional (a) and conformal (b) microstrip line feeding.

### 2.3.2 Coaxial Probe Feeding

In this configuration, the dielectric resonator is located above a ground plane and the probe exciting the antenna is connected to the dielectric resonator through a substrate placed underneath the ground plane. The probe can permeate the dielectric resonator by drilling a hole inside it or can be placed adjacently to one edge of the dielectric resonator, as shown in Figure 2.4. This feeding technique was first reported in 1983 [14]. It was proven that the location of the probe as well as the length of the inner pin of the coaxial cable penetrating the dielectric resonator, have a substantial influence on the input impedance. This feeding mechanism is capable of supplying intense coupling which results in better radiation performance, especially when the probe is permeating the slab.



However, drilling a hole in the dielectric slab is critical since the size of the hole has to exactly resemble the dimensions of the inner pin to avoid having air in-between. Additionally, it increases the fabrication complexity.

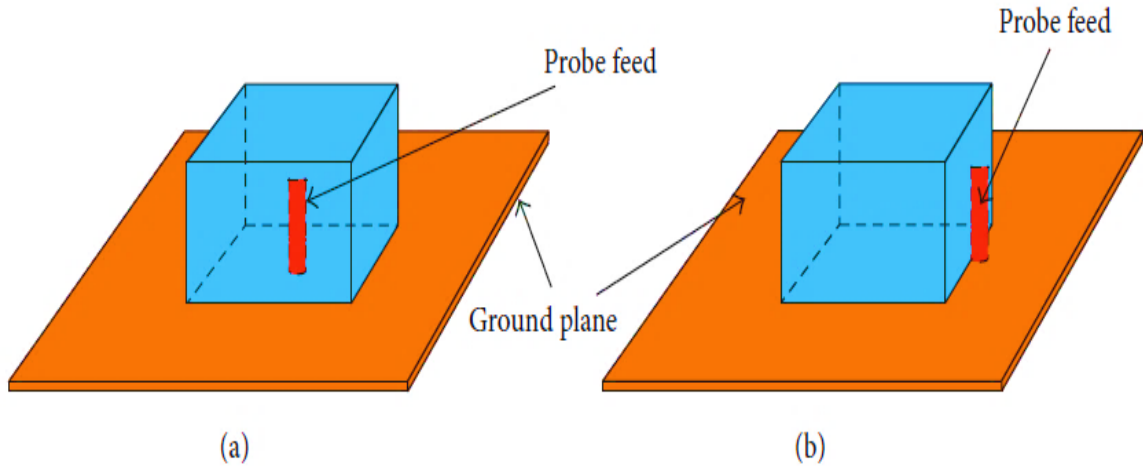


Figure 2.4: 3D view of coaxial probe penetrating (a) or adjacent to (b) the DRA

### 2.3.3 Aperture Coupling Feeding

This excitation method illustrated in Figure 2.5 is the most popular method used to feed the dielectric resonator antenna. The electromagnetic waves are guided along a transmission line printed on the bottom side of the substrate. Then, these waves propagate into the substrate heading to the dielectric resonator through a slot carved on the ground plane. The main advantage of this feeding technique is that spurious radiations from the feeding network can be minimized since the transmission line is isolated from the dielectric resonator. In fact, the displacement distance of the dielectric resonator along x and y-axis with respect to the slot was thoroughly studied. It was concluded that when the dielectric resonator is exactly centered above the aperture, the best impedance matching can be accomplished [22].

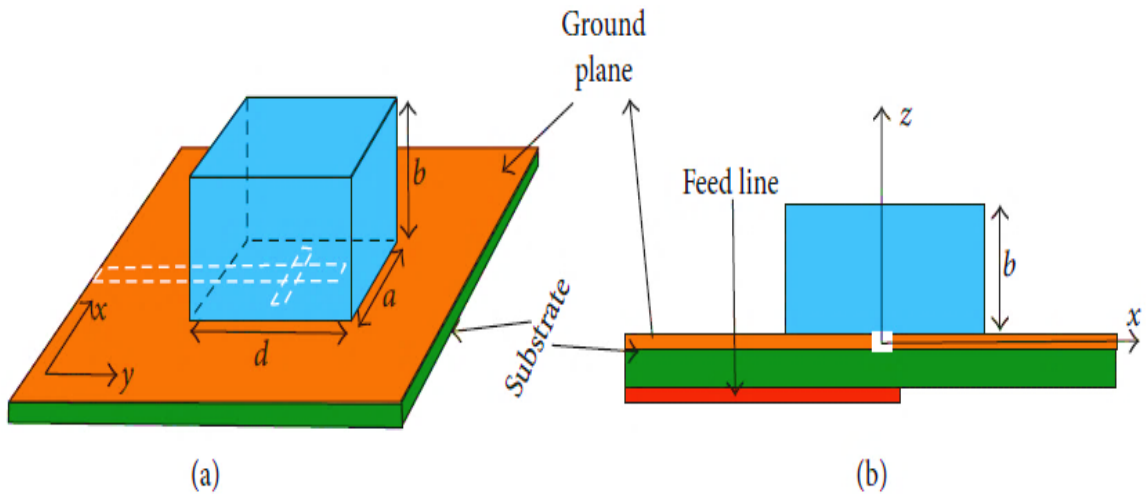


Figure 2.5: 3D view (a) and cross-sectional view (b) of an aperture-fed rectangular DRA.

## 2.4 Applications of DRAs

Dielectric resonator antennas are popular and attracting more attention since they were introduced in the mid of 1980s due to the fact that they are robust, compact, and inexpensive. They also have excellent performance, especially with millimeter wave applications. Dielectric resonator antennas have applications in many different areas such as satellite and space communication, RADAR and surveillance, and tomography and biomedical applications. Recently, dielectric resonator antennas are being involved in 5G applications due to their wide impedance bandwidth and their good performance at extremely high frequencies.

### 2.4.1 RADAR and Surveillance Applications

RADAR technology is used to detect any movable objects such as airplanes in the space or vehicles on the ground. The range of RADAR systems mainly depends on the amount of power delivered to the antenna. Since dielectric resonator antennas have minimal conducting surfaces and therefore small dissipation loss, it is suitable to deal and

handle high power which, in turn, provides longer RADAR range. Furthermore, since dielectric resonator antennas have wide frequency band, the opportunity of jamming or spoofing the RADAR is reduced because frequency hopping can be performed with wide bandwidth. Also, since dielectric resonator antennas are small in size and light in weight, this feature enables them to be mechanically rotated for broad scanning purposes using sprightly rotators [23].

#### **2.4.2 GNSS and GPS Applications**

This type of communication systems requires antennas that are capable of operating over a wide band, performing beam steering, having a lightweight and low profile, and have less mutual coupling between array elements. Dielectric resonator antennas can meet previously mentioned constraints for several reasons. Firstly, DRAs have the ability to perform beam steering and hence locate the nulls at undesired interferences. By doing so, DRAs can counteract any potential vexatious attacks such as spoofing to forbid the service or manipulate the accuracy of the navigation functionality. Secondly, due to the lack of metallic structure in DRAs, mutual coupling between GNSS arrays is diminished [24].

#### **2.4.3 Tomography and Biomedical Applications**

In this medical field, the antennas employed are designed to operate within the medical band providing significantly wide impedance bandwidth and highly localized near-field distributions. They are also desired to be small in size and compact. Therefore, due to the many advantages of dielectric resonator antennas, this type of antennas is, in fact, attracting more attention to be utilized in this field. Kishk and Huang have proposed

a flipped two-steps stair-shaped array for microwave breast cancer detection. They have successfully achieved a matching frequency ranges from 7.4 to 11.3 GHz which corresponds to a useful bandwidth of 41.7% [25]. Another approach offers a predicted 10 dB return loss bandwidth of 74% between 4.4 and 9.7 GHz [26].

## **Chapter 3**

### **RECTANGULAR DIELECTRIC RESONATOR ANTENNA CHARACTERIZATION**

Dielectric resonator antennas have a number of advantageous features that have made them more attractive recently. One of these advantages is that a DRA can have any shape. Most commonly, they come with rectangular or circular cross-sections. Since dielectric resonator antennas are volume apparatuses, they present more degrees of freedom than other types of antennas. Rectangular dielectric resonator antennas are the most adaptable as they have two degrees of freedom. At a specific resonant frequency with known dielectric constant, two of rectangular dielectric resonator antenna's dimensions can be independently selected.

#### **3.1 Overview of Analyzing Models**

Although rectangular dielectric resonator antennas are the most versatile and commonly used type, they are the hardest to be theoretically analyzed. The reason is that comparing to cylindrical or hemispherical dielectric antennas, they have more edge boundaries that make obtaining the closed-form Green's function quite complicated. However, number of numerical methods such as Finite Difference Time Domain (FDTD) and Method of Moment (MoM) can be used to solve for the resonance frequency and the

electromagnetic field. The above-mentioned techniques are known to consume much more time and computer memory. As a result, they are not practical to be utilized for designing or optimizing purposes.

The dielectric waveguide model (DWM), firstly proposed by Marcatili [27], has been vastly applied to analyze rectangular dielectric resonator antennas. The model was originally generated to obtain the guided wavelength inside dielectric guides having rectangular cross-sections. In this model, the fields within the guide are presumed to have sinusoidal variations while these outside the guide are presumed to have an exponential decaying trace. The wave propagation numbers in all directions as well as the attenuation constants can be obtained, after matching the fields at the boundaries, using [17]:

$$k_z = \sqrt{\varepsilon_r k_o^2 - k_x^2 - k_y^2} \quad (3-1)$$

$$k_x = \frac{m\pi}{a} \left( 1 + \frac{2}{a k_o \sqrt{\varepsilon_r - 1}} \right)^{-1} \quad (3-2)$$

$$k_y = \frac{n\pi}{b} \left( 1 + \frac{2}{b k_o \sqrt{\varepsilon_r - 1}} \right)^{-1} \quad (3-3)$$

$$\alpha = \frac{1}{\sqrt{(\varepsilon_r - 1)k_o^2 - k_x^2}} \quad (3-4)$$

$$\gamma = \frac{1}{\sqrt{(\varepsilon_r - 1)k_o^2 - k_y^2}} \quad (3-5)$$

where  $k_x$ ,  $k_y$ , and  $k_z$  are the wavenumbers in the x-, y-, and z-direction.  $\alpha$  and  $\gamma$  are the attenuation constants in the x- and y-direction, respectively.

and  $k_o$  is the free-space wave number given by:

$$k_o = \frac{2\pi}{\lambda_o} = \frac{2\pi f_o}{c} \quad (3 - 6)$$

where  $c$  is the free-space speed of light,  $f_o$  is the operating frequency, and  $\lambda_o$  is the free-space wavelength. However, when the fields' leakage is minimal and the fields are well confined, the further approximation is valid:

$$k_x = \frac{m \pi}{a} \quad (3 - 7)$$

$$k_y = \frac{n \pi}{b} \quad (3 - 8)$$

where  $a$  and  $b$  are the length and width in x- and y-direction, respectively; also,  $m$  and  $n$  are the number of field extrema in the x- and y-direction, respectively inside the guide.

For the sake of modeling a dielectric resonator antenna, the waveguide assumed above is truncated along the z-direction at  $\pm d/2$  with magnetic walls. Thus, it can be utilized in practical cases where a DRA is placed on top of a ground plane. As a result of the ground plane existence, image theory can be utilized here to remove the ground plane and double the height of the DRA.

### 3.2 Field Distribution

The lowest order mode of a rectangular dielectric resonator antenna with dimensions of  $a$ ,  $b$ , and  $h$  is  $TE_{1\delta 1}^y$  for a source wave in the y-direction and  $0 < \delta \leq 1$ . The DRA practically is mounted on a ground plane at  $z=0$ . Considering the image theory, the ground plane can be removed and thus the rectangular dielectric resonator antenna can be

treated as an isolated one having the dimensions of  $a \times b \times d$  where  $d= 2h$ . By applying the boundary conditions and solving the wave function inside the dielectric slab, the eigenfunction  $\Psi_{mnp}$

$$\Psi_{mnp} = \sin \left[ k_x \left( x + \frac{a}{2} \right) \right] \cos(k_y y) \sin \left[ k_z \left( z + \frac{d}{2} \right) \right] \quad (3 - 9)$$

where  $k_x$ ,  $k_y$ , and  $k_z$  are:

$$k_x = \frac{m\pi}{a} \quad (3 - 10)$$

$$k_y \tan \left( \frac{k_y b}{2} \right) = \sqrt{(\epsilon_r - 1)k_0^2 - k_y^2} \quad (3 - 11)$$

$$k_z = \frac{p\pi}{d} \quad (3 - 12)$$

Hence, the fields inside the rectangular dielectric resonator antenna can be approximated as follows [28]:

$$H_x = \frac{jA(k_x k_y)}{\omega \mu \epsilon} \cos \left[ k_x \left( x + \frac{a}{2} \right) \right] \sin(k_y y) \sin \left[ k_z \left( z + \frac{d}{2} \right) \right] \quad (3 - 13)$$

$$H_y = \frac{-jA(k_x^2 + k_z^2)}{\omega \mu \epsilon} \sin \left[ k_x \left( x + \frac{a}{2} \right) \right] \cos(k_y y) \sin \left[ k_z \left( z + \frac{d}{2} \right) \right] \quad (3 - 14)$$

$$H_z = \frac{jA(k_y k_z)}{\omega \mu \epsilon} \sin \left[ k_x \left( x + \frac{a}{2} \right) \right] \sin(k_y y) \cos \left[ k_z \left( z + \frac{d}{2} \right) \right] \quad (3 - 15)$$

$$E_x = \left( \frac{Ak_z}{\epsilon} \right) \sin \left[ k_x \left( x + \frac{a}{2} \right) \right] \cos(k_y y) \cos \left[ k_z \left( z + \frac{d}{2} \right) \right] \quad (3 - 16)$$

$$E_y = 0 \quad (3 - 17)$$



$$E_z = \left( \frac{-Ak_x}{\varepsilon} \right) \cos \left[ k_x \left( x + \frac{a}{2} \right) \right] \cos(k_y y) \sin \left[ k_z \left( z + \frac{d}{2} \right) \right] \quad (3 - 18)$$

where  $A$  is a magnitude constant, and

$$k_x^2 + k_y^2 + k_z^2 = \varepsilon_r k_o^2 \quad (3 - 15)$$

The parameter  $\delta$  corresponds to a fraction of a cycle of the field variation in the  $y$ -direction.

### 3.3 Radiation Characteristics

To evaluate the radiation pattern of a rectangular dielectric resonator antenna, all the surfaces of the slab are assumed to be perfect or imperfect magnetic walls. Since the fields inside the slab are not completely confined and  $\hat{n} \times \vec{H} = 0$  is not satisfied, the surfaces  $x = \pm a/2$  and  $z = \pm d/2$  are assumed to be perfect magnetic conductors (PMC) whereas  $y = \pm b/2$  surfaces are assumed to be imperfect magnetic conductors [29], [30.], and [31]. By applying the equivalence principle to find the magnetic surface current ( $\vec{M}_s$ ) or the electric surface current ( $\vec{J}_s$ ) on the corresponding surfaces, the electric field in the far zone can be expressed as follows [32]:

$$E_\theta = - \frac{j k_o e^{-jk_o r}}{4\pi r} x [L_\varphi + \eta_o N_\theta] \quad (3 - 16)$$

$$E_\varphi = \frac{j k_o e^{-jk_o r}}{4\pi r} x [L_\theta - \eta_o N_\varphi] \quad (3 - 17)$$

where:

$$N_\theta = A_x \cos(\theta) \cos(\varphi) + A_y \cos(\theta) \sin(\varphi) - A_z \sin(\theta) \quad (3 - 18)$$

$$N_\varphi = -A_x \sin(\varphi) + A_y \cos(\varphi) \quad (3-19)$$

$$L_\theta = F_x \cos(\theta) \cos(\varphi) + F_y \cos(\theta) \sin(\varphi) - F_z \sin(\theta) \quad (3-20)$$

$$L_\varphi = -F_x \sin(\varphi) + F_y \cos(\varphi) \quad (3-21)$$

$$F_x = -2j E_3 I_1 I_5 \cos\left(\frac{k_y b}{2}\right) \sin\left(\frac{b}{2} \chi_2\right) \quad (3-22)$$

$$F_y = I_3 \left[ \begin{array}{l} E_3 I_5 \left\{ (-1)^m e^{\frac{j a \chi_1}{2}} - e^{-\frac{j a \chi_1}{2}} \right\} + \\ E_1 I_2 \left\{ e^{-\frac{j d \chi_3}{2}} - (-1)^p e^{\frac{j d \chi_3}{2}} \right\} \end{array} \right] \quad (3-23)$$

$$F_z = 2j E_1 I_2 I_4 \cos\left(\frac{k_y b}{2}\right) \sin\left(\frac{b}{2} \chi_2\right) \quad (3-24)$$

$$A_x = 2 H_3 I_2 I_4 \sin\left(\frac{k_y b}{2}\right) \cos\left(\frac{b}{2} \chi_2\right) \quad (3-25)$$

$$A_y = 0 \quad (3-26)$$

$$A_z = -2 H_1 I_1 I_5 \sin\left(\frac{k_y b}{2}\right) \cos\left(\frac{b}{2} \chi_2\right) \quad (3-27)$$

$$\chi_1 = k_o \sin(\theta) \cos(\varphi) \quad (3-28)$$

$$\chi_2 = k_o \sin(\theta) \sin(\varphi) \quad (3-29)$$

$$\chi_3 = k_o \cos(\theta) \quad (3-30)$$

$$I_1 = f(P = a, Q = a, R = 1, S = 2, U = k_x, V = \chi_1) \quad (3-31)$$

$$I_2 = f(P = a, Q = a, R = -1, S = 2j, U = k_x, V = \chi_1) \quad (3-32)$$

$$I_3 = f(P = b, Q = 0, R = 1, S = 2, U = k_y, V = \chi_2) \quad (3 - 33)$$

$$I_4 = f(P = d, Q = d, R = 1, S = 2, U = k_z, V = \chi_3) \quad (3 - 34)$$

$$I_5 = f(P = d, Q = d, R = -1, S = 2j, U = k_z, V = \chi_3) \quad (3 - 35)$$

Here,  $E_1, E_3, H_1, H_2,$  and  $H_3$  are the strength of the fields  $E_x, E_z, H_x, H_y,$  and  $H_z$  respectively, and

$$f(P, Q, R, S, U, V) = \left[ \left( \frac{P}{S} \right) e^{j\frac{UQ}{2}} J_0 \left( \frac{(V + U)P}{2} \right) \right] \\ + \left[ \left( \frac{RP}{S} \right) e^{-j\frac{UQ}{2}} J_0 \left( \frac{(V - U)P}{2} \right) \right] \quad (3 - 36)$$

where  $J_0(x) = \frac{\sin(x)}{x}$  and  $P, Q, R, S, U,$  and  $V$  are constants.

### 3.4 Resonant Frequency and Higher-order Modes

The process of solving for the resonant frequency is mathematically intensive and requires a computer programming as a transcendental equation is involved. Equations (3-10), (3-12), and (3-15) are first substituted into equation (3-11), and this transcendental equation is solved for  $k_y$ . Then, the resonant frequency can be calculated by solving for  $k_o$  in (3-15) and substitute its value in (3-6). In [17], the aabove-mentioned equations have been utilized to plot the curves shown in Figure 3.1. The normalized frequency ( $F$ ) is plotted as a function of the ration of rectangular dielectric resonator antenna dimensions  $d/b$  for different ratios of  $a/b$ .

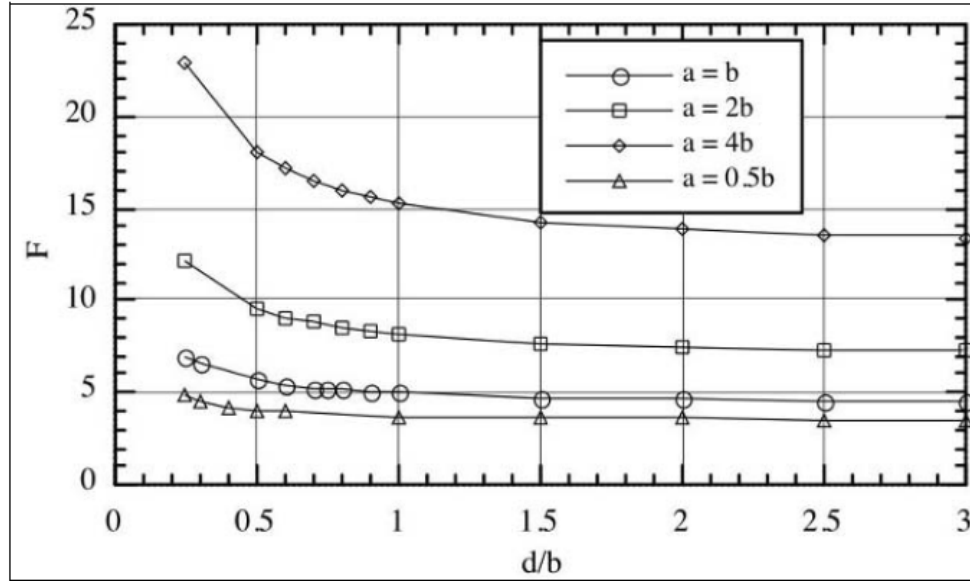


Figure 3.1: Normalized frequency of a rectangular dielectric resonator antenna [17]

Once the value  $F$  is obtained from the above plot, the resonant frequency can be calculated as follows:

$$f_o = \frac{F c}{2\pi a \sqrt{\epsilon_r}} \quad (3 - 37)$$

Although the above curves and formula can be utilized to quickly evaluate the resonant frequency, there still are some limitations regarding the choices of slab dimensions ratios. However, in [33], a formula has been developed by Leung *et al.* to calculate the resonant frequency based on previously known dimensions, and vice versa. For a rectangular dielectric resonator antenna with length  $a$ , width  $b$ , and height  $d$ , with  $a > b$ , the resonant frequency can be calculated using:

$$f_r = \frac{c}{2\pi a \sqrt{\epsilon_r}} \left( \frac{s_1}{s_2 + e^{s_3 p}} + s_4 \right) \quad (3 - 38)$$

where:

$$s_1 = -5.29q^4 + 15.97q^3 - 17.74q^2 + 8.812q - 3.198 \quad (3 - 39)$$

$$s_2 = 0.2706q^4 - 0.7232q^3 + 0.7857q^2 - 0.4558q - 1.023 \quad (3 - 40)$$

$$s_3 = -8.03q^4 + 23.06q^3 - 24.53q^2 + 11.75q - 3.588 \quad (3 - 41)$$

$$s_4 = 43.18q^4 - 124.7q^3 + 134.5q^2 - 65.85q + 15.37 \quad (3 - 42)$$

with  $p = b/a$  and  $q=d/a$ . The error comparing to DWM is negligible over the range of  $0.4 \leq p \leq 1$ ,  $0.2 \leq q \leq 1$ , and  $6 \leq \epsilon_r \leq 100$ .

Inversely, if the resonant frequency is specified, the length  $a$  of a rectangular dielectric resonator antenna can be calculated as:

$$a = \frac{c}{2\pi f_r \sqrt{\epsilon_r}} \left( \frac{s_1}{s_2 + e^{s_3 p}} + s_4 \right) \quad (3 - 43)$$

Once the length  $a$  is calculated, the width  $b$  and the height  $d$  can be obtained using the ratios of  $p$  and  $q$ , respectively. However, if the ratios of  $p$  and  $q$  are not identified, they can assume any value within the previously mentioned valid ranges.

Typically, a feeding source can excite an infinite number of operating modes of a rectangular dielectric resonator antenna. Recently, exciting higher order modes have been widely utilized in various DRA for gain enhancement and wide impedance bandwidth designs. The latter is basically based on exciting two consecutive modes with low-frequency ratio. Figure 3.2 illustrates both E- and H-fields of the fundamental  $TE_{111}^x$  mode and higher order modes  $TE_{113}^x$  and  $TE_{115}^x$  within a grounded rectangular DRA. Due

to the existence of the ground plane, even modes such as  $TE_{112}^x$  and  $TE_{114}^x$  are short-circuited.

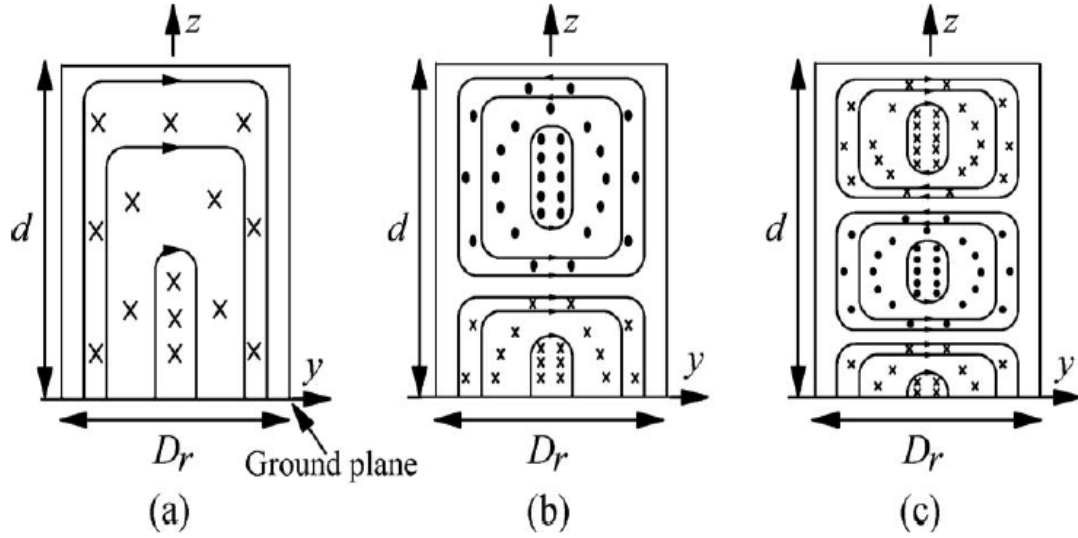


Figure 3.2: E-field (lines) and H-field (dots and crosses) of (a)  $TE_{111}^x$ , (b)  $TE_{113}^x$ , and (c)

$TE_{115}^x$  modes inside a grounded rectangular DRA [34].

## Chapter 4

### ARRAY ANTENNAS AND STANDING WAVES

#### 4.1 History of Array Antenna and Its Development

Typically, the radiation characteristics of a single antenna are limited. A single element generally generates a relatively wide radiation pattern and comparatively low gain and, therefore, restricted directivity. In numerous applications especially long-distance communications, it is mandatory to have antennas providing exceedingly directive properties. Electrically enlarging the size of the antenna is the sole approach to meet these directional properties. Although increasing the dimensions of an antenna makes it electrically larger, it is impractical to excessively increase it. One approach to electrically enhancing the antenna system without increasing the physical size of the antenna is to compose a collection of multiple radiating antennas coordinated in a specific configuration. This set of antennas is known as an array.

Array antenna can be defined as a system or a set consisting of two or more antennas located at particular distances. The separation distances are usually fractions of the wavelength with different or identical amplitudes and phases of the currents feeding each element. Arrays are advantageous because of the ability to manipulate the radiation pattern by adjusting the spacing as well as the excitation amplitude and phase. Moreover, arrays possess the susceptibility of angularly scanning the pattern either electrically or dynamically.

Arrays antenna have been known for more than a century. At their early stage, they were under less investigation having minimal interest due to the certain limitations as in numerical calculations. This underestimation of arrays capabilities had to wait around fifty years. In 1940, World War II skyrocketed their prominence by utilizing them in air defense for martial applications as they promote the transmission and the receiving of radio waves of antennas utilized in these communication systems [35]. Thenceforth, the rapid evolutions of computers and solid-state devices as well as the tremendous advances in numerical computing and simulation software have made arrays a very precious tool in radio frequency systems.

The first array antenna was successfully created by Brown in 1899. He was able to improve the directivity of a monopole by attaching another monopole half wavelength apart excited out of phase. These two vertical elements are the first end-fire array system [36]. Marconi, in early 1900's, carried out number of experiments to improve the gain of multiple antennas [37]. Nobel Prize winner Ferdinand Braun is the inventor of the phased array [38]. He located three monopoles in a triangle shape, as shown in Figure 4.1. It was assumed that the RF power exciting antennas A and B, placed at corners of an equilateral triangle, are equal in phase. However, excitation signals are delayed by a quarter of a cycle of feeding signal related to antenna C, which resides in the third corner of the triangle. Braun was the first to prove the ability to steer and orient the main array radiation beam via adjusting the feeding phases of the elements.



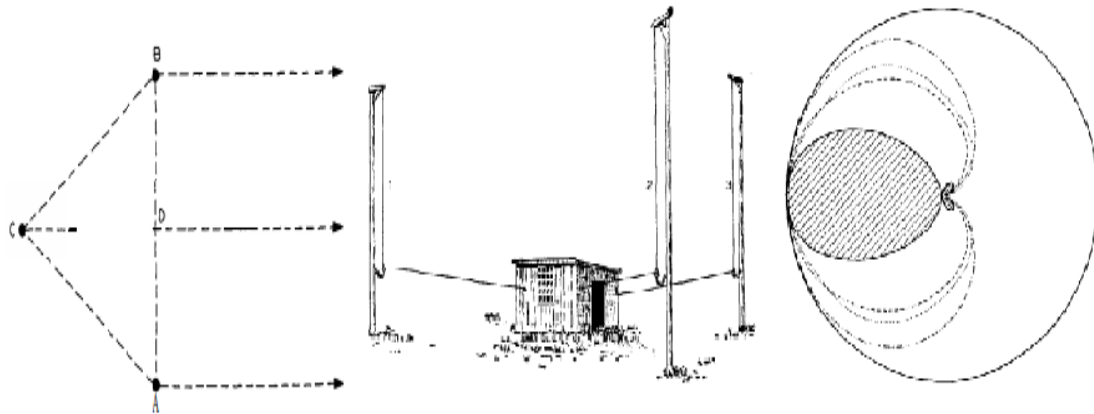


Figure 4.1: Braun's three-element array [38]

In 1919, Frank Adcock designed an array that composed of four uniformly weighted elements situated at the corners of a square. The spacing between each element is much less than half wavelength [39]. The antennas on the same diagonal line are excited out of phase with those on the other diagonal line.

During the World War II era, it was strongly demanded to develop radar systems to remotely detect enemies' vehicles, ships, and aircraft. Consequently, interest scope started turning toward arrays. In 1960, Unz has performed the first array performance enhancement attempt [40]. His work was on linear arrays. By manipulating the location of individual elements while feeding them uniformly, more directive radiation beam can be achieved. King and his colleagues investigated the beamwidth of linear arrays along with the limitations due to grating lobes [41]. They efficiently have eliminated number of elements maintaining the same beamwidth by unequally distributing the remaining elements. Also, they were able to replace the grating lobes by sidelobes of less amplitude. Stutzman in 1972 was able to obtain comparable radiation patterns of unequally spaced linear arrays to those of equally spaced arrays [42]. His proposed technique is based on

Gaussian quadrature formula employing unpretentious calculations. Moreover, he demonstrated the possibility of reducing the number of elements of an array while preserving the overall performance. He found that by properly locating arrays elements, number of them happen to exist in a region with less excitation, and thus they can be ineffectively opted out from the structure.

Dolph [43], Riblet [44], DuHamel [45], Tennant [46], and others, each in his own way, have contributed to the development of array including but not limited to spacing optimization algorithms and sidelobes reduction.

## **4.2 General Concept of Array Antenna**

Since an array antenna consists of a number of elements, so practically it can have as few as 2 elements and as many as thousands of elements. For illustration purposes, the most basic form of an array, the two-element array, will be assumed in this section. Array analysis starts by utilizing elements which uniformly radiate in all directions, known as isotropic radiators. Although there is no physical isotropic antenna, it can be said, hypothetically speaking, an isotropic antenna transmits and receives the RF power evenly in all directions. A method called the inspection method as well as the phasor summation approach will take place in this demonstration at its first stage [47]. The two isotropic sources are fed with identical amplitude and phase currents, and located one-half wavelength apart. Figure 4.2 explains the idea of applying the inspection approach in order to appreciate the concept of arrays.

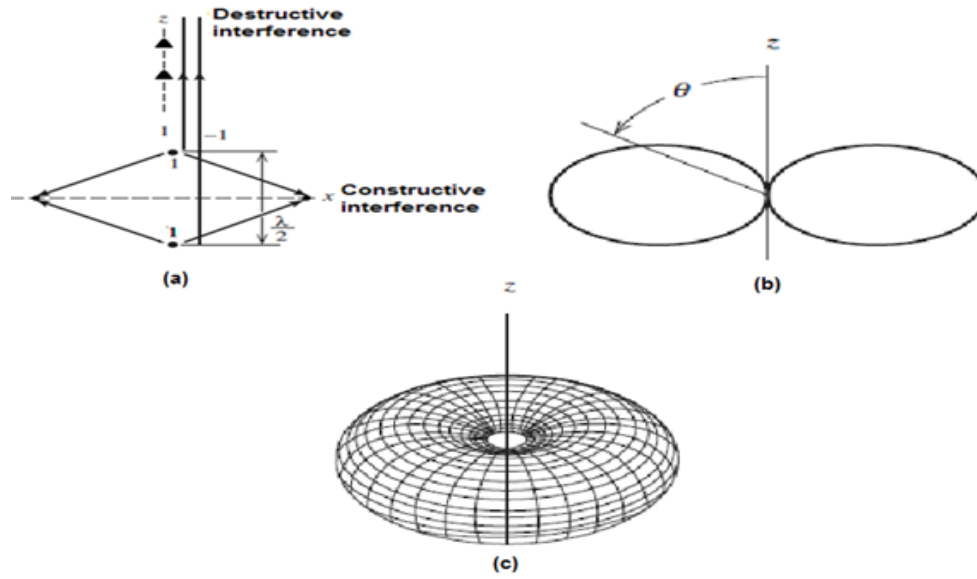


Figure 4.2: (a) Inspection Approach, (b) Array factor plot, and (c) 3D array factor plot.

Since the currents feeding the two isotropic sources are identical in both the amplitude and the phase, the waves received at the far field points along the x-axis are equal in amplitude and are in phase. Therefore, the total field is doubled. Considering the top part of the vertical line, z-axis, waves coming from the bottom source are delayed by one-half wavelength from those coming from the source on the top, i.e. 180-degree phase lag. Then, these waves produced by the two sources keep moving to the top point on the z-axis, preserving this phasor behavior in the far field. Consequently, these waves from the two sources arrive 180 out of phase to the observation point in the far field along the z-axis. This incident is a result of the separation distance between the sources. Not to mention that the amplitude of these waves is identical since the sources fed by identical current amplitude. Therefore, complete and pure cancellation is observed at that point and the total field is zero. The same dialectics applies to the opposite side of the z-axis. As a result, the total pattern has a relative value of 2 in the x-direction (assuming each source point is fed by the amplitude of 1), 0 in the z directions, and a harmonic variation

in between. The radiation pattern of an array of the two isotropic elements is called the array factor. It can be predicted utilizing phases corresponding to the path length differences shown in 4.3.

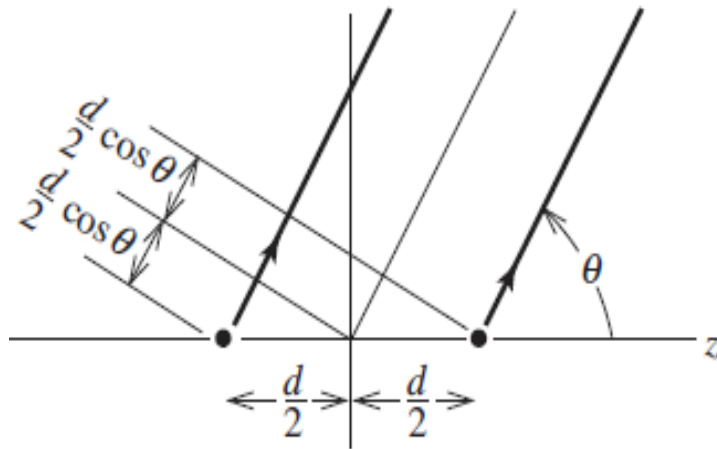


Figure 4.3: Geometry for pattern calculation using rays

The array factor is the sum of two phasors:

$$AF = 1 e^{-j\beta(d/2) \cos \theta} + 1 e^{j\beta(d/2) \cos \theta} = 2 \cos \left( \beta \frac{d}{2} \cos \theta \right) \quad (4-1)$$

The separation between the two elements is  $= \lambda/2$ , therefore  $\beta d/2 = \pi/2$ .

Hence, equation (4-1) becomes:

$$AF = 2 \cos \left( \frac{\pi}{2} \cos \theta \right) \quad (4-2)$$

The normalized array factor for the maximum value of unity is given by:

$$f(\theta) = \cos \left( \frac{\pi}{2} \cos \theta \right) \quad (4-3)$$

The maximum value of  $f(\theta)$  occurs when  $\theta = \pi/2$ , i.e.  $f(\theta) = \cos\left(\frac{\pi}{2} \cos \frac{\pi}{2}\right) = 1$  and minimum the value is observed when  $\theta = 0$ , i.e.  $f(\theta) = \cos\left(\frac{\pi}{2} \cos 0\right) = 0$ .

To generalize the concept of antenna arraying, let us consider  $N$  elements having identical amplitudes and each succeeding element has a progressive phase lead current excitation related to the preceding element. If the array elements are different than isotropic sources, the total radiation pattern can be obtained by multiplication of the array factor of the isotropic sources by the radiation pattern of a single element. This is known as the pattern multiplication rule and it can be used in a uniform array solely [48]. Then, the array factor can be calculated as:

$$AF = 1 + e^{+j(kd \cos \theta + \beta)} + e^{+2j(kd \cos \theta + \beta)} + \dots + e^{j(N-1)(kd \cos \theta + \beta)} \quad (4-4)$$

$$AF = \sum_{n=1}^N e^{j(n-1)(kd \cos \theta + \beta)} \quad (4-5)$$

For simplicity, (4-5) can be written as follows:

$$AF = \sum_{n=1}^N e^{j(n-1)\psi} \quad (4-6)$$

Where  $\psi = kd \cos \theta + \beta$

Since the overall array factor for the array is nothing but the summation of exponent functions, it can be expressed as the vector sum of  $N$  phasors, each of unity amplitude and progressive phase relative to the previous element. Therefore, equation (4-6), after multiplying both sides by  $e^{j\psi}$ , can be expressed as:

$$(AF) e^{j\psi} = e^{j\psi} + e^{j2\psi} + \dots + e^{j(N-1)\psi} + e^{jN\psi} \quad (4-7)$$

Subtracting (4-6) from (4-7), we get:

$$AF (e^{j\psi} - 1) = (-1 + e^{jN\psi}) \quad (4-8)$$

This can be written as:

$$\begin{aligned} AF &= \frac{e^{jN\psi} - 1}{e^{j\psi} - 1} = e^{j[(N-1)/2]\psi} \left[ \frac{e^{j(N/2)\psi} - e^{-j(N/2)\psi}}{e^{j(1/2)\psi} - e^{-j(1)\psi}} \right] \\ &= e^{j[(N-1)/2]\psi} \left[ \frac{\sin\left(\frac{N}{2}\psi\right)}{\sin\left(\frac{1}{2}\psi\right)} \right] \end{aligned} \quad (4-9)$$

If the center of the array is chosen as a reference point, equation (4-9) can be written as:

$$AF = \left[ \frac{\sin\left(\frac{N}{2}\psi\right)}{\sin\left(\frac{1}{2}\psi\right)} \right] \quad (4-10)$$

The normalized array factor is given by:

$$(AF)_n = \frac{1}{N} \left[ \frac{\sin\left(\frac{N}{2}\psi\right)}{\sin\left(\frac{1}{2}\psi\right)} \right] \cong \left[ \frac{\sin\left(\frac{N}{2}\psi\right)}{\frac{N}{2}\psi} \right] \quad (4-11)$$

In conclusion, it can be said that the array factor is a function of both the separation distances between array elements and the phase of the current feeding each element. By manipulating these two factors, the functional properties of the array factor and hence the total radiation pattern of the array can be optimized.

### **4.2.1 Multidimensional Array Antennas**

One-dimensional linear arrays typically suffer from certain limitations. For example, the radiation pattern beamwidth in the plane orthogonal to the line of element centers is broad. It corresponds to the element beamwidth in that plane which, in turns, restricts the realizable gain. Furthermore, if linear array antennas are utilized in phase scanning applications, the process of scanning can be performed only in the plane parallel to the array axis. Therefore, multidimensional array antennas are effectively utilized in applications where a pencil-shaped beam, high gain, or beam scanning in any direction is desired. With advances in fabrication techniques, the fabrication of large multidimensional arrays is efficient with reasonable efforts and cost. Multidimensional arrays can be classified based on three factors: The geometrical configuration of the surface on which the element centers are placed, the external circumference of the array structure, and the internal geometrical distribution of the elements [47]. The surface on which elements are placed can be circular, planar, etc. The perimeter of planar arrays typically possesses the shape of a square, rectangle, or circle. The elements allocation grid (also called lattice) can have equal or unequal vertical and horizontal spacings. A planar array with element spacings along x- and y-axis,  $d_x$  and  $d_y$  respectively, in the principal planes is referred to as a rectangular grid. When the spacing  $d_x = d_y$ , the lattice is said to be square.

### **4.3 Dielectric Resonator Antenna Arrays**

Dielectric resonator antenna arrays, like any other type of arrays, exhibit any geometrical configuration. They can be configured as linear or planner arrays. Moreover, adaptive or smart arrays with beam steering ability can be constructed utilizing dielectric

resonator antenna elements. It has been proven in the literature that DRA arrays possess promising directional characteristics generating more directed radiation pattern and hence improved gain if the spatial locations and excitations the array elements are chosen appropriately.

The concept of dielectric resonator antenna arraying was experimentally presented for the first time by Birand and Gelsthorpe in 1981 [49]. The structure consisted of a dielectric waveguide utilized as a feeding line that excites a set of rectangular dielectric slabs arranged linearly. The expediency of this type of array has been illustrated. An acceptable agreement has been observed between the experimental results and these theoretically anticipated. Shortly after hence, investigative studies have been well presented in the literature providing promising capabilities of dielectric resonator antenna arrays. An excellent investigation of various feeding mechanisms and their performance evaluation was carried out in 1995 by Petosa et al [50]. The study discussed linear array with microstrip line and dielectric image guide feed at a super high-frequency band, K band precisely. Despite the fact that the insertion loss is minimal in dielectric image guide feeding technique comparing to that of the microstrip line, it suffers from considerable undesired spurious radiation generated by the waveguide launchers. This drawback unfavorably influences the array gain eventually. On the other hand, the microstrip feeding line method behaves progressively worse as the operating frequency increases due to conduction losses. Yet, it provides a radiation pattern with higher gain and lower sidelobes comparing to the other feeding method.



The radiation pattern of a dielectric resonator antenna array can be calculated by multiplying the radiated electric field of the single element by the array factor. Thus, the radiation pattern in the far-field region can be expressed as

$$E = n \times E_0 \times AF \quad (4 - 12)$$

Where  $n$  is number of array elements utilized,  $E_0$  is the electric field of a single element located at the array origin, and  $AF$  is nothing but the array factor. However, the radiation pattern along with other characterizing factors, including but not limited to the resonant frequency and the directivity, can be negatively affected by mutual coupling between the array's elements due to the electromagnetic interaction between them. Number of factors plays an important role in the mutual coupling level. These factors are the separation distance between elements, the geometrical shape of the array, the dielectric constant of the individual element, and the operation mode order. It was also proven that the level of mutual coupling between array elements depends of the thickness of the substrate and the slabs dimensionality, essentially the height [17].

To conclude, arrays that are constructed of dielectric resonator elements have similar advantageous capabilities of these in single element dielectric resonator with exceeding radiation efficiency. Microstrip feeding line is most proper and convenient feeding mechanism to excite an array, especially at lower gigahertz frequency range. However, with this feeding arrangement, the performance at higher frequency ranges becomes drastically diminished due to severe conduction losses in the feeding network. Consequently, utilizing the dielectric waveguide as a feeding network is more profitable. Wu [17] has summarized the role factors affecting the eventual performance of dielectric

resonator antenna arrays. He has claimed that non-uniformity of dielectric materials between elements, air gaps and fabrication errors of dielectric elements and the feed structure, mutual coupling between array elements, losses in the feed network, size of the ground plane, and element mounting and alignment technique will mainly impact the radiation efficiency and overall performance of the array.

#### **4.4 Standing-Wave Arrays**

Generally, antenna array can be classified into two main categories based on the feeding network arrangement. The first type is called coplanar corporate feed. In this feeding mechanism, each element is independently excited by a specific magnitude and phase of a traveling electromagnetic wave from the feeding network. In such a feeding scheme, it is mandatory to have several quarter-wavelength transformers and power dividers. This, in turns, leads to high configuration complexity and usually generates spurious undesirable radiation. Therefore, the antenna efficiency is reduced especially at high frequencies due to metallic surfaces losses, also known as conduction losses [11] and [51-54]. Figure 4.4 illustrates various array structures with a corporate feeding network being utilized.

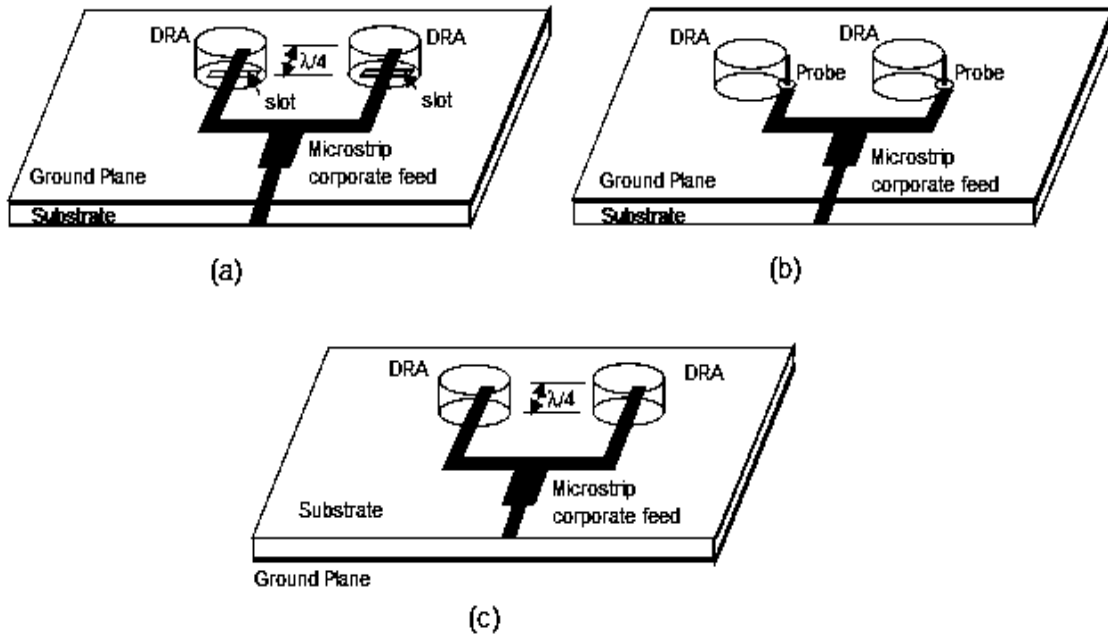


Figure 4.4: Illustration of (a) slot, (b) probe and (c) microstrip coupling corporate feed arrangements of DRA arrays

The second type is called inline series feed. In series-fed arrays, the input signal that is fed from one location on the feeding transmission line travels serially to feed the array elements one after another. Since the number of interconnecting lines and microstrip discontinuities is reduced in this feeding arrangement, its compact feeding network is one of the major advantages that make it more attractive than corporate feeding method. Figure 4.5 demonstrates an array structure with inline series feeding mechanism being used.

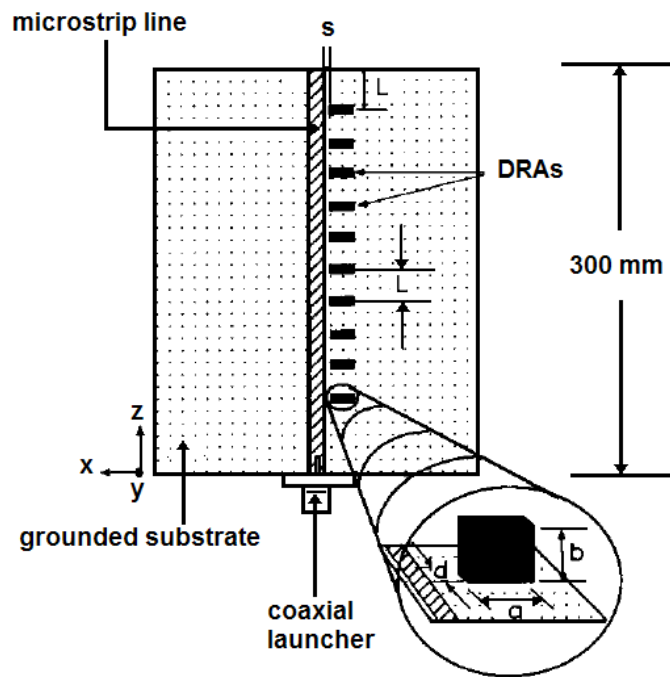


Figure 4.5: Inline series feeding method

In fact, the two aforementioned feeding networks share the same wave nature which is known as a traveling wave. A wave is considered to be traveling if it spatially changes its peaks with respect to time in the direction of propagation. As the wave crest moves through the medium transporting energy, it excites array elements either in parallel or serial manner. On the other hand, resonant cavity antennas such as microstrip patch and dielectric resonator antennas can be excited by forming stationary standing waves within the antenna structure. A standing wave generates an oscillating pattern within a medium. This phenomenon occurs when the resonant frequency of the wave generator produces waves that bounce back and forth from the medium boundaries to constructively interfere with waves latterly incident from the source. However, at a frequency different than the resonant frequency, the interference between incident and reflected waves becomes destructive which creates a disturbance of dissimilar and

unsystematic pattern within the medium. The figure below provides more insight into the wave behavior as a function of time.

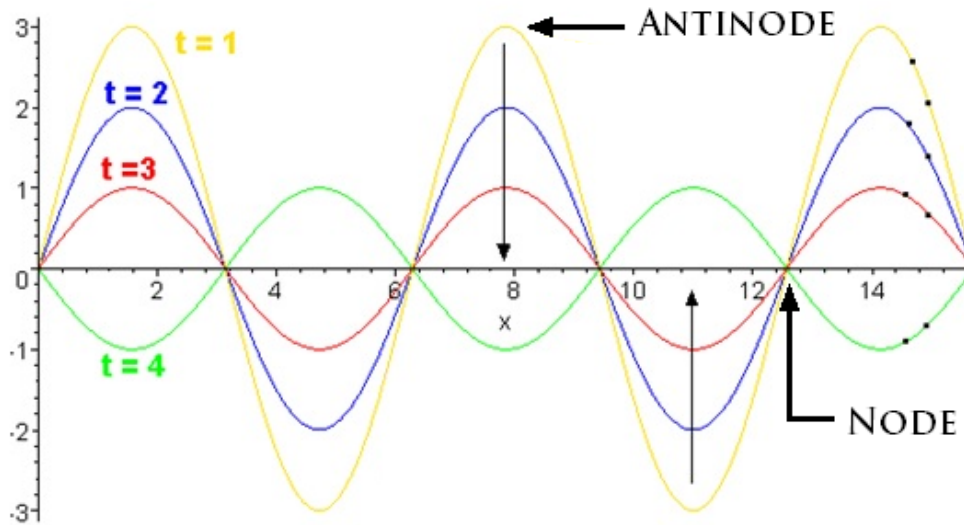


Figure 4.6: Standing wave pattern as a function of time

The name of this type of waves is inspired by the fact that this interference happens in a way that certain points within the medium behave to be stationary or standing still. The points at which the amplitude of the waves is minimal are known as Nodes whereas the points at which the amplitude is maximal are known as Antinodes.

That is to say, standing waves are formed by the superposition of two traveling waves oriented in opposite direction. In fact, when the multiple-bouncing waves become precisely constructive, maximum energy can be stored in the structure and it is said to be resonant [55]. Indeed, this feeding mechanism where a standing wave is formed excites the radiating elements of an array with equal magnitudes and equal (or opposite) phases for maximum directivity. The effectiveness of standing wave formation to excite a

dielectric resonator array structure will be thoroughly discussed in chapter 5 as the physical intuition will be provided as well.

#### **4.4.1 Corporate Feed Drawbacks**

Corporate feed networks are resilient and common in dielectric resonator array antennas. This type of feeding networks consists of numerous quarter-wave transformers and power dividers that are considered to a substance in the design. In dielectric resonator array antennas, radiating slabs, quarter-wave transformers, and transmission lines are independently designed. Nevertheless, corporate feeding networks possess some drawbacks, especially when operating at high gigahertz frequency bands. A conventional corporate-fed traveling wave array structure has noticeably long transmission lines in the power divider network that can be lossy [55]. The microstrip discontinuities can result in spurious radiations and coupling which negatively influence the performance of the array including the maximum observed gain [53-54]. Additionally, corporate feed networks are susceptible to changes in the phase [11]. On the other hand, dielectric resonator array antenna design utilizing standing waves in the structure can ultimately alleviate, to an excellent extent, these disadvantageous impacts of the corporate feed network lines. Hence, a better array performance can be achieved.

#### **4.5 Antenna Gain**

The parameter gain is one of the important quantitative that describes the performance of an antenna. It describes how much an antenna concentrates energy in a certain direction with respect to radiations observed in other directions. Although the gain of an antenna is closely related to its directivity, it is a measure that takes into account the efficiency of the antenna as well as its directional capabilities. The gain of an antenna, in

a given direction, can be defined as “the ratio of the intensity, in a given direction, to the radiation intensity that would be obtained if the power accepted by the antenna were radiated isotropically. The radiation intensity corresponding to the isotropically radiated power is equal to the power accepted by the antenna divided by  $4\pi$  [48].

Antenna gain can be theoretically calculated by:

$$Gain = 4 \pi \frac{\text{radiation intensity}}{\text{total input power}} \quad (4 - 13)$$

$$Gain = e_{cd} \times Directivity \quad (4 - 14)$$

where  $e_{cd}$  is the antenna radiation efficiency.

From equation (4-14), it can be observed that the gain can be exactly equal to the directivity of the antenna when the efficiency is 100%. Indeed, when the direction is not stated, the gain is typically observed in the direction of the maximum radiation.

There are two types of antenna gain,

#### **4.5.1 Matched Gain**

According to the IEEE Standards, evaluation of gain does not count for losses generated from polarization and impedance mismatches [2]. Therefore,

$$G_0 = G(\theta, \Phi)|_{max} = e_{cd} D(\theta, \Phi)|_{max} = e_{cd} D_0 \quad (4 - 15)$$

In fact, the above equation does take into account the losses of the antenna element itself. However, it does not take into account the losses when the antenna element is connected to a transmission line.

### 4.5.2 Realized Gain

This type of gain is also called an absolute gain  $G_{abs}$  that takes into consideration the reflection or mismatch losses that occurs due to the connection of the antenna element to a transmission line or coaxial cable probe. It can be written as:

$$\begin{aligned} G_{abs}(\theta, \Phi) &= e_r G(\theta, \Phi) = (1 - |\Gamma|^2) G(\theta, \Phi) \\ &= e_r e_{ccd} D(\theta, \Phi) = e_o D(\theta, \Phi) \end{aligned} \quad (4 - 16)$$

From the above equation, it can be observed that if the antenna is perfectly matched with the feeding source, meaning that input impedance  $Z_{in}$  is equal to the characteristic impedance of the transmission line  $Z_o$ ,  $|\Gamma|^2 = 0$  and  $e_o = 100\%$ . Therefore realized gain is equal to the matched gain.

### 4.6 Electrically Large High-gain Array Antennas

For communications performed over relatively long distances, it strongly recommended having a transmitter and receiver possess high gain for the sake of the fact that the received power has to be more than the minimum required level for the receiving system. This is an explicit ramification of FRIIS transmission formula; that is:

$$P_r = \frac{P_t G_t G_r \lambda^2}{(4\pi R)^2} \quad (4 - 17)$$

where the parameters  $P_r, P_t, G_t,$  and  $G_r$  are the received power, the transmitted power, the transmitter gain, and the receiver gain, respectively.



According to antenna theory, as the operating frequency increases, the aperture size of the antenna decreases. Therefore, the free space path loss factor increases due to the antenna size reduction for the same gain. The free space path loss factor can be expressed as:

$$FSPL = \left( \frac{4\pi R}{\lambda} \right)^2 \quad (4 - 18)$$

As a consequence, the receiver captures a small fraction of the incident power. Therefore, the link budget of the system is reduced. This dilemma becomes more significant at mm-wave frequency band. To improve the gain of a transmitter or receiver, the aperture size of the array antenna utilized has to be increased and while preserving the electrical size of the array elements, simultaneously. This condition adds to the feeding network design complexity.

To put it more simply, according to Friis equation, the captured or transmitted power is reduced as the size of the antenna shrinks when increasing the operational frequency. However, to avoid this obstacle, it is strongly preferred to have a relatively high gain to maintain the received or transmitted power intensity within the acceptable range.

## Chapter 5

### STANDING WAVE DIELECTRIC ARRAY ANTENNAS

Dielectric resonator antennas are typically low gain antennas. The gain is approximately limited to 5 dBi. This deficient fact unfavorably affects the advantages that dielectric resonator antennas offer in terms of fabrication easiness and cost-efficient. In fact, one simple and straightforward way to overcome this drawback is to assemble dielectric resonator antennas in a certain manner to form an array that is capable of achieving relatively high gain. However, the main obstacle evokes when designing the array to operate at high frequency. Spurious radiations from the feeding network are considerable and negatively influence the overall array performance. Moreover, in corporate feed arrays, it is mandatory to have several quarter-wavelength transmission lines and power dividers which, in turns, lead to high configuration complexity. These power dividers are extremely sensitive to the phase change. Different configurations of dielectric resonator array antennas will be reviewed and studied in section 5.2.

#### 5.1 Motivations

In the last few decades, dielectric resonator antennas have been attracting more attention in the literature especially for high-frequency applications due to the advantageous features they have. According to antenna theories, as the operating frequency increases, the size of the antenna decreases. Therefore, according to Friis equation, the captured or transmitted power is reduced as the size of the antenna shrinks.

However, to avoid this specific obstacle, it is strongly preferred to have a relatively high gain to maintain the received/transmitted power amount within an acceptable range when increasing the operational frequency. As previously mentioned, one of the well-known methods to improve the gain is by arraying additional individual elements. One substantial disadvantage escalates when increasing the operational frequency. Spurious radiations from the feeding network are considerable and unfavorably influence the array performance. Additionally, it is compulsory to have a number of quarter-wavelength transmission lines and power dividers which, in turns, leads to high configuration complexity. Therefore, it is really appreciated and beneficial to feed an array structure with a single feeding port without the need to have complex and phase sensitive feeding network. In this case, the undesired spurious radiation coming from the feeding network is minimized and, hence, the array efficiency and performance can be improved when operating at higher frequency bands.

Furthermore, dielectric resonator antennas have been observed as an excellent candidate to be utilized in 5G communication systems. Since it is anticipated that the unlicensed 60 GHz band will be released, existing antenna, such as a microstrip patch antenna, will suffer from a limitation in radiation efficiency at this frequency band. Hence, DRAs can be used providing excellent radiation efficiency since the conduction losses are minimized due to the lack of metallic surfaces. In fact, the size of the DRA is *o*proportional to  $\lambda_0/\epsilon_r$ . Therefore, the size can be reduced by choosing dena se material with high relative permittivity.

Lastly, these novel and creative dielectric resonator antenna array designs have been proposed for the first time in the area of dielectric resonator array antennas. It has been proven that the two prototypes produce excellent and comparable gain and impedance bandwidth comparing to those existing configurations in the literature.

## 5.2 Previous Work

To the best of the author's knowledge, no one has ever utilized the concept of standing wave to excite dielectric resonator array antennas before. As a consequence, all the previously proposed work that is discussed and examined in this section will be based on either corporate or series traveling wave feeding networks.

In [56], a cylindrical dielectric resonator antenna array was proposed, shown in Figure 5.1. The maximum achievable gain is 5.7 dBi and 8.3 dBi for two and four elements linear array, respectively. In this configuration, every single element in the array is fed independently by a coaxial cable which, in turn, increases the fabrication costs and complexity. The usable impedance bandwidth is measured to be 5.2% of 6.8 GHz for two-element array and 3.7% of 3.825 GHz for four-element array.

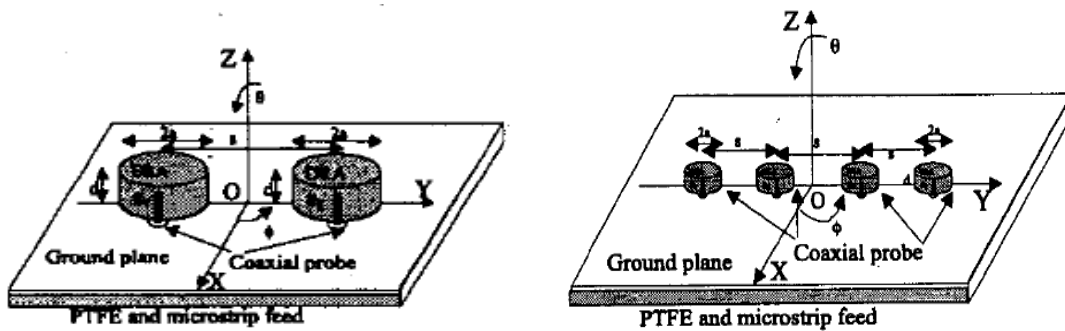


Figure 5.1: Cylindrical dielectric resonator array antenna [56]

In [57], a 10 element rectangular dielectric resonator array antenna was proposed. The presented configuration produces a gain of 13.2 dBi at the boresight. Although this design uses a single transmission line for the feeding, the number of coupling apertures utilized makes this configuration increases the design complexity. Furthermore, the length of the transmission line that passes by all the array elements will result in spurious radiations when operating at higher frequency bands.

In [58], two elements rectangular dielectric resonator array antenna was proposed, shown in Figure 5.2. The maximum achieved gain is 6.18 dBi comparing with 4.7 dBi for the single element at 5.8 GHz operating frequency. The feeding network is based on aperture coupling transmission line feeding. Although it is simple, utilizing it with a higher number of elements is impractical. In the case of higher elements number, the need to have quarter-wavelength transmission lines and power dividers becomes mandatory. This, in turn, will increase undesired radiations.

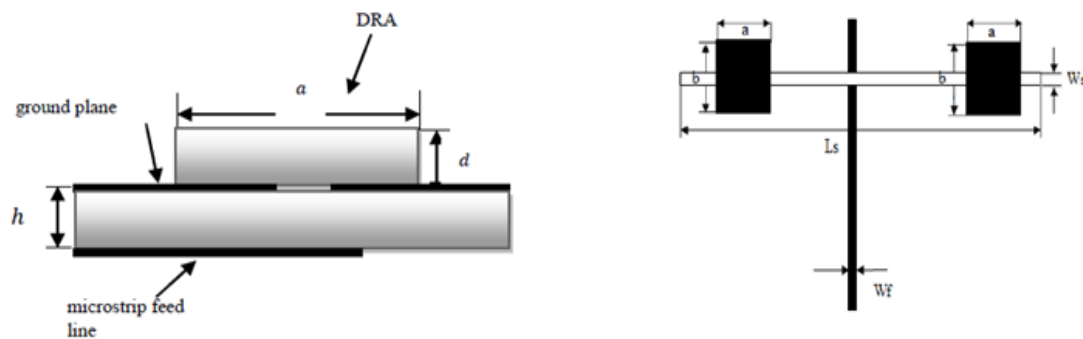


Figure 5.2: Rectangular dielectric resonator array antenna [58]

Another rectangular dielectric resonator linear array is proposed in [59], depicted in Figure 5.3. The gain of a single element is obtained to be 4.14 dBi with a useful impedance bandwidth of 6.35 of 5.8 GHz. The array configuration produces a gain of

8.28 dBi and 9.53 dBi with a bandwidth of 8.48% and 9.53% for two and four-element array, respectively. Although this configuration produces relatively wide impedance bandwidth, the design suffers from complexity where the feeding network consists of a number of quarter-wave impedance transformers.

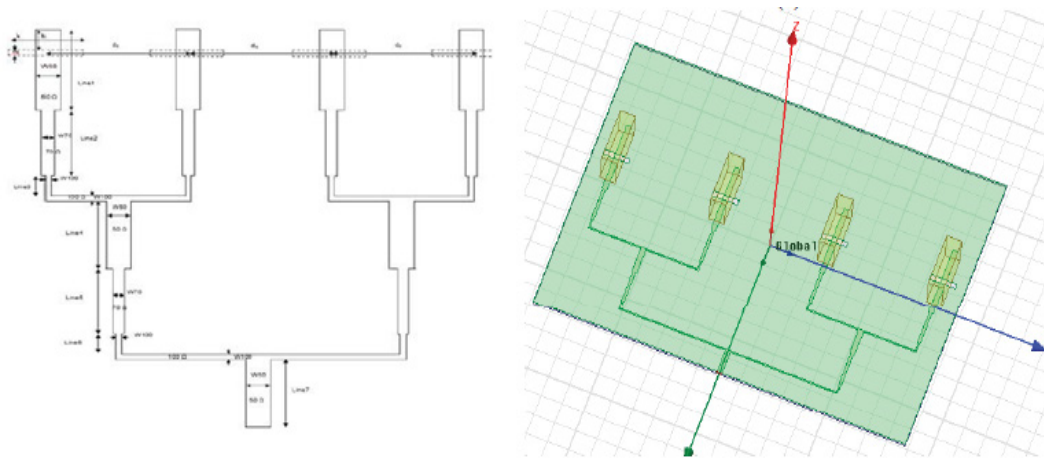


Figure 5.3: Four-element rectangular dielectric resonator array antenna [59]

In [61], a 3x3 planar array with hard horn excitation was proposed, shown in Figure 5.4. A pyramidal horn that produces a uniform field distribution was utilized to feed the array elements which were placed at the horn aperture. The horn itself was fed by a coaxial probe. Although this proposed design is capable of operating over a wide useful bandwidth of 15%, it suffers from some disadvantages. For example, to assure that the horn produces uniform field distribution, hard walls along the horn were used. Another drawback is that as the elements are placed in close proximity, the mutual coupling between them is considerable and, hence, two metal plates were introduced to minimize the mutual coupling. Lastly, it can be said that the design is impractical as its size is voluminous.

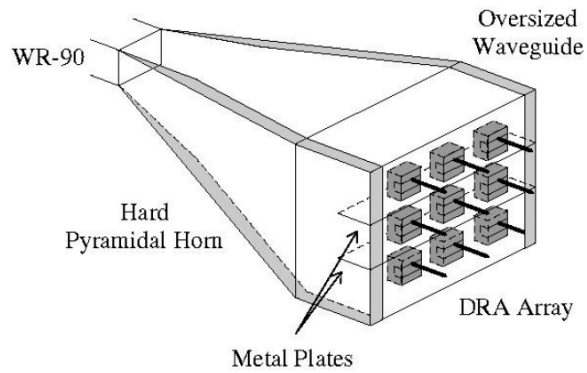


Figure 5.4: Geometry of coaxial probe-fed embedded DRA array inside a pyramidal hard horn [61]

Another planar dielectric resonator antenna array was proposed in [62] and depicted in Figure 5.5. In this design, numbers of perforated bonding dielectric rods are utilized to facilitate the fabrication process. These rods were designed to be thin enough to avert guiding waves around the operating frequency of the array itself. The feeding network is based on corporate feeding method which produces undesired spurious radiation at higher frequency bands. The maximum achieved gain was not stated, however, the matched bandwidth was about 21.8%.

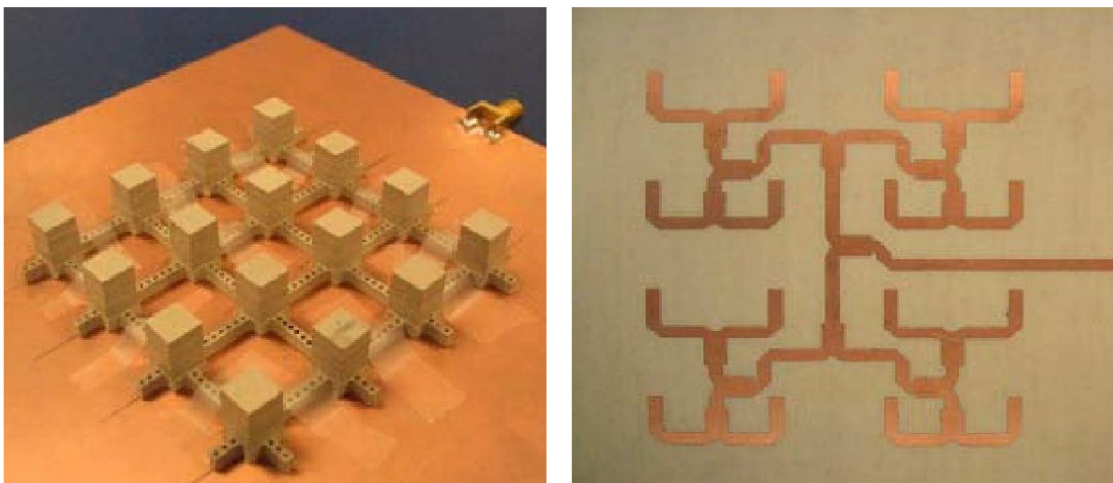


Figure 5.5: Prototype of 16-element DRA array with perforated connecting rods [62]

The tables below summarize the above-mentioned configurations of dielectric resonator array antennas as well as other examples.

Table 5.1 Summary of linear DRA array examples

Ref	DRA Shape	No. of DRAs	$f_o$ (GHz)	DRA Feed	Array Feed	Gain (dBi)	Bandwidth (%)
[56]	Cylindrical	1	6.7	Probe	-----	3.4	12.1
		2	6.86		Probe	5.7	5.2
		3	3.8			8	3.7
[57]	Rectangular	10	8	EM Coupling	Microstrip	13.2	8
[58]	Rectangular	1	5.8	Aperture	-----	4.7	-----
		2			Aperture	6.18	2.25
[59]	Rectangular	1	5.8	Aperture	-----	4.14	6.35
		2			Microstrip	8.28	8.48
		4				10.41	9.53

Table 5.2 Summary of planar DRA array examples

Ref	DRA Shape	No. of DRAs	$f_o$ (GHz)	DRA Feed	Array Feed	Gain (dBi)	Bandwidth (%)
[60]	Rectangular	4	7	Aperture	Microstrip	11.3	18
[61]	Rectangular	9	X-band	Probe	Waveguide Horn	----- --	15
[62]	Rectangular	16	10	Aperture	Microstrip	----- --	21.8
[63]	Square	16	X-band	Cross-Aperture	Microstrip	18	-----
[64]	Square	64	20	H-Slot	Microstrip	21.8	-----



## 5.3 Design, Analysis, Fabrication, and Measurement of Planar Standing-wave Dielectric Array Antennas

### 5.3.1 Single Element Design

The design procedure starts by designing a single rectangular dielectric resonator antenna that its higher-order mode  $TE_{115}$  is realized at the desired operating frequency which is 5.3 GHz. COMSOL Multiphysics Modeling Software is used at most of the simulation stages. The structure of the antenna is depicted in Figure 5.6 below.

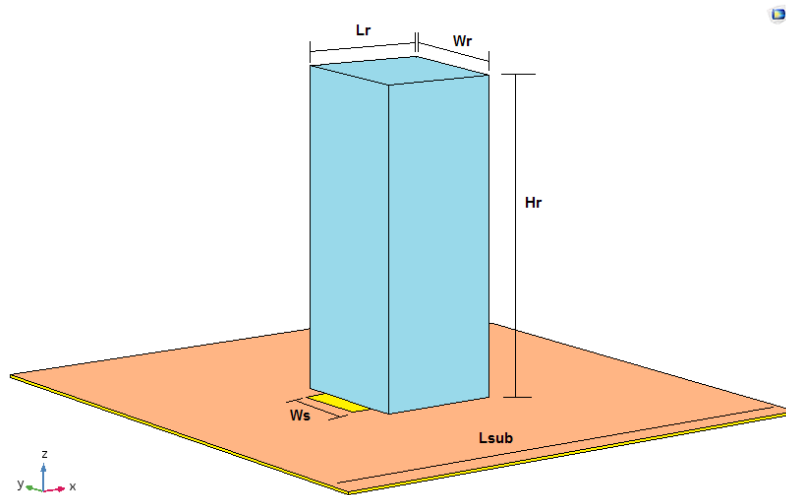


Figure 5.6: Proposed single rectangular dielectric resonator antenna

The dimensions of the radiating slab are 25mm x 25mm x 65 mm ( $L_r \times W_r \times H_r$ ), and it is made of PLA (Poly Lactic Acid). This type of material is widely utilized in 3D printers. The dielectric constant is  $\epsilon_r = 2.5$  and the dissipation factor is 0.005. The dielectric element is located at the center of a substrate with the dimensions of 110 mm<sup>2</sup> ( $L_{sub}^2$ ). The substrate is made of Arlon 25N with low dielectric constant  $\epsilon_{r\_sub} = 3.38$  and dissipation factor = 0.0015 with a thickness of 20 mils (0.508mm). The utilized feeding mechanism is aperture-coupled microstrip-line feed. The transmission line and the matching stub are attached to the bottom surface of the substrate with dimensions of 1.13

mm x 40.8 mm and 1.13 mm x 2.59 mm along the y-axis, respectively. The coupling slot is engraved at the top surface of the substrate with dimensions of 34.95mm x 14.83 mm ( $L_s \times W_s$ ). As shown in Figure 5.7 and 5.8, excellent impedance matching of -31 dB is achieved at  $f = 5.3$  GHz. A wide useful bandwidth is observed due to the fact that the dielectric slab is made out of material with low relative permittivity ( $\epsilon_r$ ).

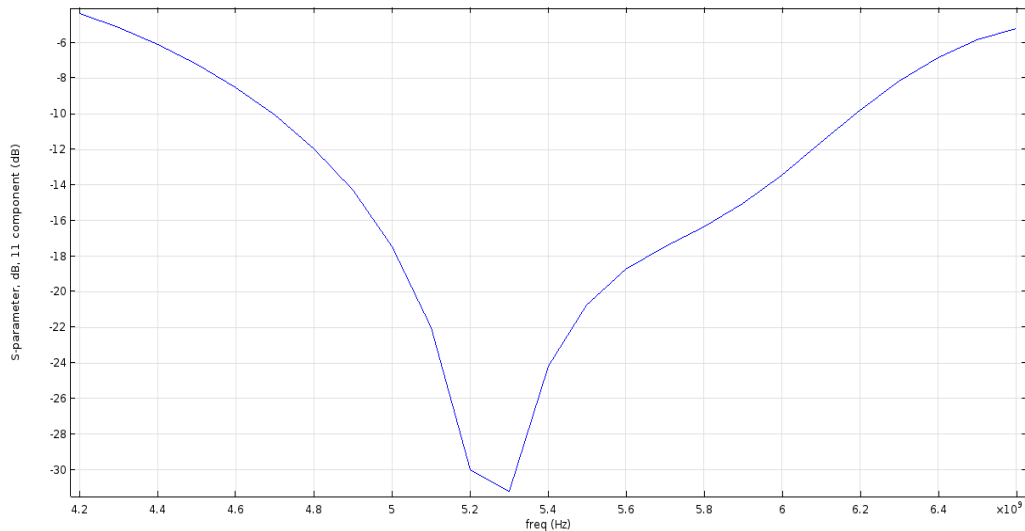


Figure 5.7: Return loss S11 vs frequency of the single rectangular dielectric antenna

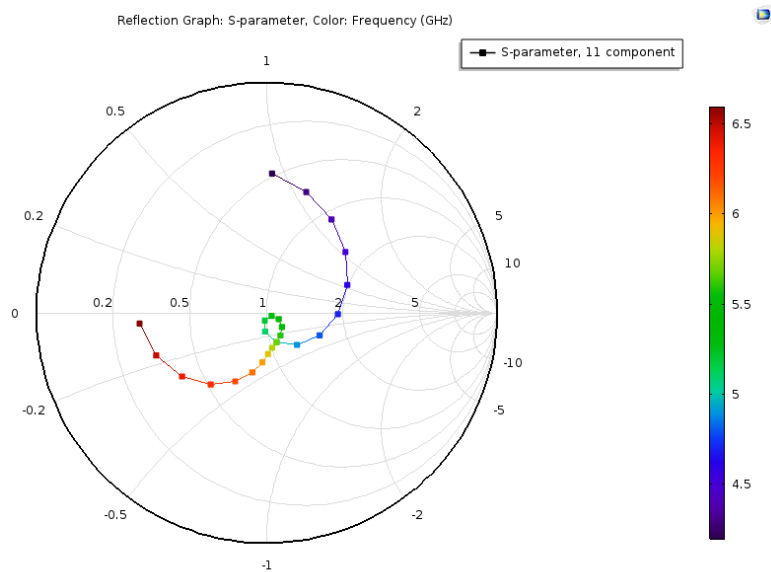


Figure 5.8: Input impedance on Smith chart of the single rectangular dielectric antenna

The antenna produces a focused radiation pattern at the boresight with a peaked gain of 8.2 dBi at 5.3 GHz, as shown in Figure 5.9 and 5.10.

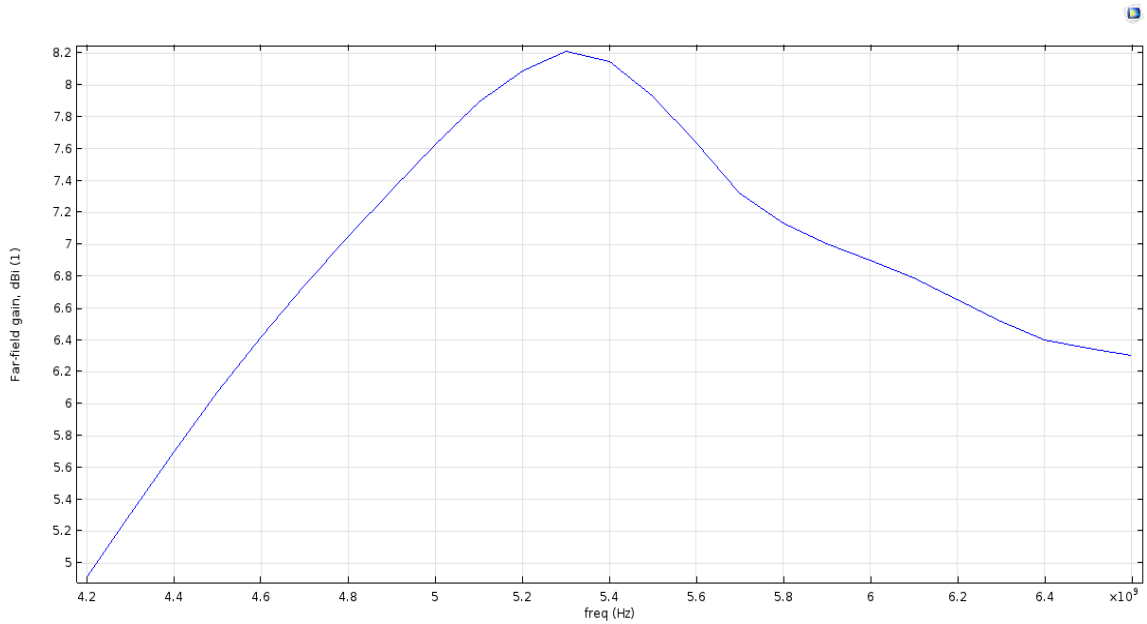


Figure 5.9: Realized gain vs Frequency at TE<sub>115</sub> mode

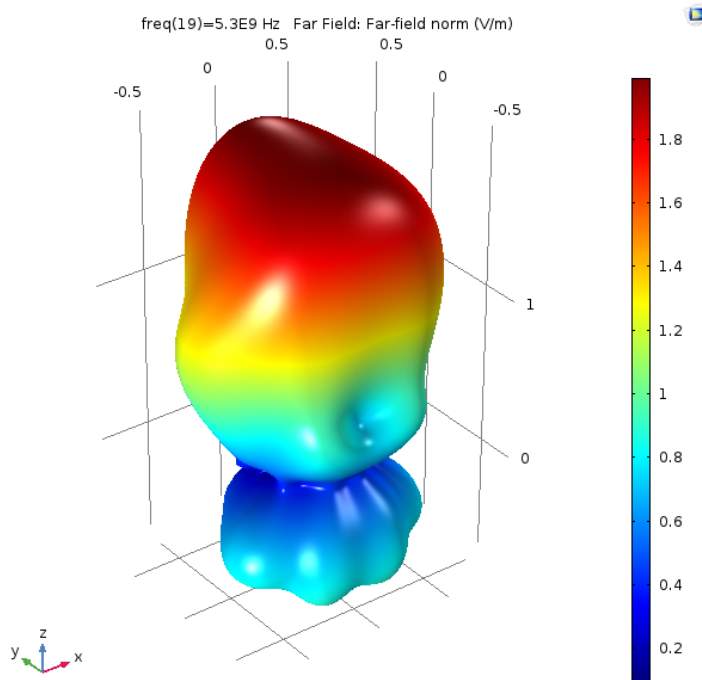


Figure 5.10: 3D radiation pattern of the single rectangular dielectric antenna at  $f = 5.3$  GHz

The 2D plots of the far electric field in both x-z and y-z planes are shown in Figure 5.11.

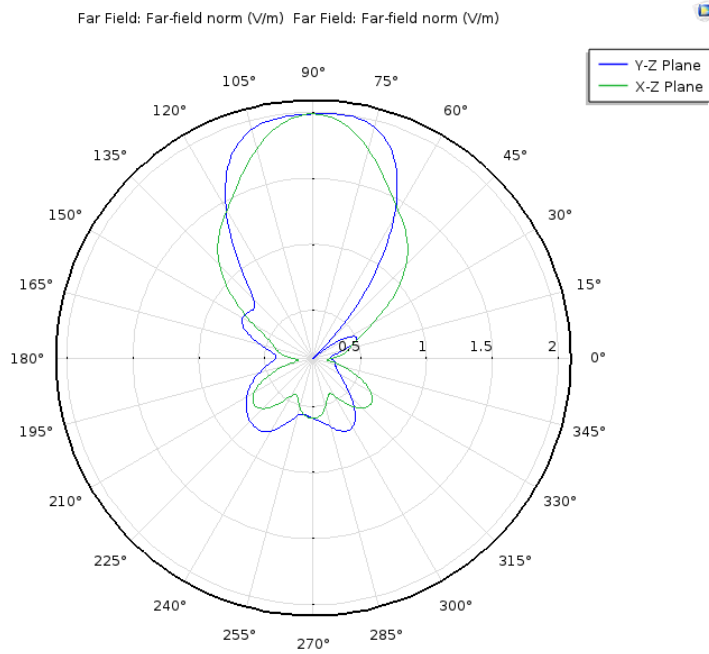


Figure 5.11: 2D far electric fields in both x-z and y-z planes at  $f=5.3$  GHz

The electric field distribution inside the slab is shown in Figure 5.12. It is observed that the mode  $TE_{115}$  is excited which is intentionally achieved to start the array design.

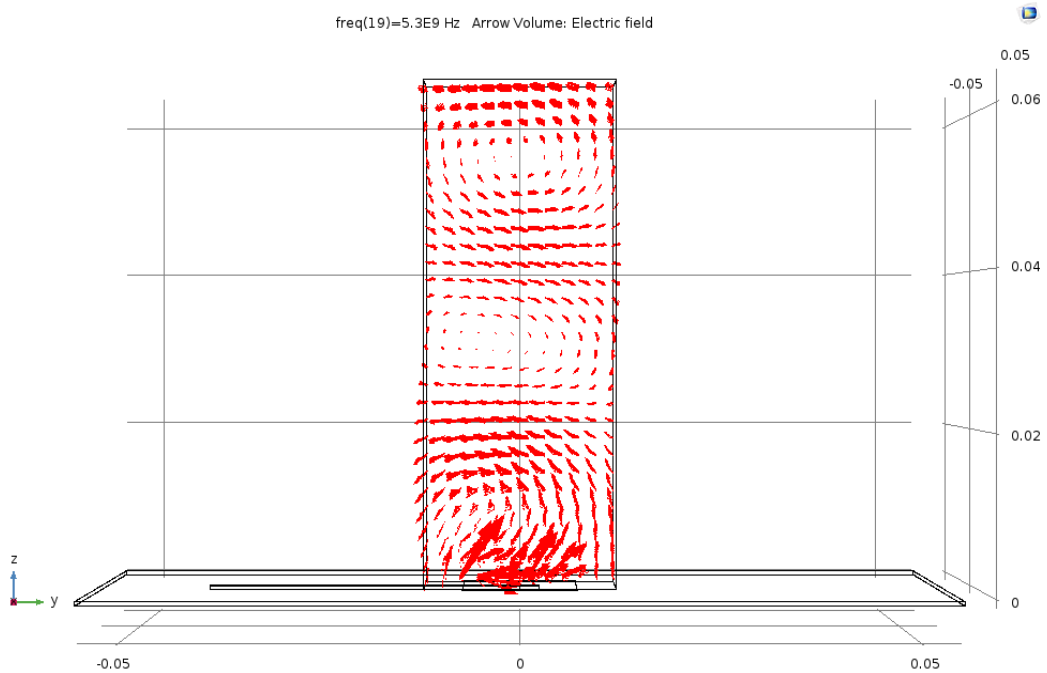


Figure 5.12: Field distribution inside the slab at the resonance frequency

### 5.3.2 Three Elements Linear Array Design (Parallel to the Feeding Line)

Before starting the planar array design, it is better to first verify the validity of standing wave array concept in linear geometry. As the feeding mechanism is based on standing wave, it is required to create a medium connecting the array elements so that the standing waves become distributed among all the array elements. Figure 5.13 depicts the array geometry.

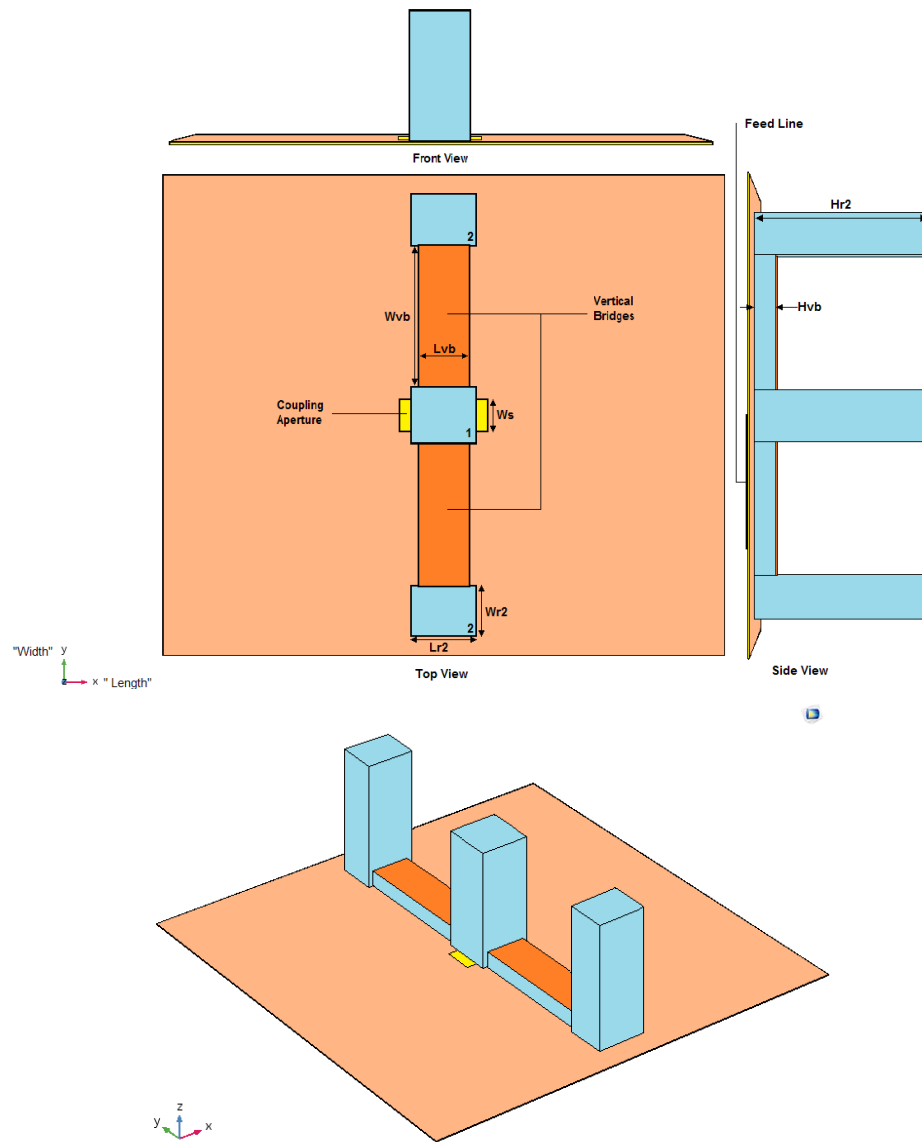


Figure 5.13: Top, front, side, and 3D views of the proposed linear array antennas

In this novel design, the center dielectric slab accepts the power from the transmission line located under the substrate. Then, it feeds this power to the neighboring elements through the vertical dielectric bridges. Therefore, at the resonance frequency, the entire structure resonates at once due to the multiple bouncing between the structure boundaries. The radiating slabs are initially designed identically to the single element antenna. However, due to the variation in the boundary conditions between the center element (labeled as 1) and other neighboring elements (labeled as 2), the latter were further optimized. It was chosen to fix their length and height and vary the width. Then, the width is optimized to be 20.75 mm. That is to say, the dimensions of the center element are 25mm x 25mm x 65 mm ( $L_r \times W_r \times H_r$ ); referring to Figure 5.4. And the dimensions of the top and bottom elements are 25 mm x 20.75 mm x 65 mm ( $L_{r2} \times W_{r2} \times H_{r2}$ ) as depicted in Figure 5.13.

The dielectric bridges are designed as follows: the free space wavelength of an electromagnetic wave at 5.3 GHz is 56.6 mm. However, the presence of the dielectric material slows down the wave by a factor of approximately  $1/\sqrt{\epsilon_r}$ . Therefore, the waveguide wavelength in the dielectric bridges is less than the free space wavelength. This value of the waveguide wavelength is determined to be 35.8 mm. However, if a wave is confined inside a waveguide, its wavelength can be longer. Since the electric fields inside the center slab at the surfaces facing the bridges have an absolute maximum value, the total spacing from one edge of the middle radiating slab to the first edge of its neighboring element can be either 0.5 or 1.5 times the waveguide wavelength. In order to reduce the mutual coupling between the radiating slabs and hence improve the array performance, the spacing is set to be 1.5 times the waveguide wavelength. The final

optimum dimensions of the vertical bridges are found by simulation to be 20 mm x 65 mm x 8 mm ( $L_{vb} \times W_{vb} \times H_{vb}$ ). It can be said that the spacing between any two elements along the  $y$ -axis is 1.5 times the waveguide wavelength. For the sake of having a uniform wave distribution among the array structure and minimizing the undesired radiations coming out of the bridges, the top surface of each is covered by a very thin metallic patch. Once the dimensions of the radiating elements and the bridges are optimized to produce a maximum gain at the boresight, the feeding network now needs to be tuned due to the fact the mutual coupling between the slabs has slightly deviated the resonant frequency. The new resonant frequency is found to be 5.6 GHz and the new length of the matching stub is 2.54 mm. The optimum new length of the aperture slot  $L_s$  is found to be 34.89 mm which produces the best impedance matching. It is to mention that the structure has only one coupling slot resides under the center radiating element. Figure 5.14 and 5.15 show the reflection coefficient  $S_{11}$  as a function of the frequency on both linear scale and smith chart, respectively.

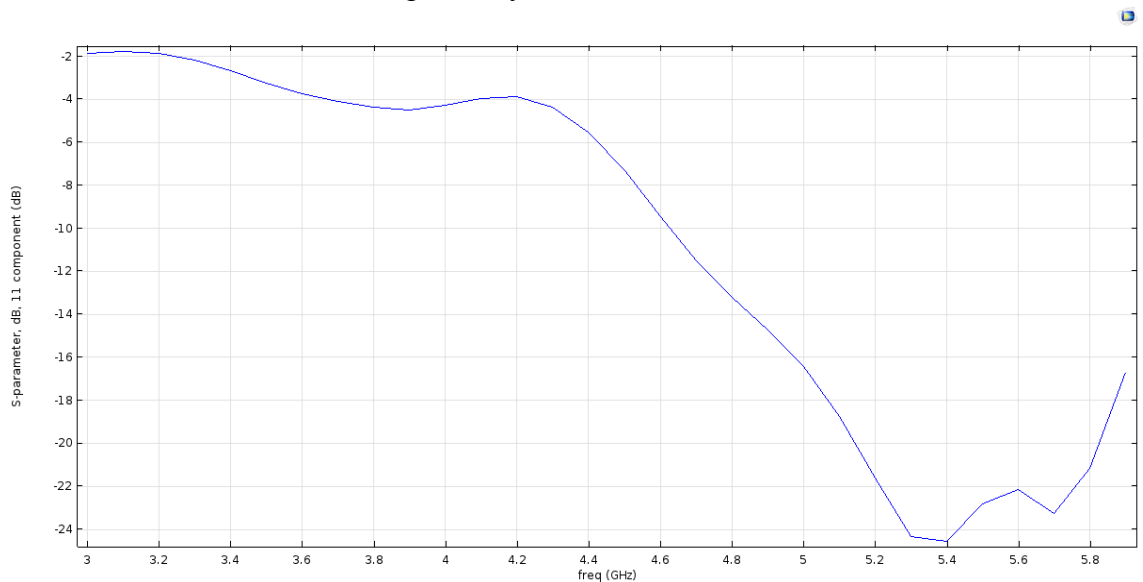


Figure 5.14: Return loss  $S_{11}$  vs frequency of three-element linear array antennas

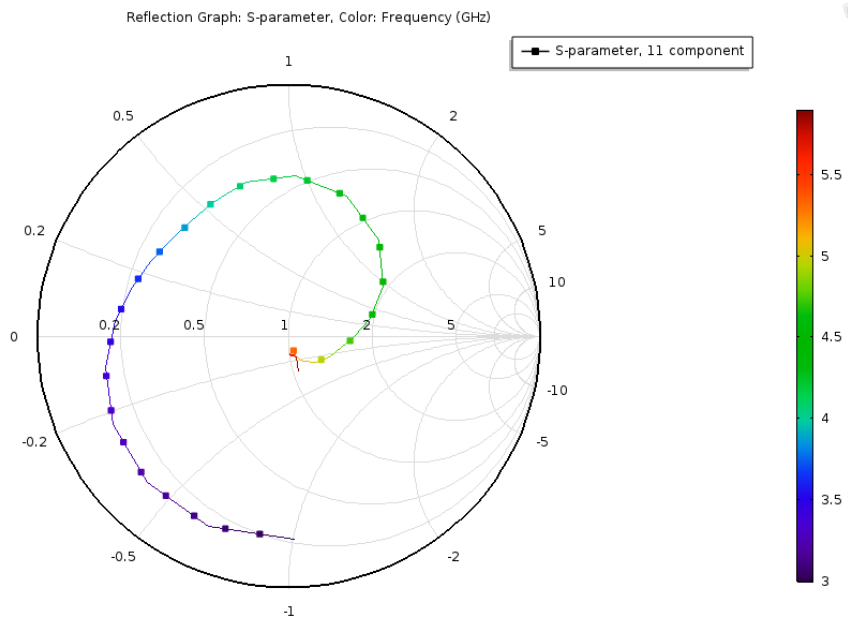


Figure 5.15: Input impedance on Smith chart of three-element linear array antennas

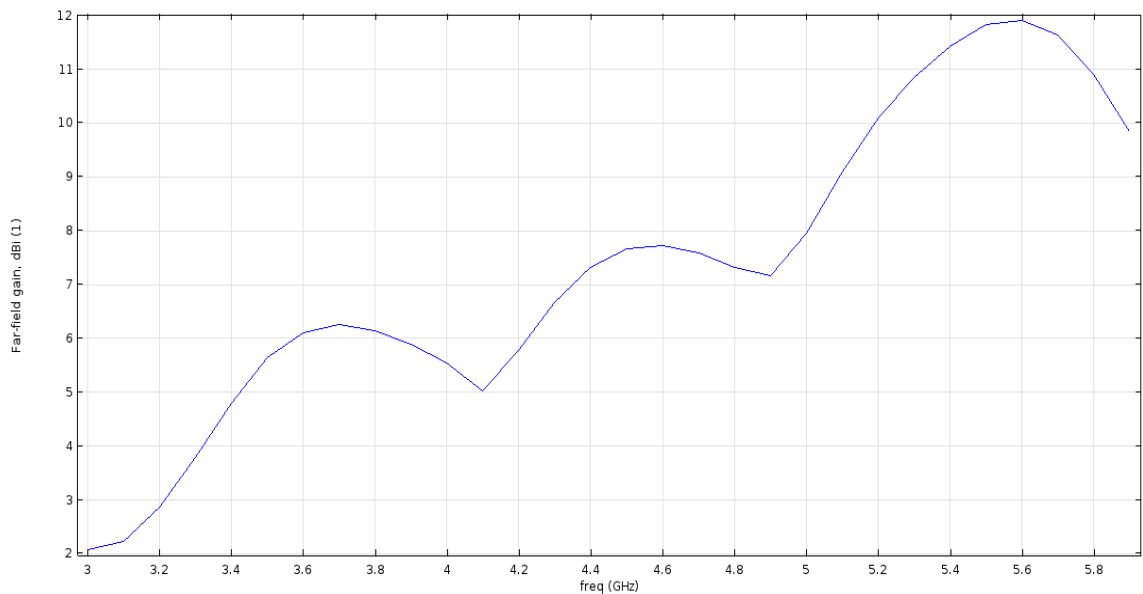


Figure 5.16: Realized gain vs Frequency of parallel three-element linear array

In Figure 5.16, the maximum observed realized gain is 11.9 dBi at the resonant frequency which corresponds to an increase of about 4 dBi comparing to the single element resonating at the higher-order mode  $TE_{115}$ . This increment in the gain was



anticipated as in the array theories each extra element in the array will roughly add 2 dBi to the gain of the single element. Since the gain increment is in excellent agreement with the array theory, it can be said that the concept of exciting the entire array structure by standing waves is valid. Another evidence of the proposed feeding mechanism validity can be observed by examining the far field radiation pattern, depicted in Figure 5.17 and 5.18. It can be clearly seen that the radiation pattern has a very narrow beam in the direction of the array; i.e. y-z plane drawn in Blue. In the opposite direction of the array, the radiation pattern has a wide beam which is reasonable and expected (drawn in Green as x-z plane).

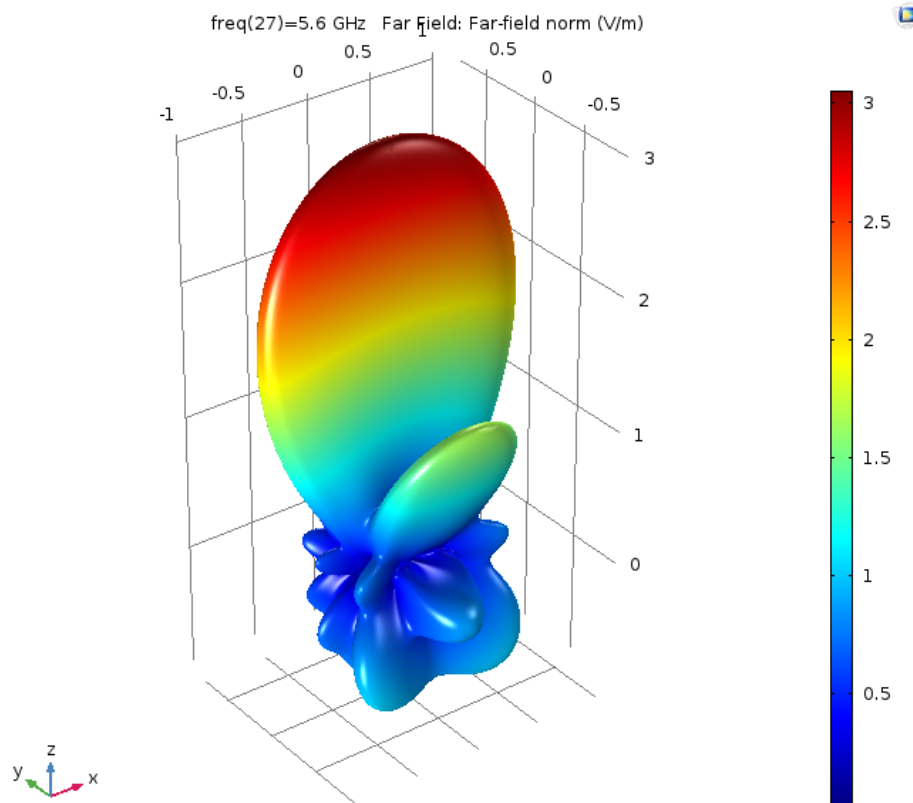


Figure 5.17: 3D radiation pattern of parallel three-element array antennas at  $f = 5.6$  GHz

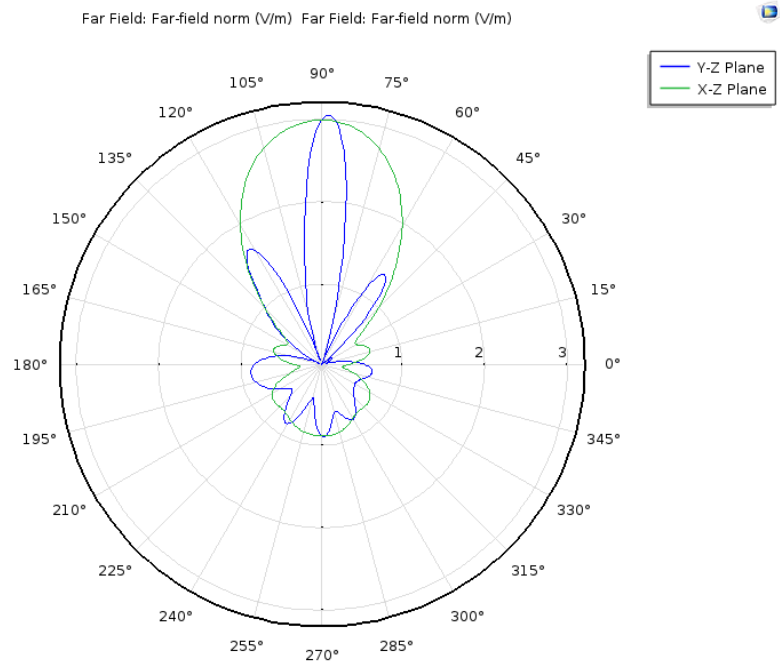


Figure 5.18: 2D far fields in both x-z and y-z planes at  $f=5.6$  GHz

Figure 5.19 demonstrates the field distribution inside the array structure. It can be noticed that the fields are almost uniformly distributed inside the radiating elements and the dielectric bridges in-between.

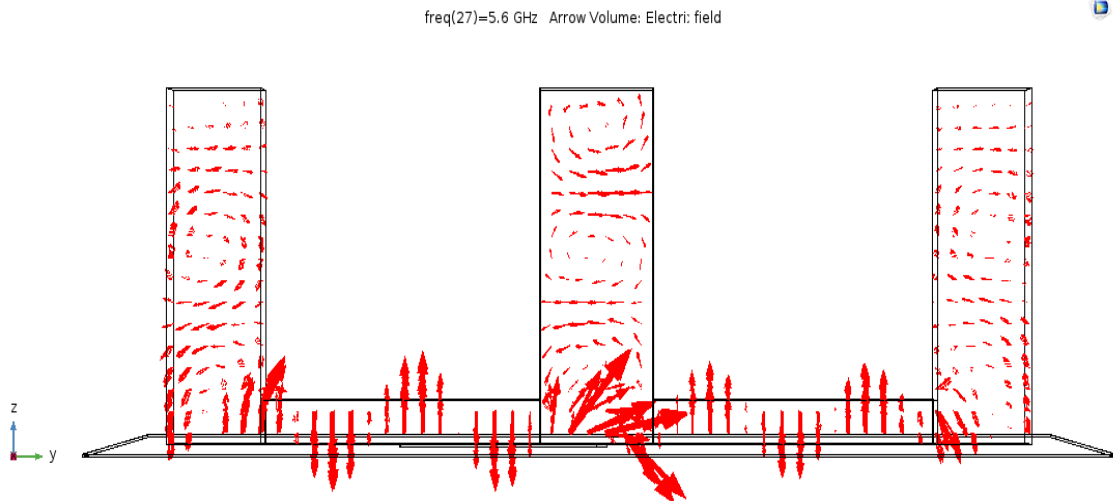


Figure 5.19: Field distribution inside the array structure at the resonance frequency

### 5.3.3 Three Elements Linear Array Design (Orthogonal to the Feeding Line)

In this section, an attempt has been made to apply the same design concept and steps. The array direction, in this case, is along the x-axis which is perpendicular to the feeding line. Figure 5.20 depicts the array geometry.

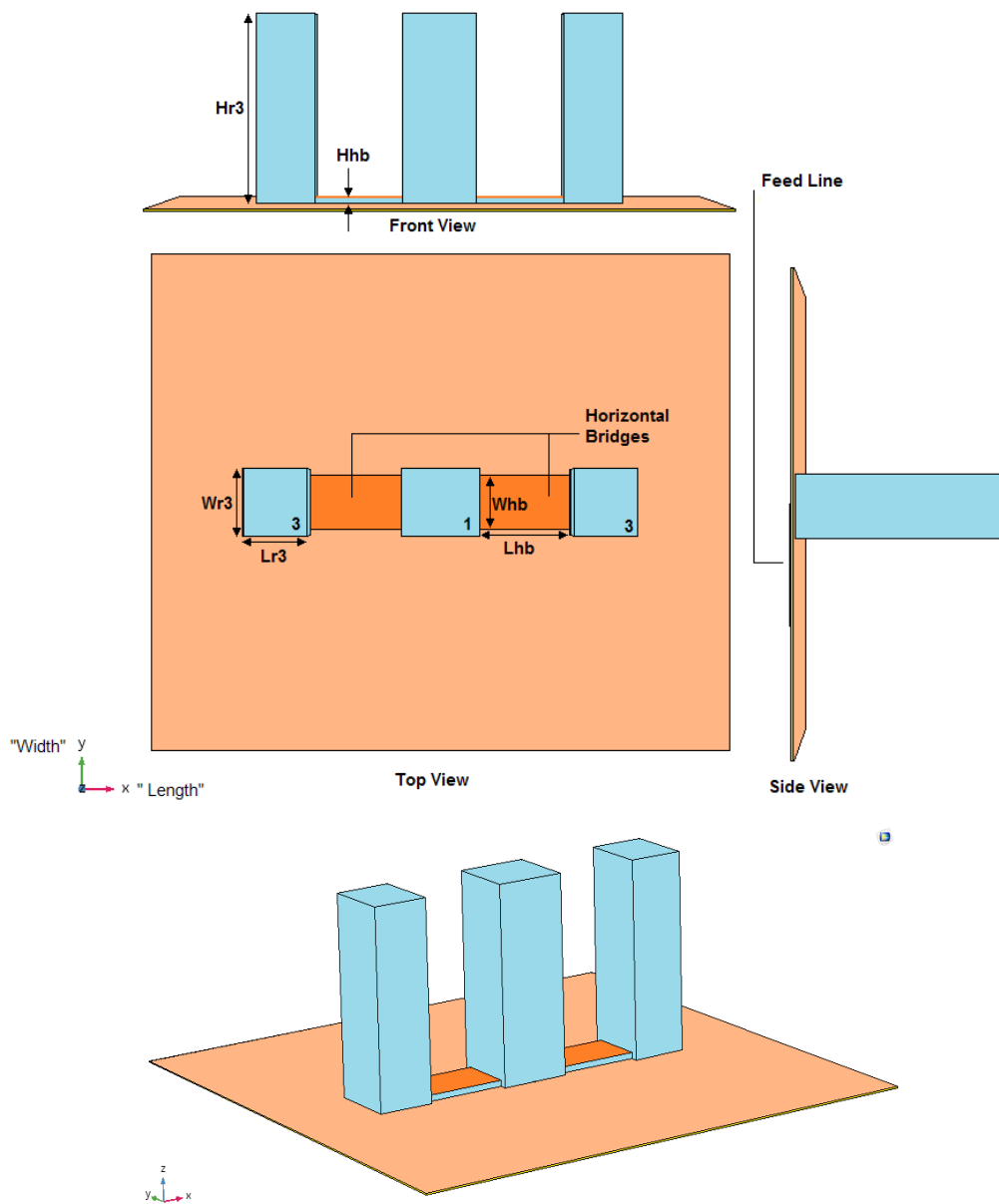


Figure 5.20: Top, front, side, and 3D views of the proposed linear array antennas

Again, due to the variation in the boundary conditions between the center element (labeled as 1) and other neighboring elements (labeled as 3), the latter were further modified. For the matter of symmetry, it was decided to fix their width and height and vary the length. The length is optimized to be 20 mm. That is to say, the dimensions of the center element are the same as before; and the dimensions of the right and left elements are 20 mm x 25 mm x 65 mm ( $L_{r3} \times W_{r3} \times H_{r3}$ ), as depicted in Figure 5.20.

Since the fields inside the center slab at its right and left sides are different than these at the front and back sides, the dimensions of the dielectric bridges are different. In this case, the total spacing from one edge of the middle radiating slab to the first edge of its neighboring element is set to be one waveguide wavelength since the fields have a sinusoidal variation at the surfaces facing the bridges. The final optimum dimensions of the horizontal bridges are found by simulation to be 30 mm x 20 mm x 2 mm ( $L_{hb} \times W_{hb} \times H_{hb}$ ). It can be said that the spacing between any two elements along the x-axis is one waveguide wavelength. Furthermore, the top surface of both horizontal bridges is covered by very thin metallic sheets to reduce the undesired radiations coming out of them as well as improving the field distribution inside the array structure.

Figure 5.21 and 5.22 show the reflection coefficient S11 as a function of the frequency on both linear scale and Smith chart, respectively. It is to notice that as the resonant frequency is the same as in the parallel linear array, the feeding network and the coupling aperture sizes are almost the same as before. About -22 dB of S11 is achieved with relatively wide useful impedance bandwidth.

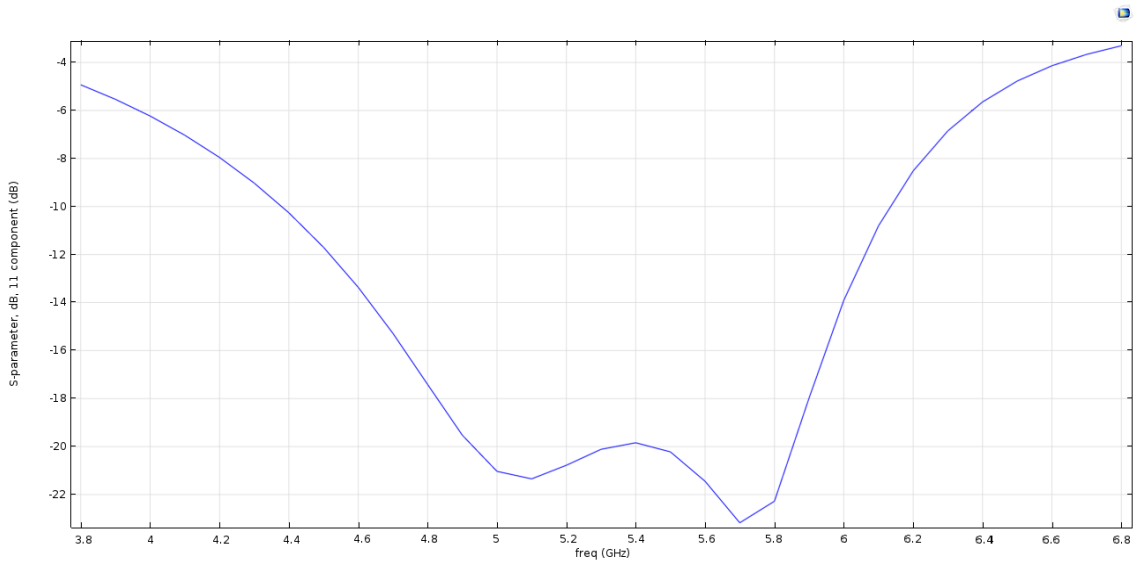


Figure 5.21: Return loss S11 vs frequency of orthogonal three-element linear array antennas

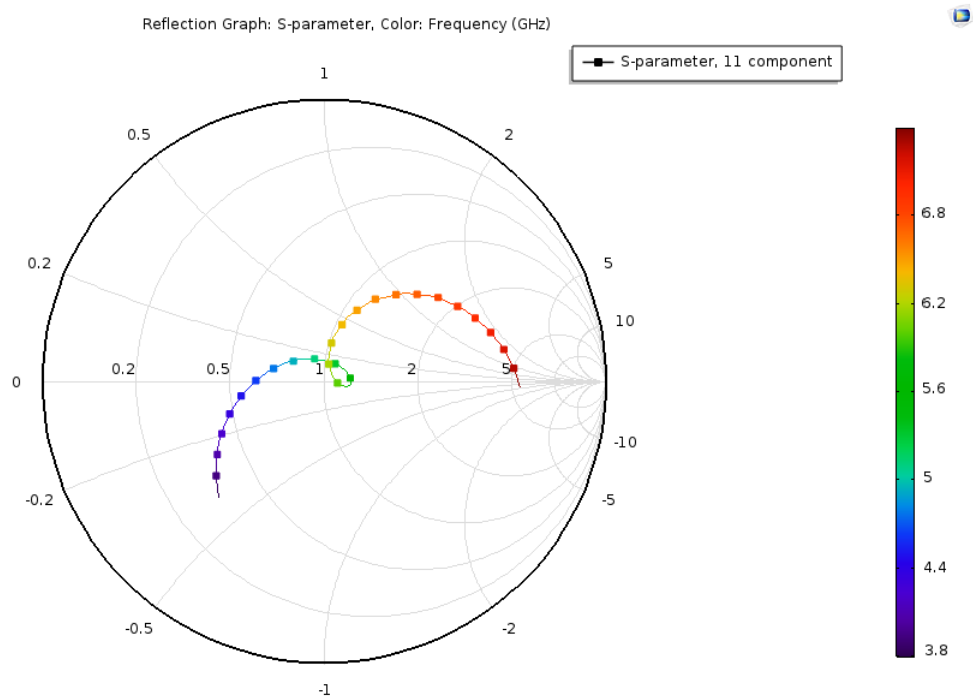


Figure 5.22: Input impedance on Smith chart of three-element linear array antennas

As in Figure 5.23, the maximum observed realized gain is almost 11.75 dBi at the resonant frequency 5.6 GHz which corresponds to an increase of 3.6 dBi comparing to that of single element resonating at the higher-order mode  $TE_{115}$ . Since the gain increment is in excellent agreement with the linear array theory, it can be said that the concept of exciting the entire array structure by generating standing waves inside the structure is valid for this case where the arraying direction is perpendicular to the feeding line.

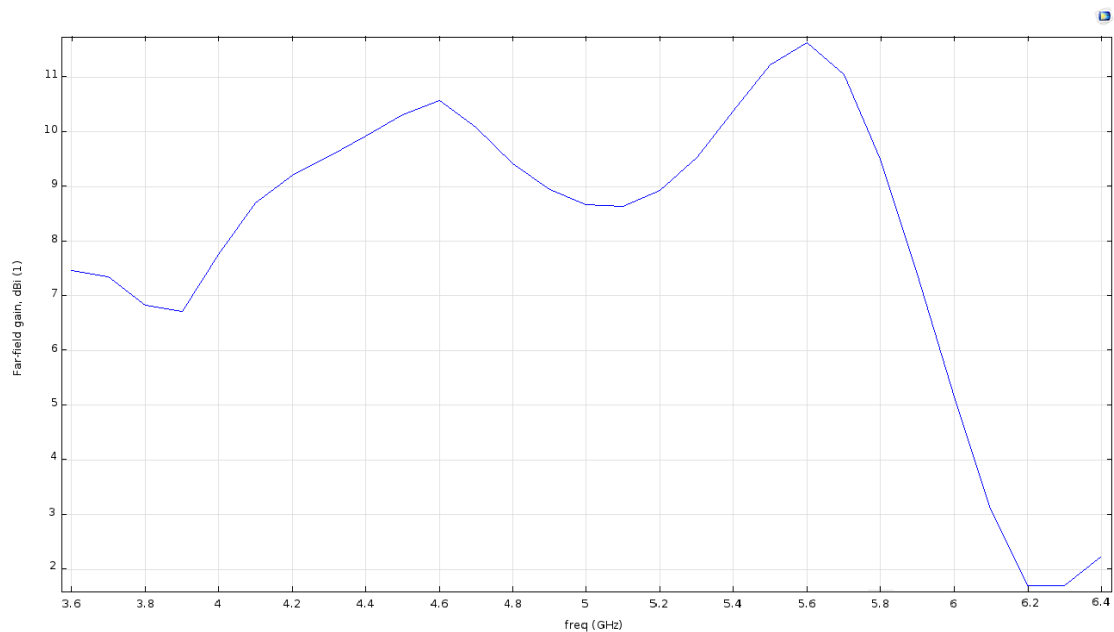


Figure 5.23: Realized gain vs Frequency of orthogonal three-element linear array

Another evidence of the validity of the proposed feeding mechanism can be observed by examining the far field radiation pattern, depicted in Figure 5.24 and 5.25. It can be clearly seen that the radiation pattern has a very narrow beam in the direction of the array; i.e. x-z plane drawn in Green. On the other hand, along the opposite direction of the array, i.e. y-z plane drawn in Blue, the radiation pattern has a wide beam which is expected.

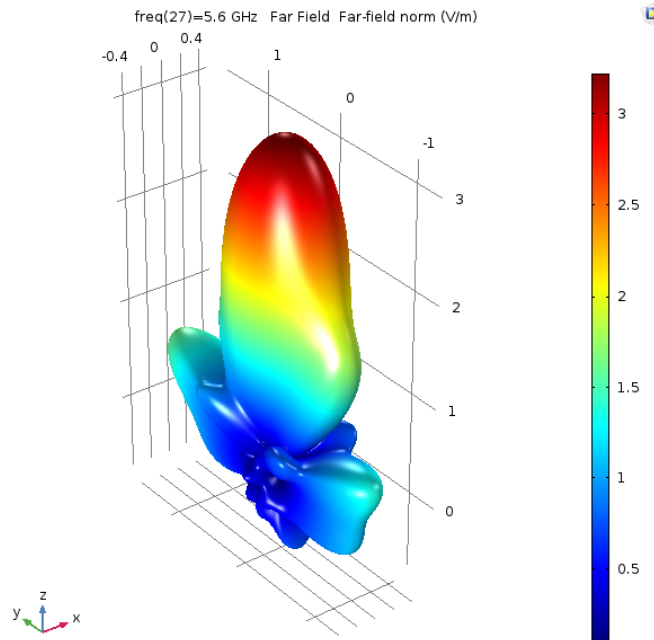


Figure 5.24: The 3D radiation pattern of orthogonal three-element array antennas at  $f = 5.6$  GHz

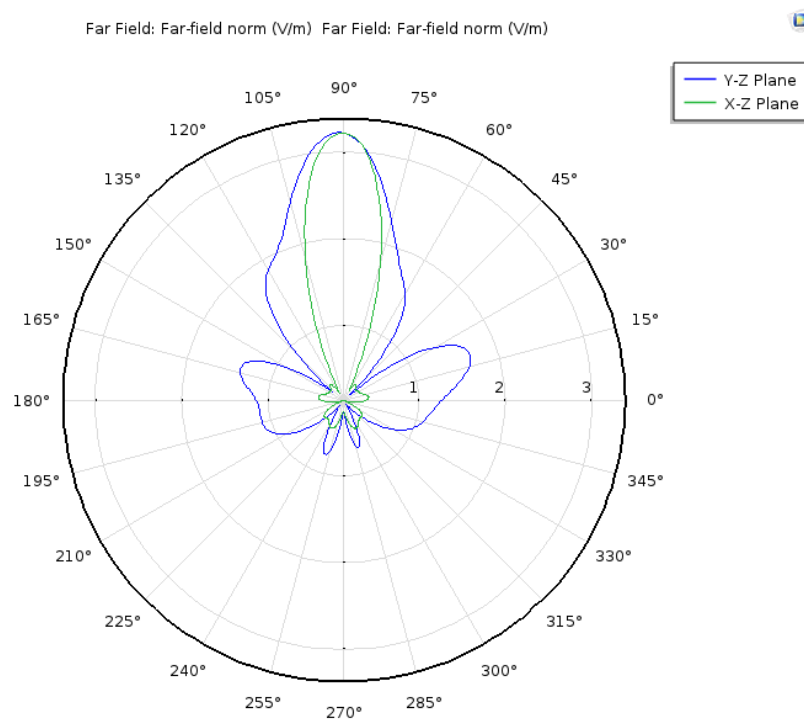


Figure 5.25: The 2D far fields in both x-z and y-z planes at  $f = 5.6$  GHz

### 5.3.4 Final 3x3 Planar Dielectric Array Antennas Design

The ultimate objective of this proposed feeding mechanism is to efficiently excite two-dimensional planar array antennas. Since the proposed solution is successfully approved in linear array structures parallel and orthogonal to the feeding line, all to do now is to combine both structures as one array. In addition, extra radiating elements and dielectric bridges were introduced to form a symmetric 3x3 planar array antennas. The proposed planar array prototype is depicted below in Figure 5.26 and 5.27.

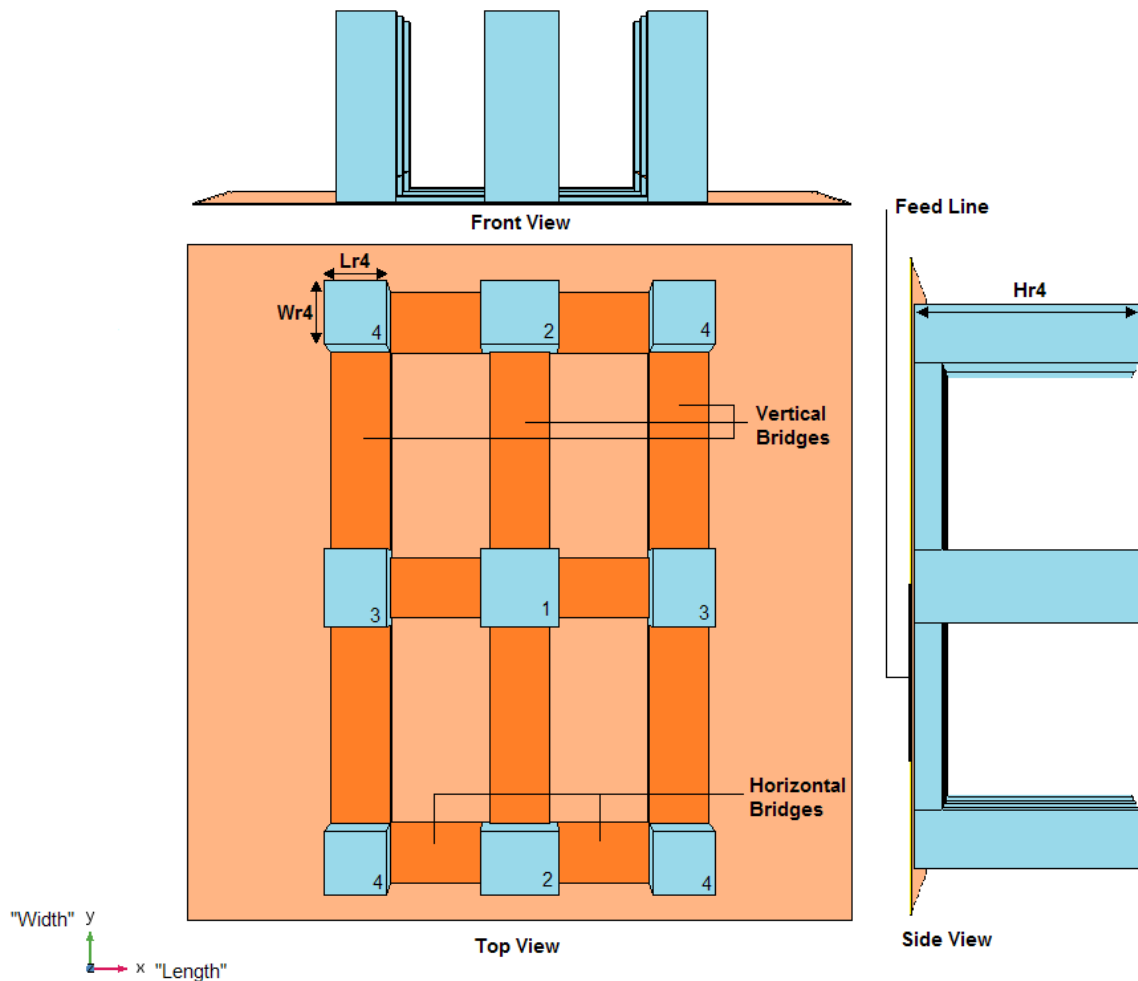


Figure 5.26: Top, front, and side views of the proposed 2D planar array antennas



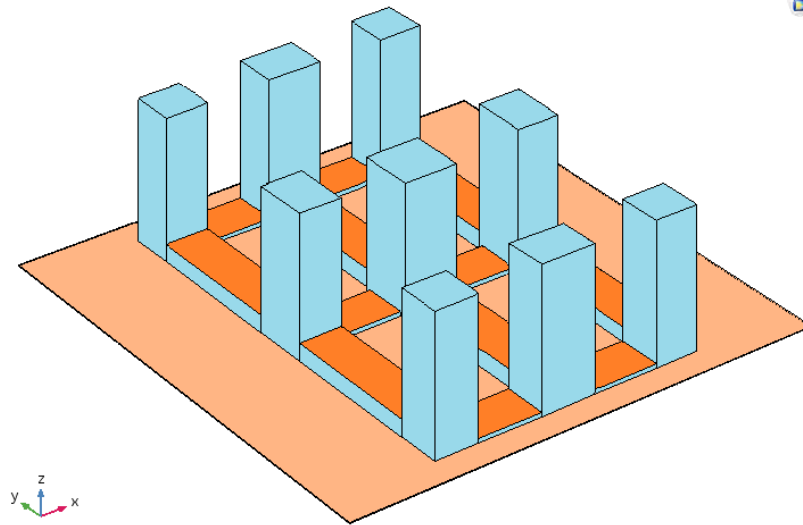


Figure 5.27: 3D view of the proposed planar array antennas

Although the design parameters in both linear array configurations (horizontal and vertical directions) have been optimized by simulation to provide a maximum gain, it is strongly recommended to investigate any potential change in the optimum values after forming the planar array. That change may result due to the mutual coupling between the array elements or due to the nearby modal excitation. In the former case, the spacings between array elements need to be increased to reduce the effect of the mutual coupling, of course with certain limitations associated with the sidelobes level and the field distribution inside the array cavity. However, in the latter case, the aspect ratios of both the resonators and the bridges have to be adjusted to mitigate such impact. The effect on the gain of the array structure was evaluated in all the parametric sweeps to assure that the eventual optimum values provide maximum gain. Indeed, achieving the maximum gain at a specific parametric value is an indication that the structure is properly resonating at the resonant frequency with respect to that particular value.

Firstly, the effect of the vertical low-profile dielectric bridges width ( $W_{vb}$ ) on the gain has been examined with values ranging from 60 mm to 70 mm. It has been found that the vertical spacing between the array elements has a strong direct impact on the gain, as expected. However, Figure 5.28 shows that the maximum gain is observed at 65 mm which is the same value obtained in the vertical linear array design. This means that the excited higher order mode is well isolated from the nearby modes that may devastatingly influence the array performance.

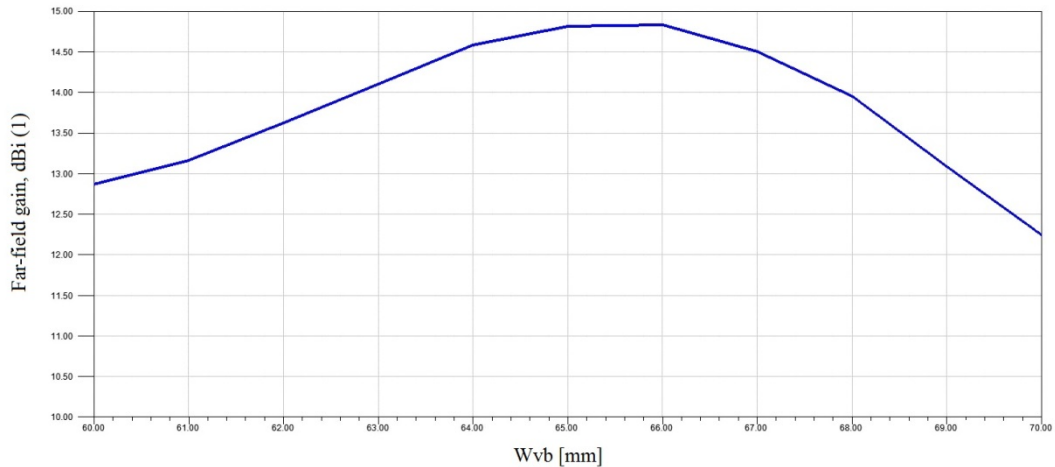


Figure 5.28: Effect of the vertical spacing (Width of the vertical bridges ( $W_{vb}$ )) on the array gain

Secondly, a parametric sweep on the horizontal spacing between the array elements which is represented by the length of the horizontal dielectric bridges ( $L_{hb}$ ) has been performed. Since  $L_{hb}$  in the horizontal linear array was optimized at one wavelength, this value may not be sufficient to reduce the mutual coupling effect. Therefore, the response of the gain with respect to values ranging from 10 mm to 50 mm was evaluated. Figure 5.29 shows that maximum gain is realized at a value of  $L_{hb}$  equals to 30 mm, which is identical to the value of  $L_{hb}$  in the linear array. It is worth noting here

that other bridges parameters such as  $W_{hb}$ ,  $L_{vb}$ ,  $H_{hb}$ , and  $H_{vb}$  have no strong effect on the gain.

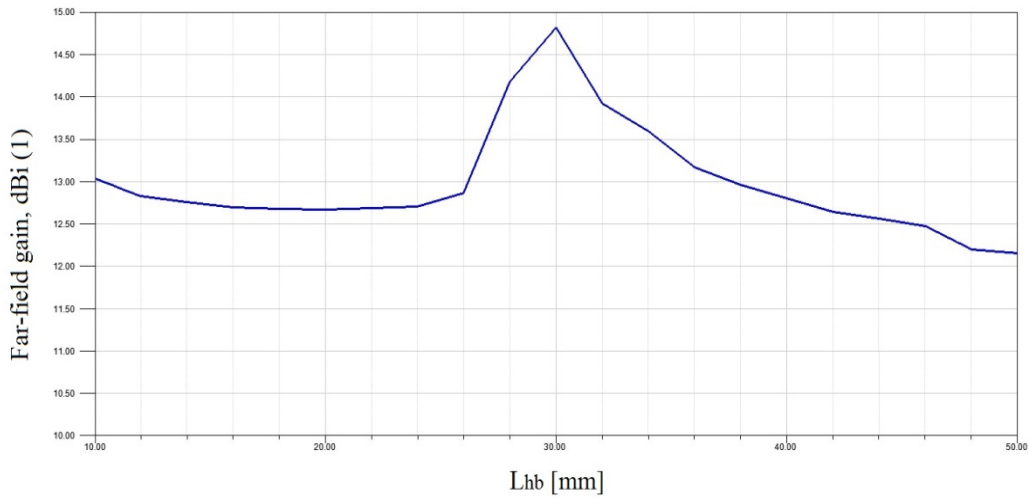


Figure 5.29: Effect of the horizontal spacing (Length of the horizontal bridges ( $L_{hb}$ )) on the array gain

Lastly, the dimensions of the dielectric resonators that have substantial impact on the gain have been optimized. These parameters are the width of the resonators labeled as 2 ( $W_{r2}$ ) and the length of the resonators labeled as 3 ( $L_{r3}$ ). It is worth noting here that the other dimensions of the resonators ( $L_{r2}$ ) and ( $W_{r3}$ ) have trivial impact on the gain in both linear configurations and their values were fixed as in the single antenna element design. Therefore, they were excluded from this study too. Also, the heights of the resonators ( $H_{r2}$ ) and ( $H_{r3}$ ) were fixed at the same initial value to not excite another mode. Figure 5.30 and Figure 5.31 illustrate that maximum gain can be achieved at parametric values slightly different than the associated ones in the linear configurations. This slight change is due to the variation in the boundary conditions after adding extra low-profile dielectric bridges in the planar array. The optimum value of  $L_{r3}$  is found to be 19.75 mm instead of

20 mm in the horizontal linear array design. For  $W_{r2}$ , its optimum value is 20 mm instead of 20.75 mm in the vertical linear array.

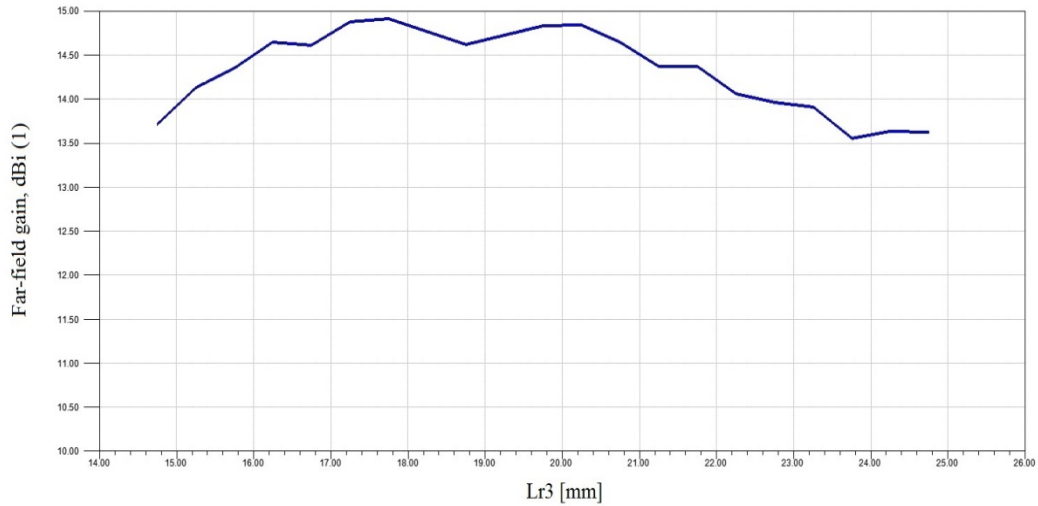


Figure 5.30: Effect of the length of resonators number 3 ( $L_{r3}$ ) on the array gain

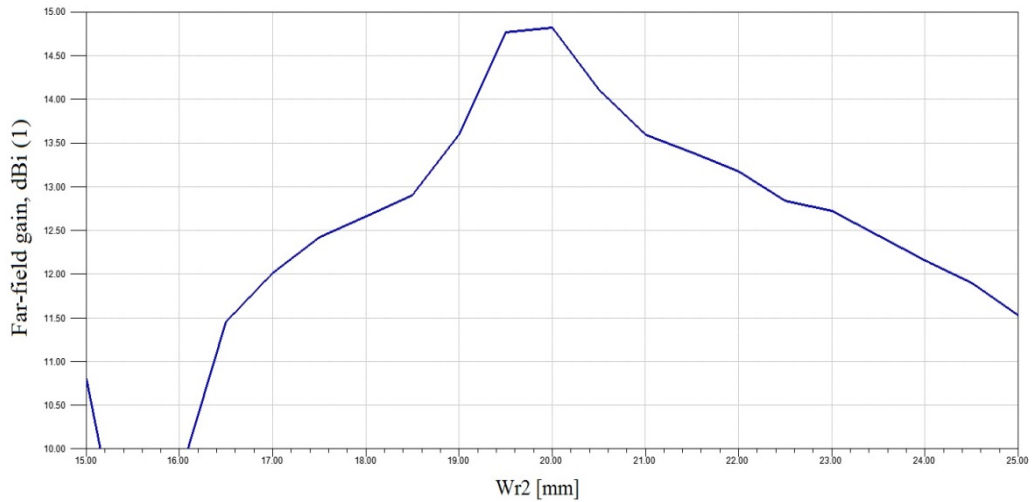


Figure 5.31: Effect of the width of resonators number 2 ( $W_{r2}$ ) on the array gain

Again, since the boundary conditions of elements numbered as 2 and 3 have changed after attaching more bridges,  $L_{r3}$  and  $W_{r2}$  were further optimized by simulation to be 19.75 mm and 20 mm, respectively. For the sake of symmetry, the dimensions of the additional radiating elements (labeled as 4) are chosen as follow, the length  $L_{r4}$  is set to be consistent with the length of elements number 3  $L_{r3}$ , and the width  $W_{r4}$  corresponds

to the width of elements number 2  $W_{r2}$ . Thus, the dimensions are 19.75 mm x 20 mm x 65 mm ( $L_{r4} \times W_{r4} \times H_{r4}$ ). Since the boundary conditions of the center radiating element have changed, its height was further optimized to be 60.5 mm. The dimensions of both vertical and horizontal dielectric bridges are fixed as in the linear array designs. The substrate is made of the same material Arlon 25N ( $\epsilon_{r\_sub} = 3.38$  and dissipation factor is 0.0015). The thickness is 20 mils (0.508mm) with a footprint area of 200 x 220 mm<sup>2</sup>. The length of the feed line and the matching stub printed at the bottom surface of the substrate are 110 mm and 1.27 mm, respectively, and the width is 1.13 mm. The size of the coupling aperture resides underneath the center slab only is 13.3 mm x 11.2 mm ( $L_s \times W_s$ ).

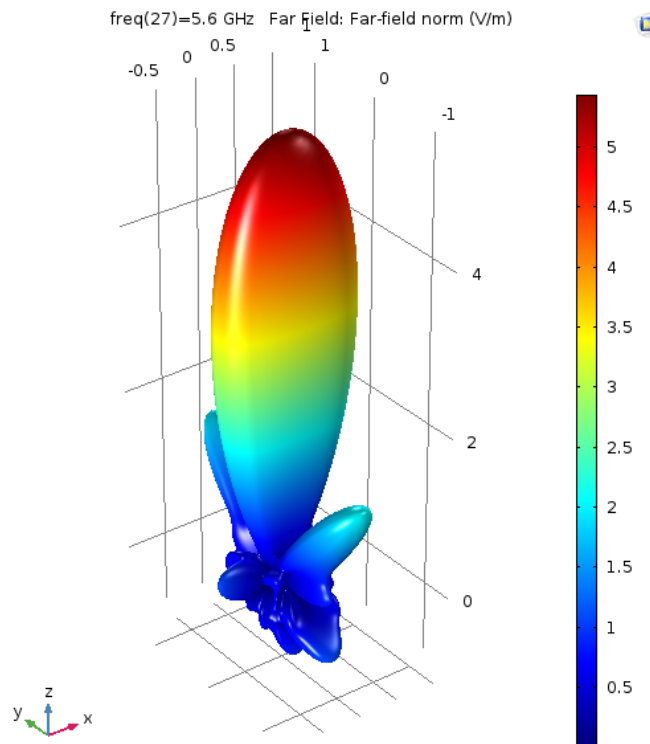


Figure 5.32: The 3D radiation pattern of the proposed 3x3 planar array antennas at  $f = 5.6$  GHz

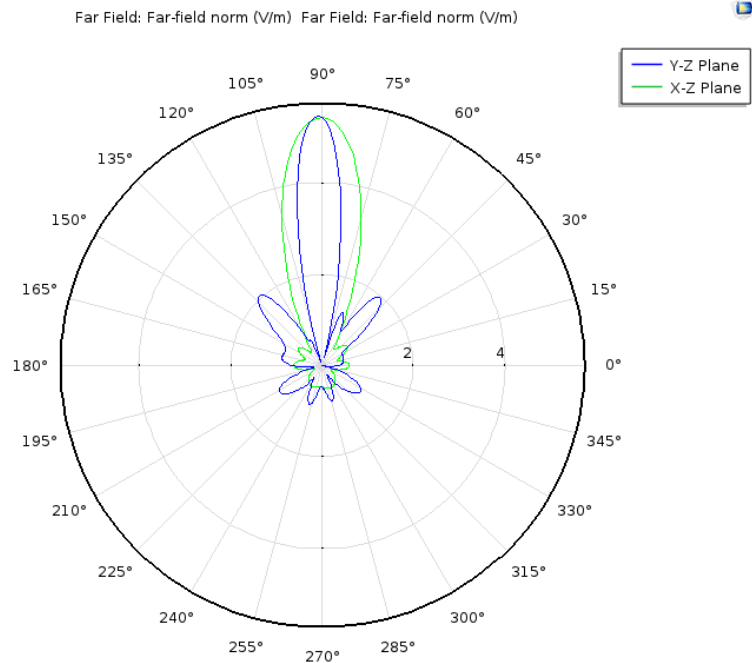


Figure 5.33: 2D far fields in both x-z and y-z planes at  $f=5.6$  GHz

The simulated radiation pattern is shown in Figure 5.32 and 5.33. It can be obviously seen that the proposed array configuration produces very narrow and directive main beam at the boresight. The 2D far-field plots prove the validity of the array excitation as having narrow beamwidth in both x-z and y-z planes.

Figure 5.34 demonstrates the field distribution inside the array structure. It can be noticed that the fields are uniformly distributed inside the radiating elements and the dielectric bridges in-between which is another proof that the proposed feeding mechanism can be effectively utilized to excite planar dielectric array antennas.

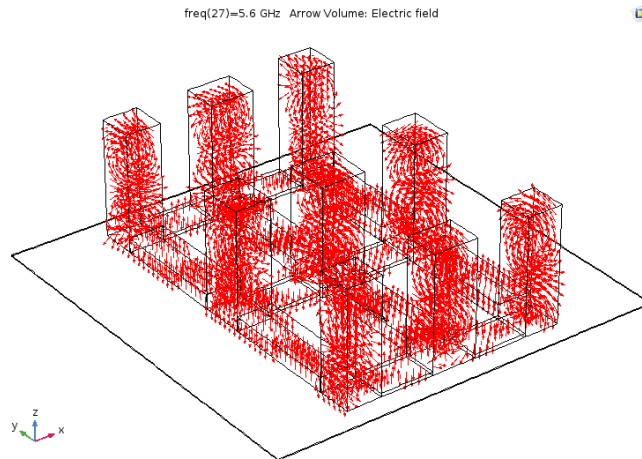


Figure 5.34: Field distribution within the proposed planar array structure

### 5.3.5 Fabrication Tolerance and Design Sensitivity

A BCN3D Sigma 3D printer has been utilized for the array fabrication. This type of printers has an accuracy of  $\pm 10 \mu\text{m}$ . The dimensions sensitivity, i.e. the fabrication tolerances, effect on the planar array gain has been carried out. In this study, each parametric value was ranging from  $\pm 5 \mu\text{m}$  to  $\pm 20 \mu\text{m}$ . As shown in Figure 5.35, four parameters that have considerable influence on the array gain have been considered in this study. Gain variations less than 1.5% can be seen for all parameters. This percentage corresponds to  $\pm 0.2 \text{ dBi}$ .

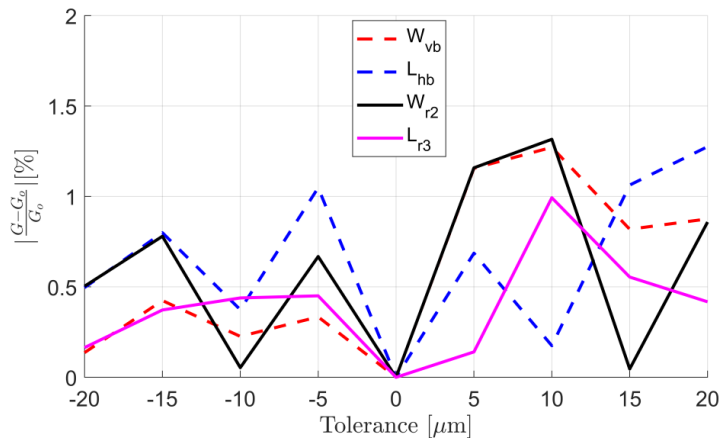


Figure 5.35: Fabrication tolerance and the sensitivity effect on the gain of the planar array

### 5.3.6 Fabrication and Measurements Results, and Discussion

The proposed standing-wave dielectric resonator array shown in Figure 5.36 is analyzed using numerical simulation and experimental measurement. The numerical simulation is done by COMSOL Multiphysics and HFSS software. Both are based on the Finite Element Method (FEM) that presumes an infinite ground plane. This presumption is equivalent to doubling the sources as a consequence of the image theory, whereas the fabricated antenna has a truncated ground plane. In fact, this is anticipated to cause slight differences in the results of the experimental measurement. The fabrication is partially done by taking advantage of 3D printing technology using PLA filament. Photographs of printing and testing the proposed array prototype are shown in Figure 5.37 and 5.38, respectively.

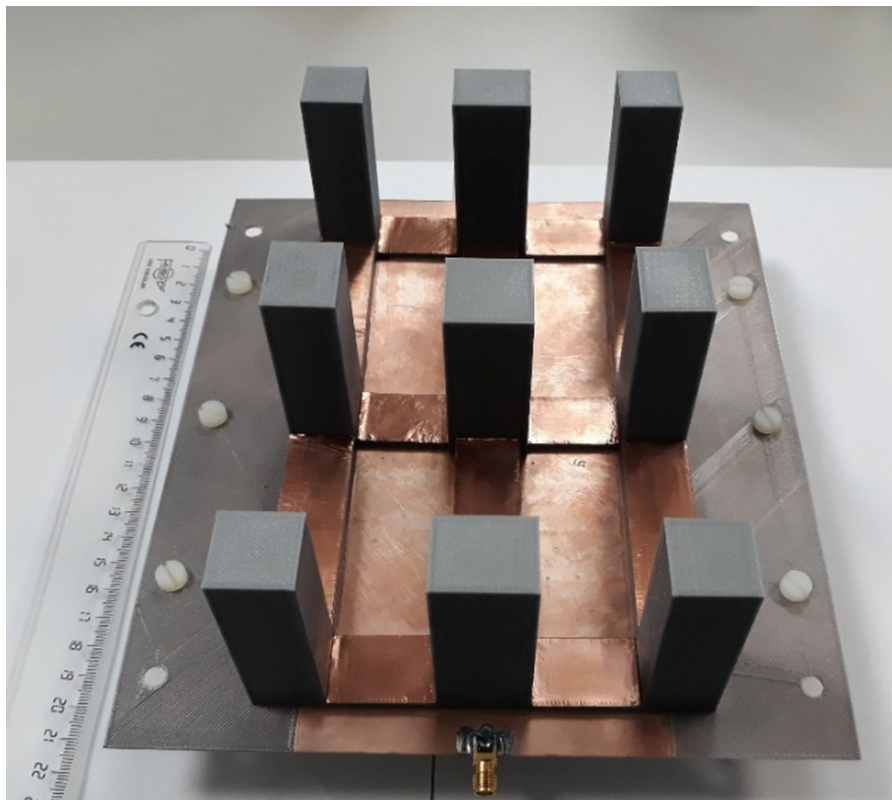


Figure 5.36: Fabricated 3x3 planar dielectric array antennas



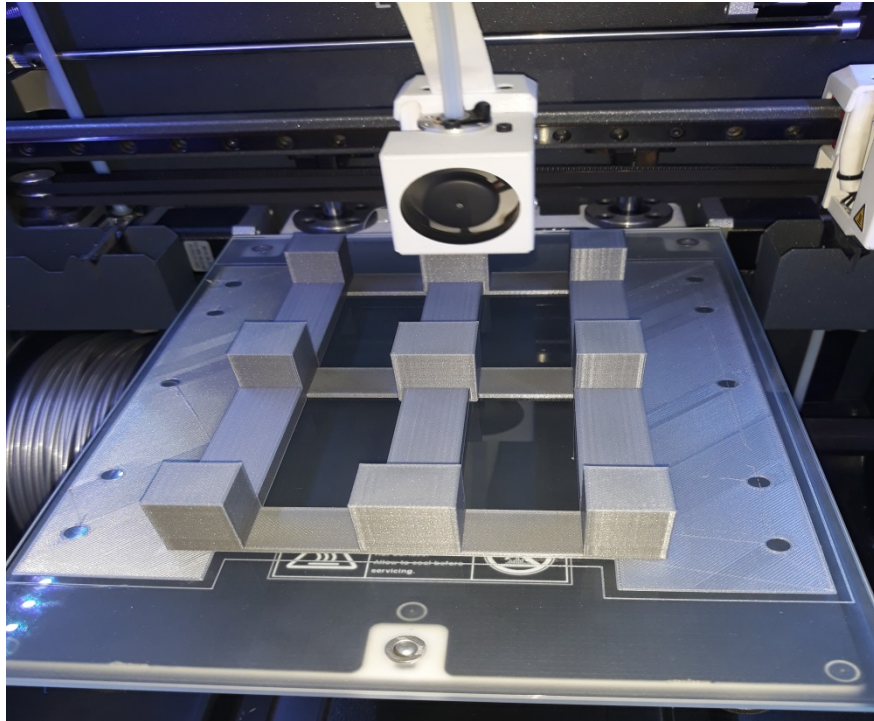


Figure 5.37: 3D printing the proposed 3x3 planar dielectric array prototype

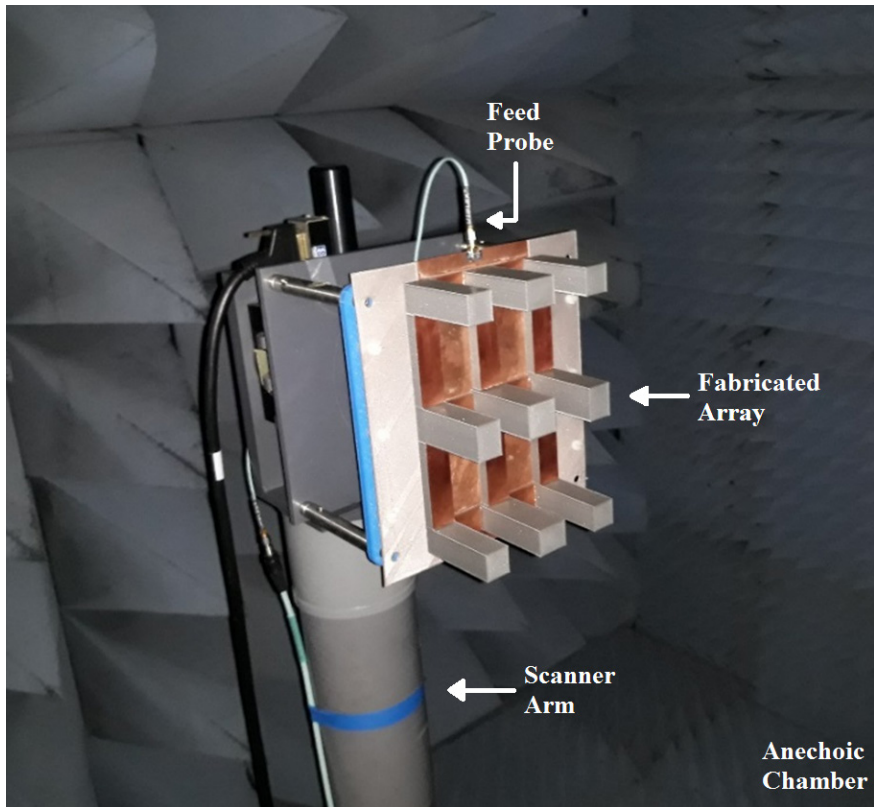


Figure 5.38: Testing the proposed 3x3 planar dielectric array prototype

The return loss as a function of frequency is plotted in Figure 5.39. The simulated curve agrees well with the measured one. The slight deviation could be due to fabrication tolerance and errors. Furthermore, the value of the resonant frequency is susceptible to the dielectric constants of the substrate and slabs' material which are subject to manufacturing tolerance. Also, the dielectric constants of both the substrate and the slabs' material may slightly alter with the frequency of operation. The measured return loss curve shows very wide useful impedance bandwidth of more than 2 GHz which corresponds to about 36% of the resonant frequency.

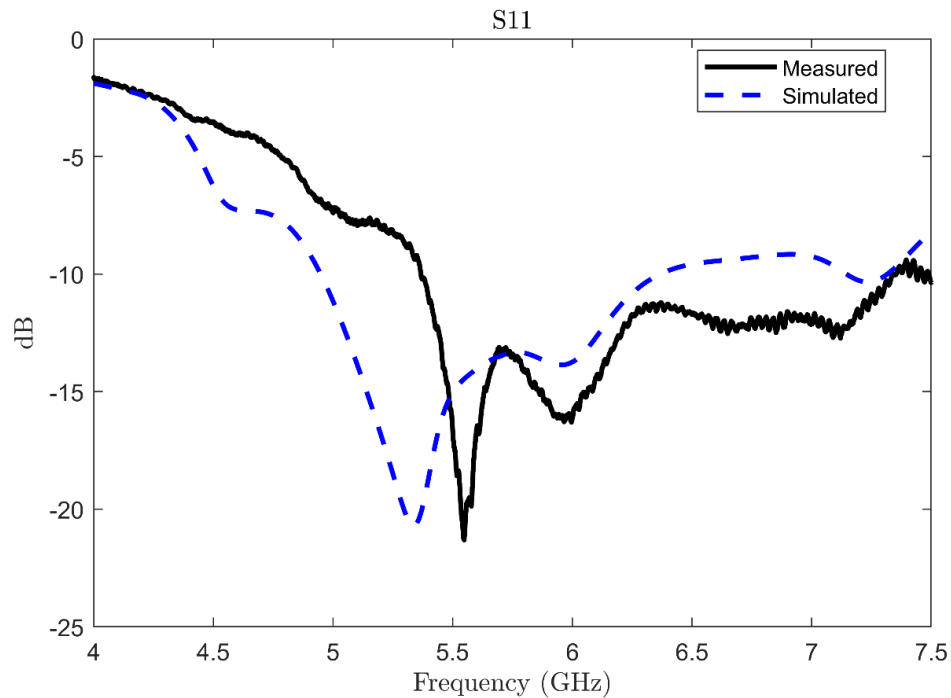


Figure 5.39: Return loss S11 vs frequency of the proposed planar array

The peaked measured gain of the array is 15 dBi which is in excellent agreement with the simulated one, as shown in Figure 5.40. Furthermore, the dB E-plane and H-plane radiation patterns are plotted in Figure 5.41. The experimental results are in good agreement with simulation results for broadside radiation. Away from the broadside, the

slight mismatch in the experimental radiation pattern levels could be due to scattering imperfections in the anechoic chamber.

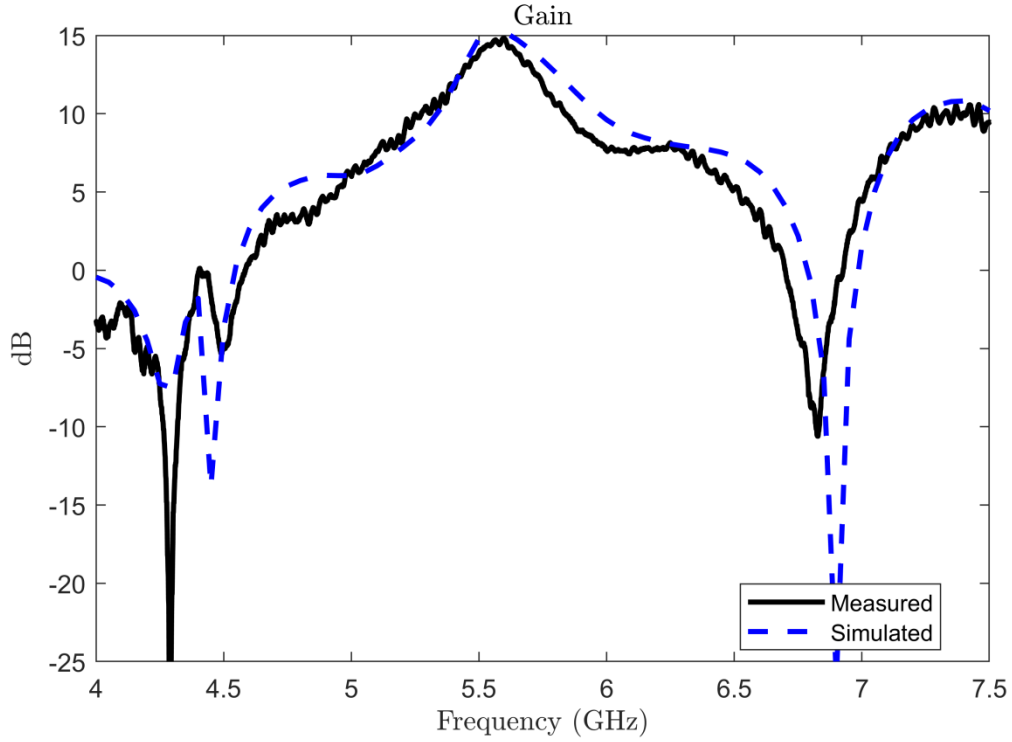


Figure 5.40: Realized gain vs frequency of the proposed planar array

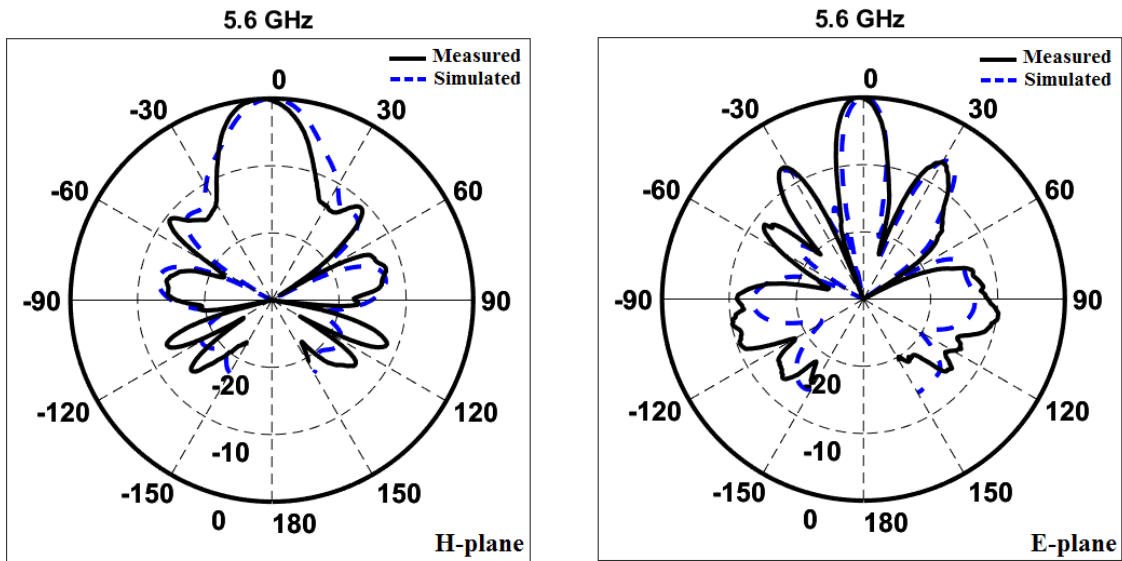


Figure 5.41: E- and H- plane radiation patterns of the proposed planar array

### 5.3.7 Summary of the Design Steps and Results

1. The design process starts by designing a rectangular dielectric resonator antenna that its  $TE_{115}$  mode is realized at or near to the desired operating frequency. This antenna will be the central element of the array.
2. Parallel to the feeding line (or the propagation direction of source wave), design two dielectric bridges of the same dielectric material used in the radiating element. The top surface of each bridge is covered by a metallic sheet of negligible thickness. The width of the bridges, i.e. the spacing distance from one edge to the next edge of the radiating elements, is 1.5 the waveguide wavelength. This condition is a consequence of the field variation inside the center element. At the front and back surfaces, parallel wavefronts, the fields have a maximum absolute value. Then, the optimum length and the height of the bridges are found by running a number of simulation iterations.
3. Orthogonal to the feeding line, repeat the previous step. However, the length of the bridges, i.e. the spacing distance from one edge to the next edge of radiating slabs, is one waveguide wavelength. Again, this is a result of the field variation inside the center slab. At the right and left surfaces, normal to a wavefront, the fields have a sinusoidal variation. Then, find the optimum width and the height of the bridges by simulation.
4. Now, add more radiating slabs of the same size as the center one (Step 1) to the end of each connecting bridge to form a five-element array of a Plus (+) sign. By simulation, vary the width of the additional elements along the feed line. The length and height remain as in the center element. Again, by simulation, vary the

length of the additional elements in the direction orthogonal to the feed line. The width and height remain as in the center element.

5. To form a 3x3 array, add more connecting bridges to each additional slab created in Step 4. The sizes of the bridges correspond to those designed in Steps 2 and 3, either parallel or orthogonal to the feed line.
6. Slightly optimize the width and length of radiating elements designed in Step 4.
7. Add four radiating elements in the four corners of the array structure between the bridges generated in Step 5. The height of these four slabs is the same as in Step 1. The length and the width should be in consistency to the optimum values obtained by simulation in Step 4.
8. As final tuning step, optimize the height of the center element designed in Step 1.

Table 5.3 Summary of design parameters and performance results of the planar array

Configuration	Dimensions (mm <sup>3</sup> )		No. of Elements	$f_o$ (GHz)	Gain (dBi)	Impedance Bandwidth (%)	Radiation Efficiency (%)
Single Element	25x25x65		1	5.3	8.2	46.9 %	-----
Linear Array (// Feed Line)	Element #1	25x25x65	3	5.6	11.9	31.6	90.6
	Elements #2	25x20.75x65					
Linear Array (⊥ Feed Line)	Element #1	25x25x65	3	5.6	11.75	32.1	-----
	Elements #3	20x25x65					
Planar Array	Element #1	25x25x60.5	9	Measured			87
	Elements #2	25x20x65		5.6	15	35.7	
	Elements #3	19.75x25x65					
	Elements #4	19.75x20x65					

## 5.4 Design, Analysis, and Simulation of Linear Standing-wave Dielectric Array Antennas

### 5.4.1 Single Element Design

In order to appreciate the potential results regarding the gain enhancement as well as the validity of the proposed standing-wave excitation concept, it is preferable to first design a single rectangular dielectric resonator antenna. Therefore, a single rectangular dielectric resonator antenna operating at the desired frequency of 3.9 GHz was first designed. COMSOL Multiphysics Modeling and HFSS Software are both used for simulation. The structure of the antenna is depicted in Figure 5.42. The dimensions of the radiating slab are 26.2 mm x 26.2 mm x 45.8 mm ( $L_r \times W_r \times H_r$ ) and is made of Poly Lactic Acid (PLA) which is widely utilized in 3D printers. The dielectric constant is  $\epsilon_r = 2.5$  and the dissipation factor is 0.005. The dielectric element is located at the center of a substrate with dimensions of 120 mm x 160 mm ( $W_{sub} \times L_{sub}$ ). The substrate is made of Arlon 25N with dielectric constant  $\epsilon_{r_{sub}} = 3.38$ , dissipation factor = 0.0015, and a thickness of 60 mils (1.524 mm).

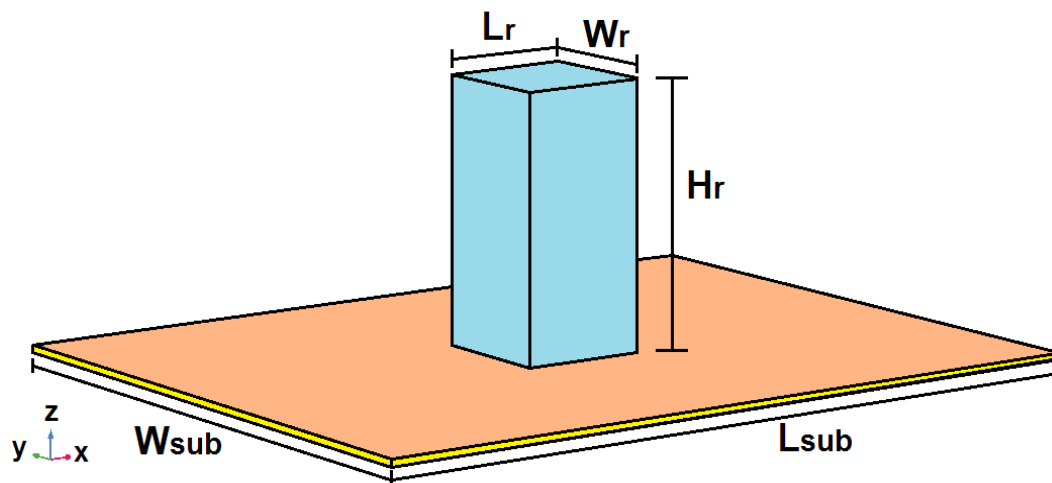


Figure 5.42: Proposed single rectangular dielectric resonator antenna

Figure 5.43 shows excellent impedance matching of -35 dB achieved at the resonant frequency of 3.9 GHz. Indeed, the impedance matching is not critical at this stage since its purpose is to find the gain of a single element for eventual comparison. In addition, the feeding mechanism will be ultimately switched to coaxial probe feeding. The antenna produces a peaked gain of 8.8 dBi at 3.9 GHz with a radiation pattern directed at the boresight, as shown in figures 5.44 and 5.45, respectively. For better visualization of the radiation pattern, the 2D plots of the electric field in the far zone in both x-z and y-z planes are depicted in Figure 5.46. The excited mode is  $TE_{113}$  which is clearly seen by depicting the field distribution inside the antenna cavity in Figure 5.47.

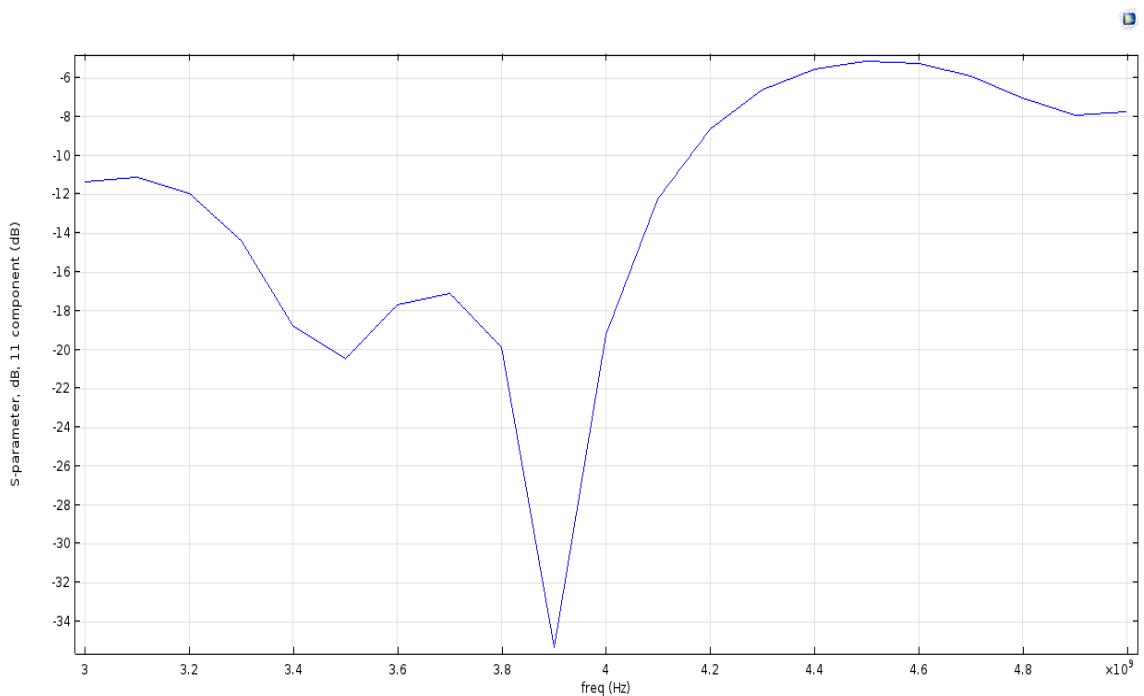


Figure 5.43: Return loss S11 vs frequency of the single rectangular dielectric antenna

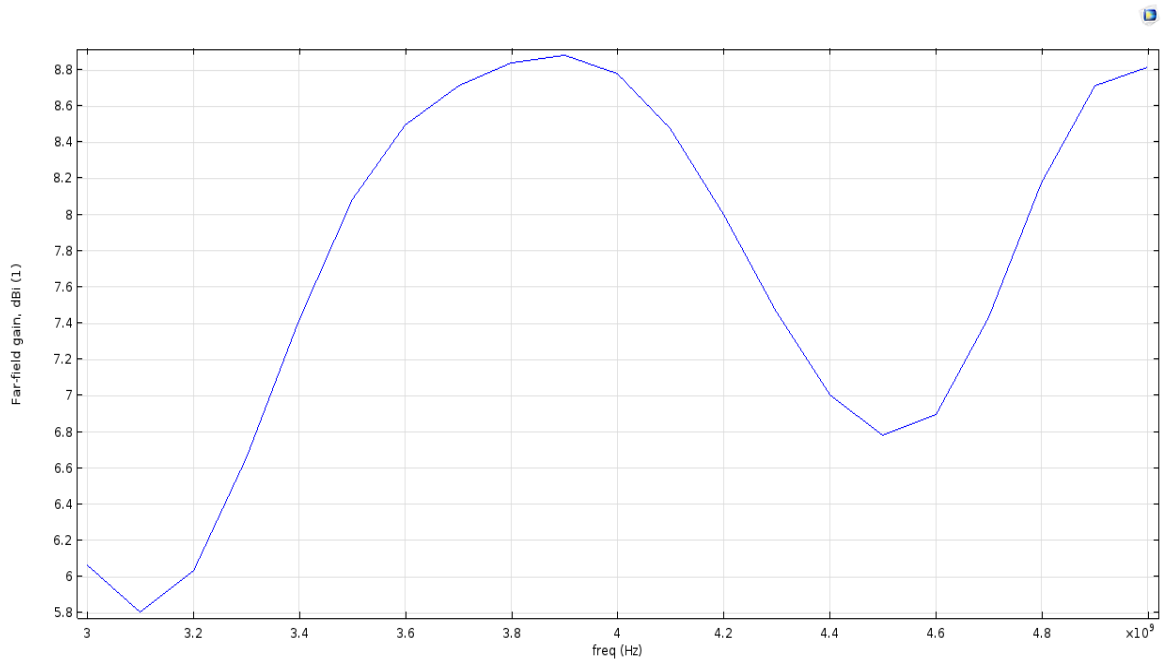


Figure 5.44: Realized gain vs Frequency of the single rectangular dielectric antenna

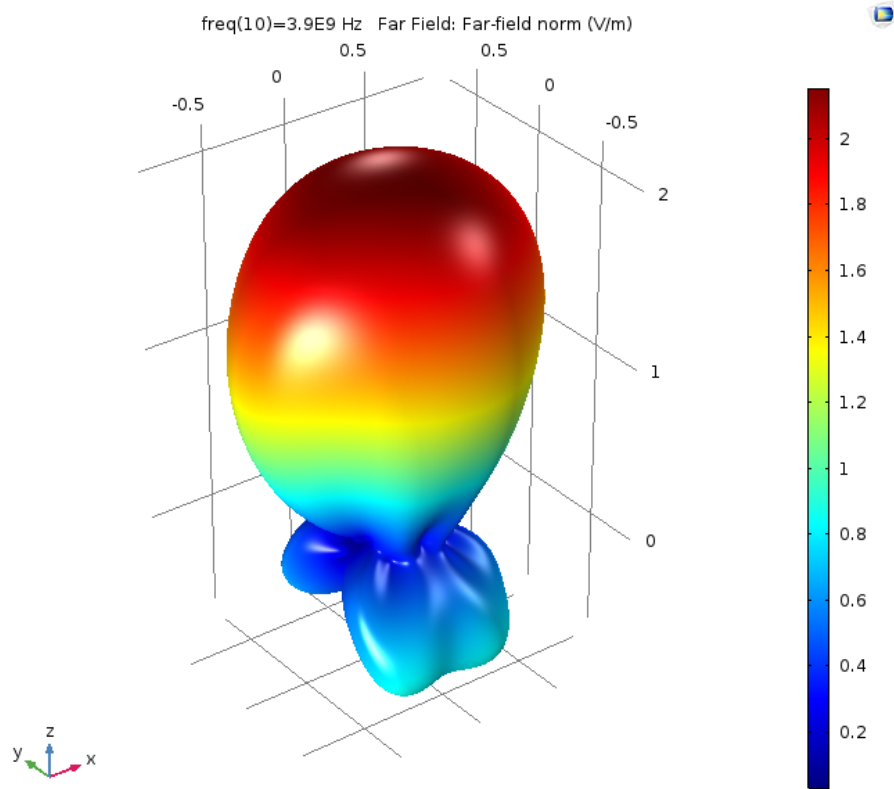


Figure 5.45: The 3D radiation pattern of the single rectangular dielectric antenna at  $f = 3.9$  GHz



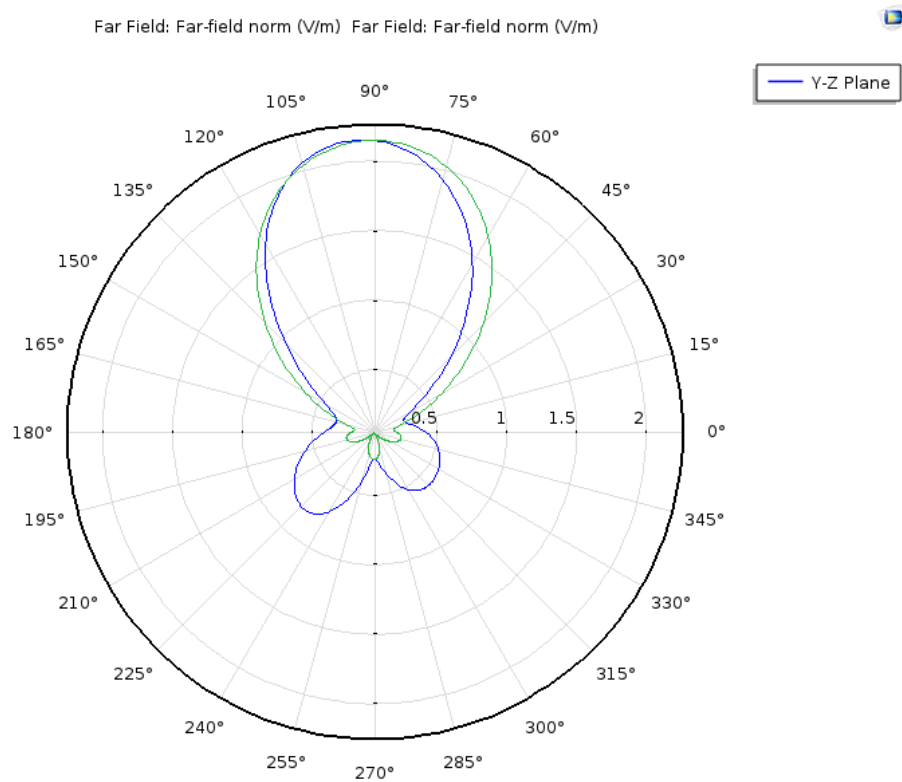


Figure 5.46: 2D far electric fields in both x-z and y-z planes at  $f = 3.9$  GHz

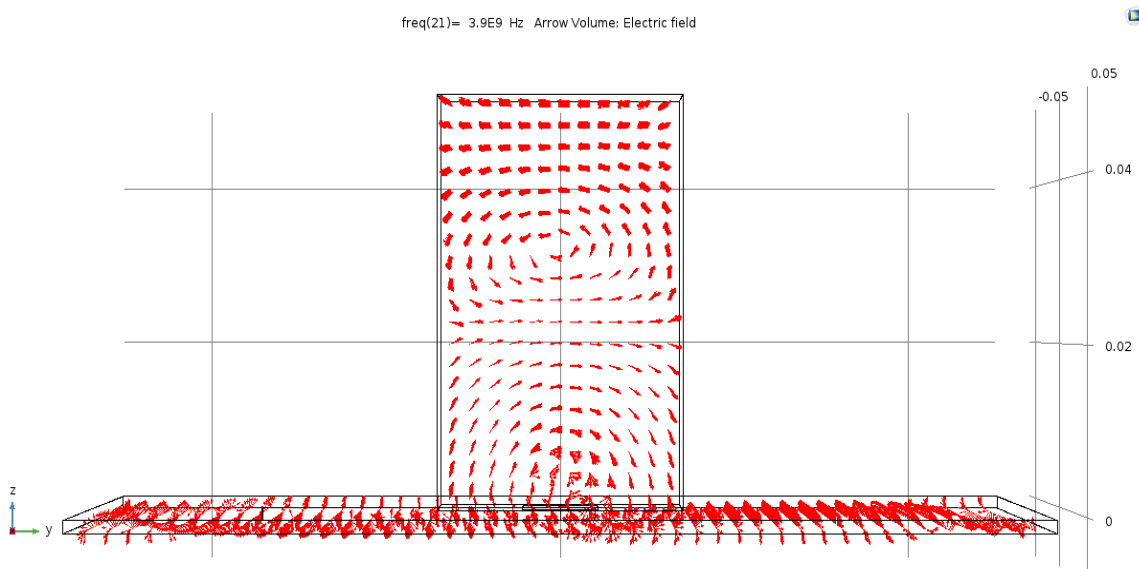


Figure 5.47: Field distribution inside the cavity at the resonant frequency 3.9 GHz

### 5.4.2 Two-Element Linear Array Design

The array design starts by designing a microstrip patch so that the length of the patch which represents the spacing between the dielectric slabs is about 1.5 waveguide wavelengths. The microstrip patch is attached to the top surface of the substrate and is fed by a coaxial cable. Then, two identical rectangular dielectric radiating elements are placed on top of the patch where its radiating edges slightly go underneath the array elements. This, in turn, will allow coupling sufficient RF power into the dielectric elements in order to radiate. Then, exactly at the center under the radiating elements, two patches of smaller size are introduced. Their function is to transfer the RF waves from the center patch, where the coaxial cable is attached to, to the radiating elements. Figures 5.48 and 5.49 illustrate the proposed array configuration.

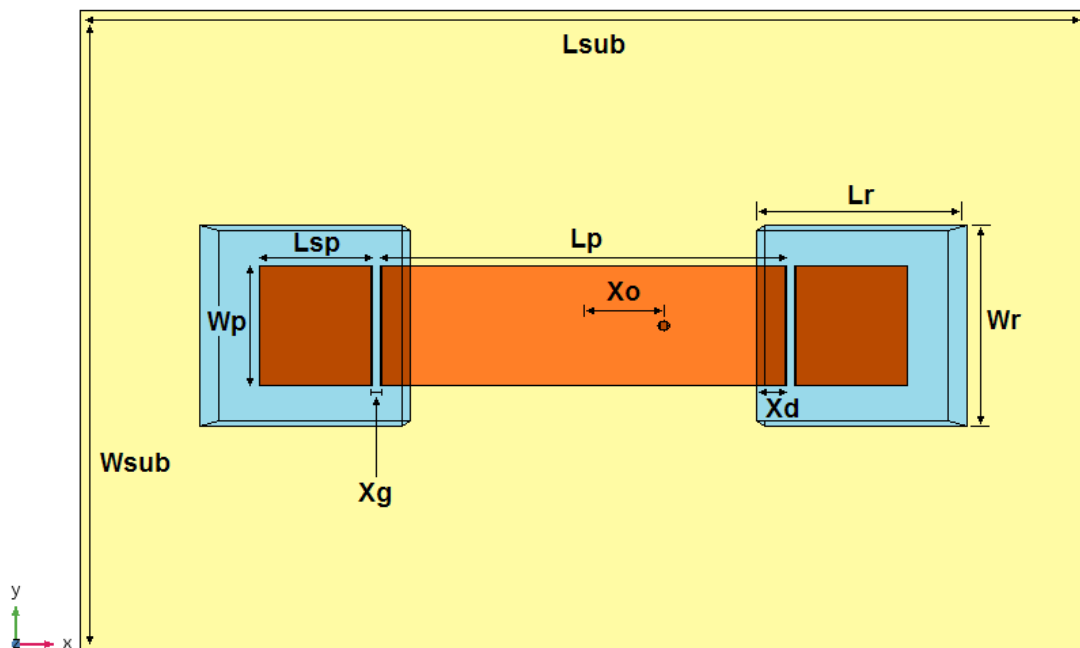


Figure 5.48: Top view of the proposed two-element linear array antennas

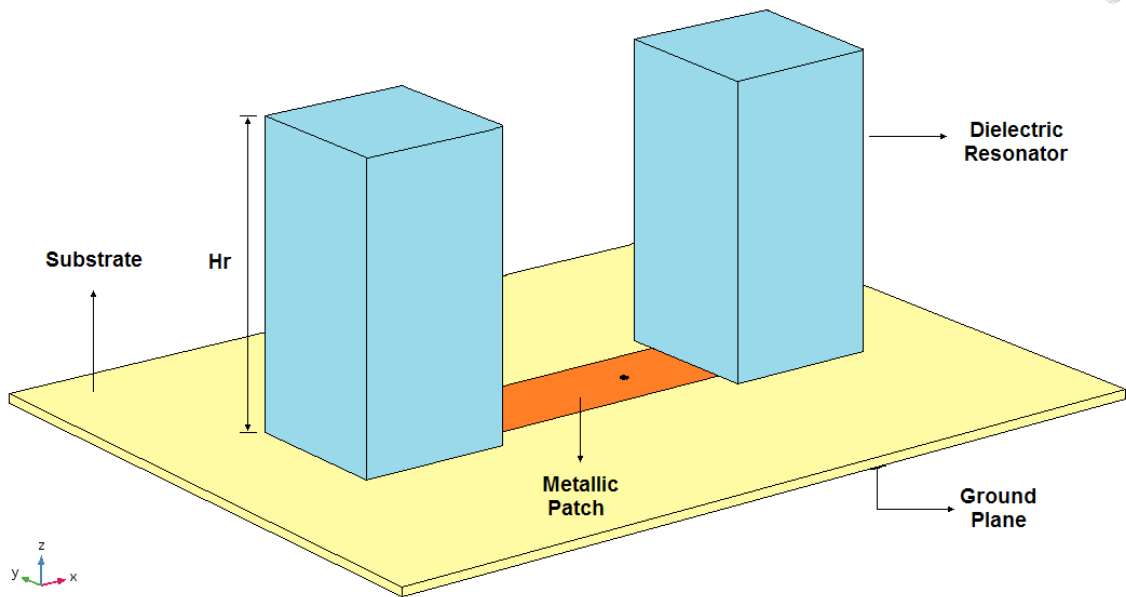


Figure 5.49: 3D view of the proposed two-element linear array antennas

The dimensions of the radiating slabs are 26.2mm x 26.2mm x 45.8 mm ( $L_r \times W_r \times H_r$ ) and are made of Poly Lactic Acid (PLA). The dielectric constant is  $\epsilon_r = 2.5$  and the dissipation factor is 0.015. The array is mounted on top of a substrate with dimensions of 400 mm x 200 mm ( $L_{sub} \times W_{sub}$ ). The substrate is made of Arlon 25N with dielectric constant  $\epsilon_{r\_sub} = 3.38$ , dissipation factor = 0.0015, and a thickness of 60 mils (1.524 mm). The dimensions of the center patches and the edge patches are 61.5 mm x 17 mm ( $L_p \times W_p$ ) and 15 mm x 17 mm ( $L_{sp} \times W_p$ ), respectively. The optimum overlapping distance  $X_d$  is found to be 4.2 mm and the gap distance  $X_g$  between any two patches is 1.4 mm. The optimum feeding location is at an offset distance  $X_o$  of 7.6 mm from the center.

Figure 5.50 depicts the return loss S11 as a function of frequency. Excellent impedance matching of about -26 dB is observed at a frequency of 3.85 GHz. It is noted that the resonant frequency is slightly deviated due to the mutual coupling between array

elements. The maximum gain of 12 dBi at the boresight is realized at the resonant frequency. Figure 5.51 plots the realized gain as a function of frequency.

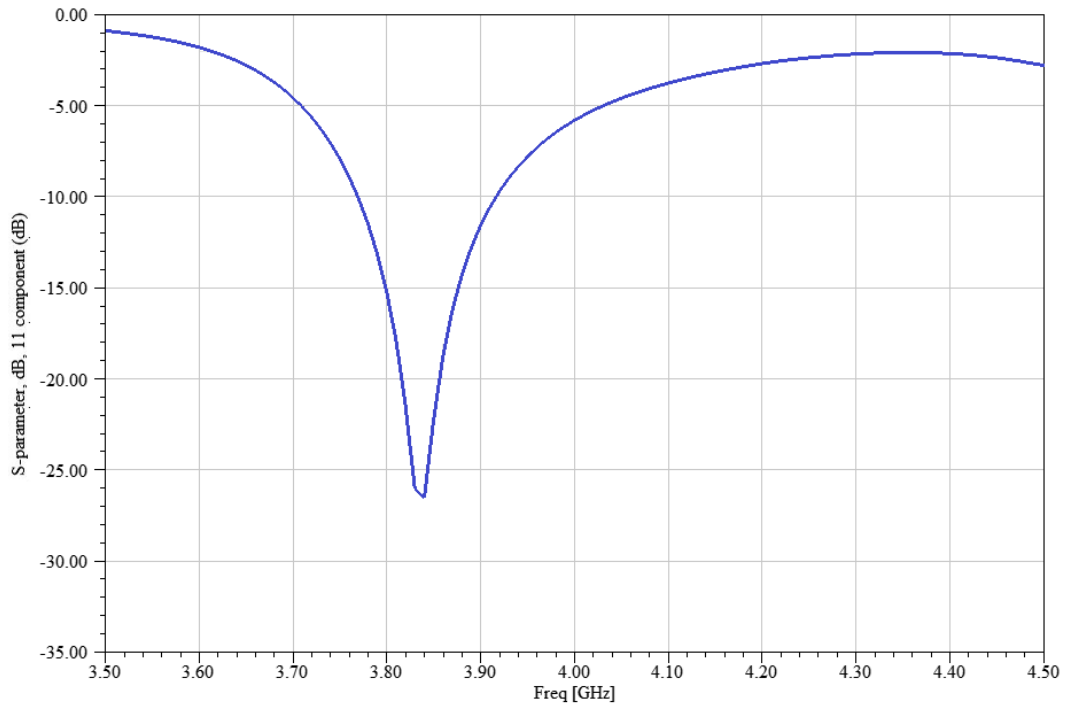


Figure 5.50: Return loss S11 vs frequency of two-element linear array antenna

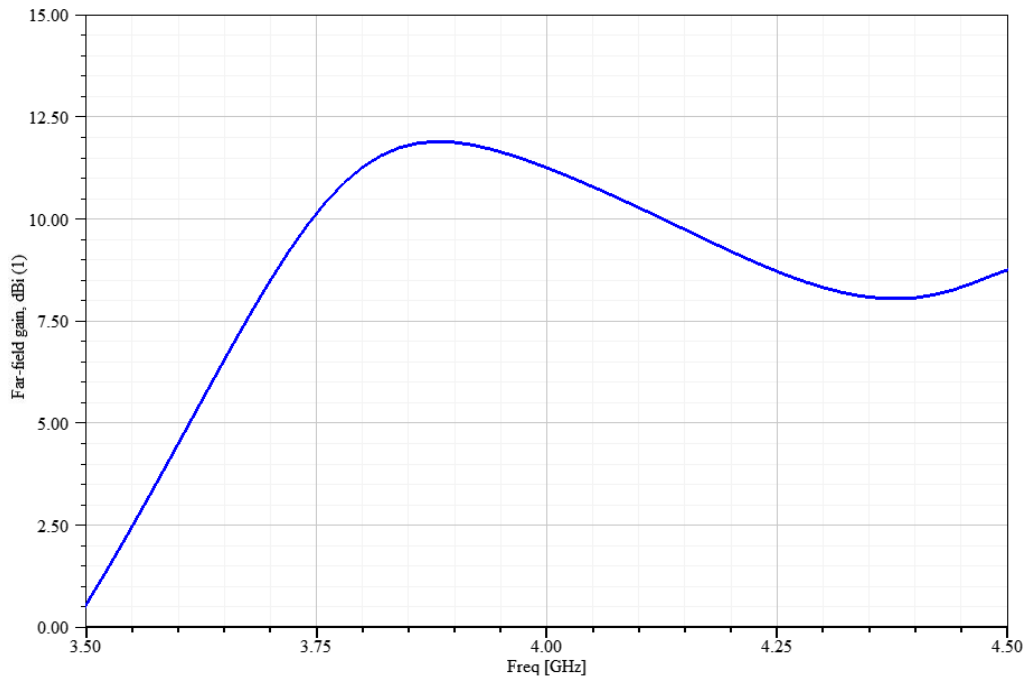


Figure 5.51: Realized gain vs frequency of two-element linear array antenna

The maximum observed realized gain is 3.2 dBi higher than the gain of the single element resonating at the higher-order mode  $TE_{113}$ . Since the gain increment is in excellent agreement with the array antenna theory, it can be said that the concept of exciting the dielectric resonator array structure by forming standing waves in microstrip patches is valid. Another evidence of the validity of the proposed feeding mechanism can be observed by examining the far field radiation pattern, depicted in Figures 5.52 and 5.53. It can be clearly seen that the radiation pattern has a very narrow beam in the direction of the array; i.e. x-z plane drawn in Green. In the opposite direction of the array, the radiation pattern has a wide beam which is reasonable and expected (drawn in Blue as y-z plane).

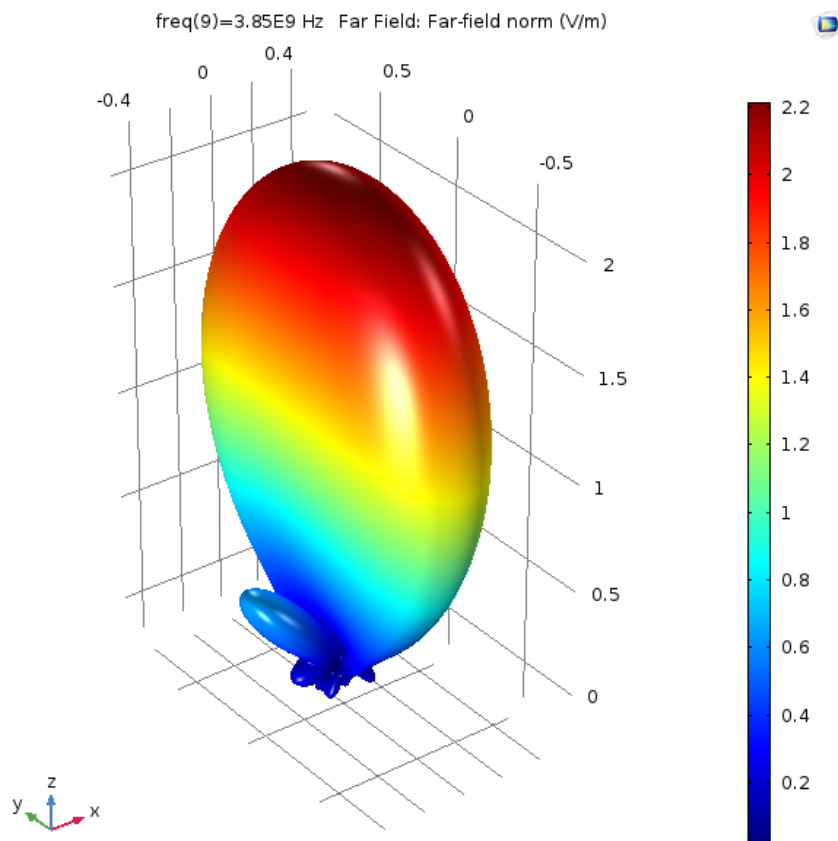


Figure 5.52: The 3D radiation pattern of two-element linear array antennas at  $f = 3.85$  GHz

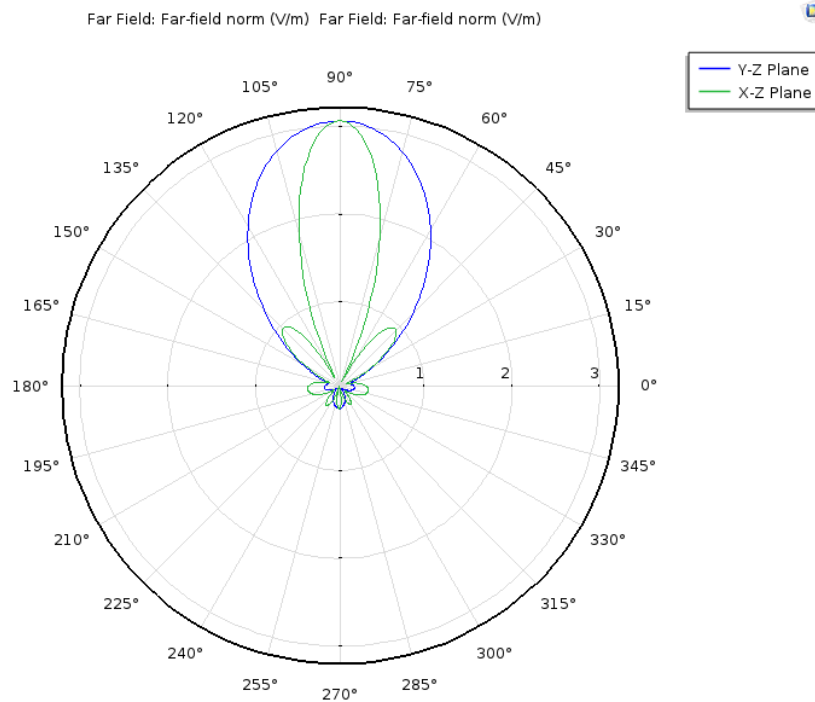


Figure 5.53: 2D far fields in both x-z and y-z planes at  $f=3.85$  GHz

Figure 5.54 demonstrates the field distribution inside the array structure. It can be clearly seen that the fields are almost uniformly distributed inside the array elements which is another evidence of the proposed configuration validity.

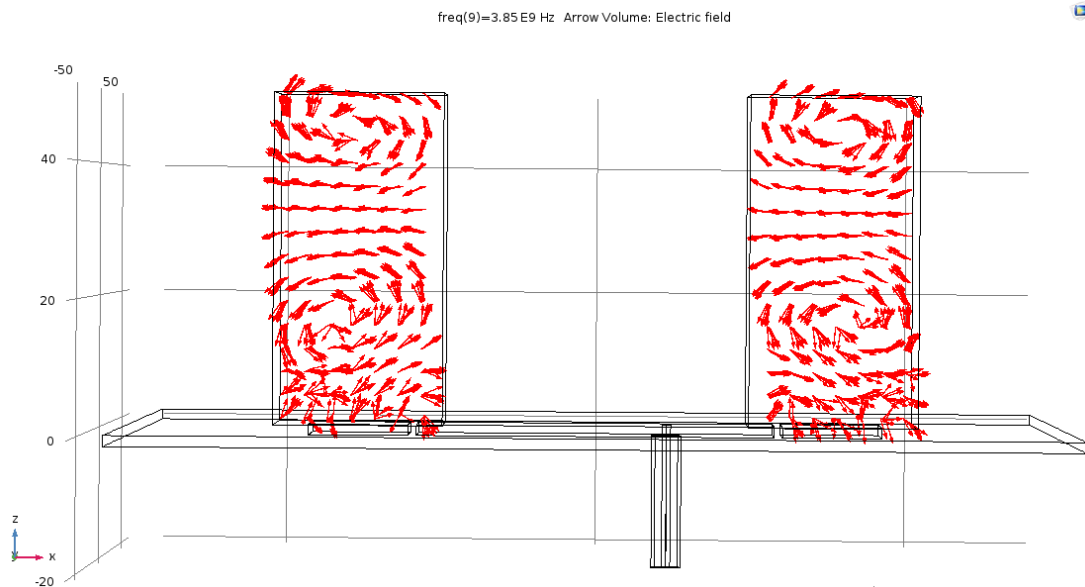


Figure 5.54: Field distribution inside the array structure at the resonance frequency

### 5.4.3 Four-Element Linear Array Design

The proposed configuration is now extended to form four-element linear array antenna following exactly the same procedure. Two extra dielectric radiating elements are introduced along with two additional main patches and two smaller patches possessing the same dimensions in the two-element array prototype. Figure 5.55 illustrates the array geometry.

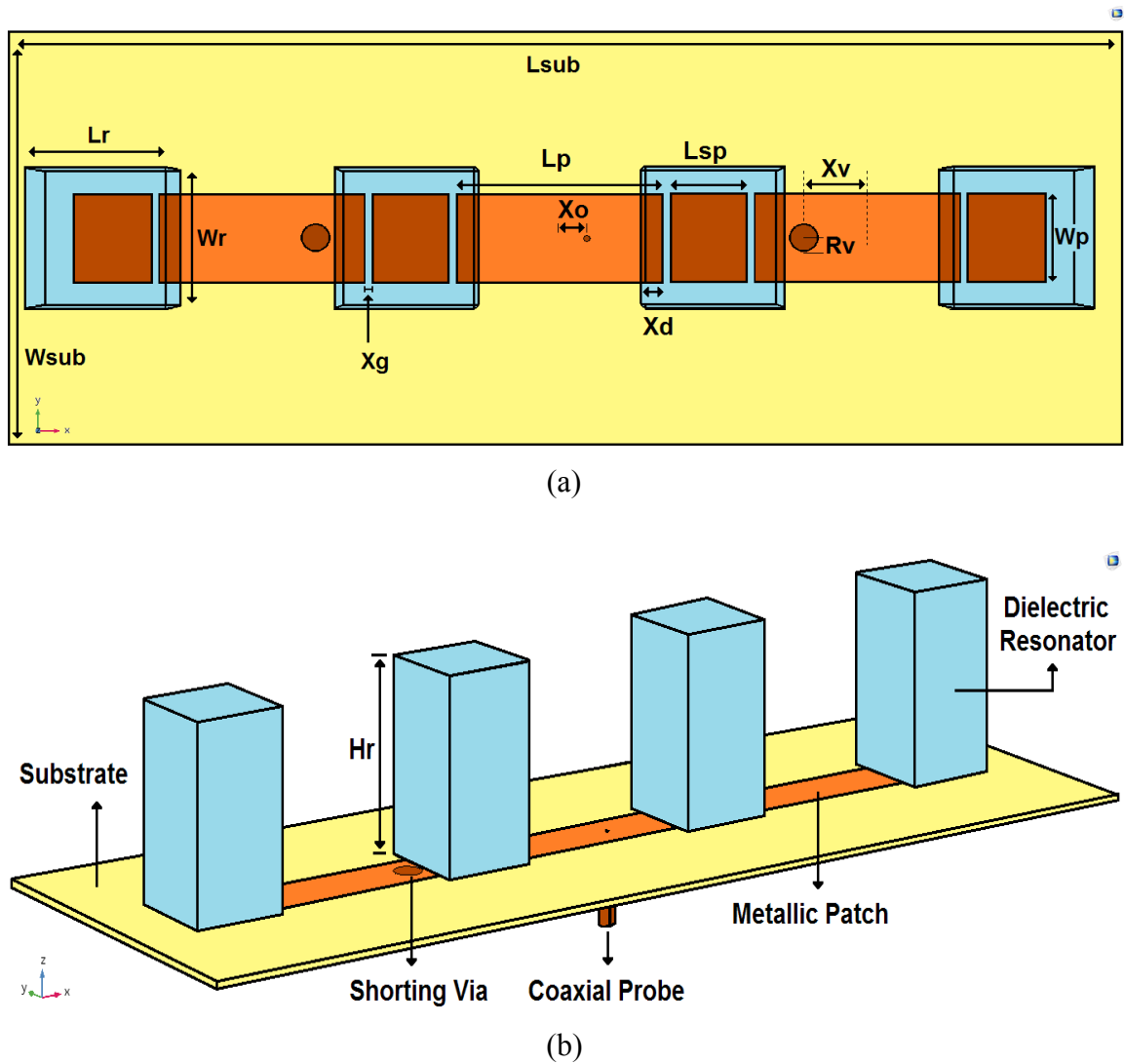


Figure 5.55: (a) Top and (b) 3D view of the proposed four-element linear array antennas

The dimensions of dielectric radiating elements and the patches are the same. The array is mounted on top of a substrate with the same dimensions. In this proposed configuration, there are two shorting vias of a radius of  $R_v = 4$  mm located at an offset distance of  $X_v = 22$  mm from the center of the patch where each via is attached to. They are made of copper with a thickness consistent with the thickness of the substrate. The shorting vias are soldered with the patches from the top and with the ground plane from the bottom. The reason these vias are considered in this configuration is that undesired mode was excited within the patches. This mode produces a radiation pattern with null at the boresight and, hence, considerable gain reduction was observed. The location of these shorting pins was chosen carefully and precisely at the null in order to suppress that mode. Better radiation pattern and gain are achieved after hence.

Figure 5.56 shows the return loss S11 as a function of frequency. Excellent impedance matching of about -45 dB is observed at a frequency of 3.9 GHz. Negligible slight frequency shift is noted due to the mutual coupling between array elements. The maximum peaked gain of 15 dBi at the boresight is realized at the resonant frequency. Figure 5.57 plots the realized gain as a function of frequency. The sidelobe level is in excellent state since 12 dBi is observed between the main lobe and the side lobes at an angle  $\theta$  of  $60^\circ$  as shown in Figure 5.58.



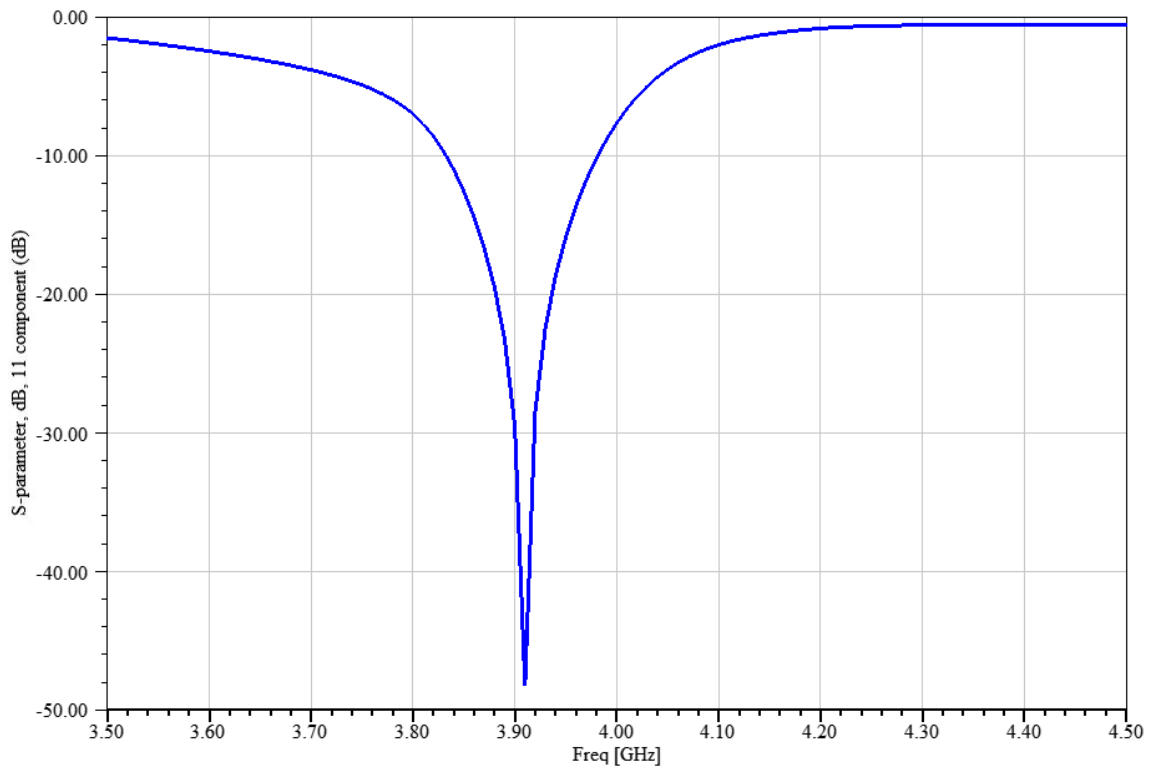


Figure 5.56: Return loss S11 vs frequency of the four-element linear array antenna

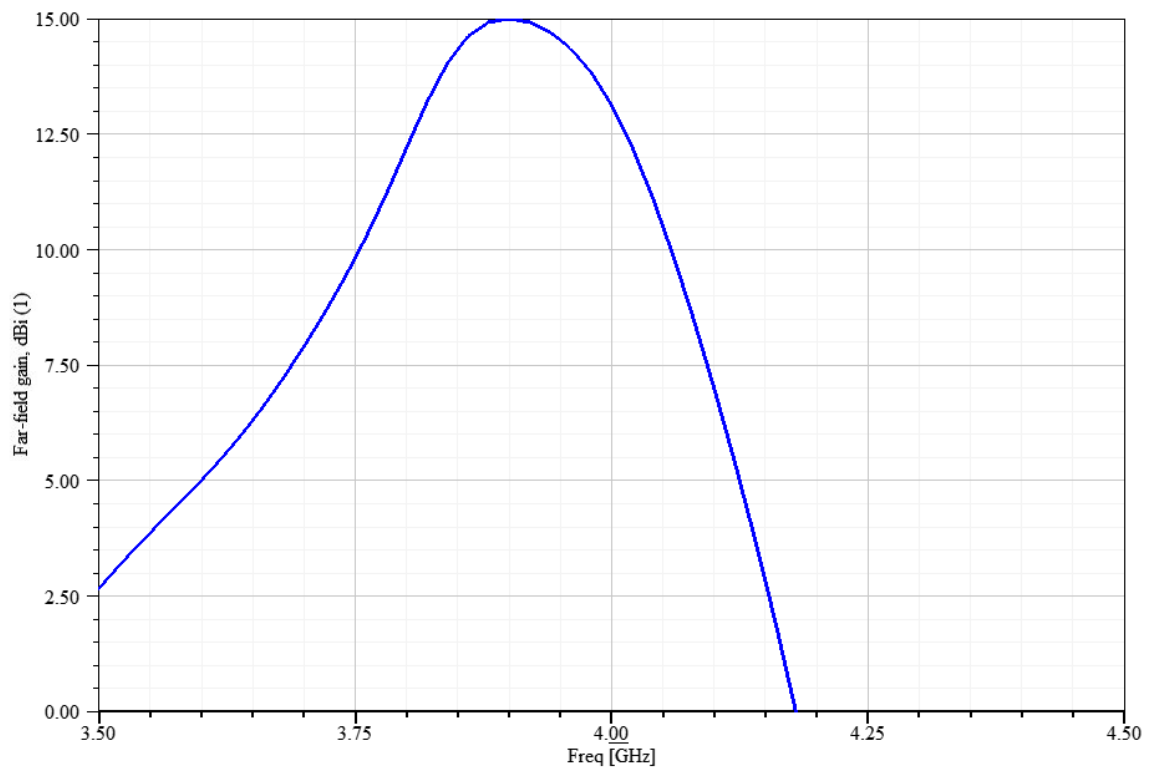


Figure 5.57: Realized gain vs frequency of the four-element linear array antenna

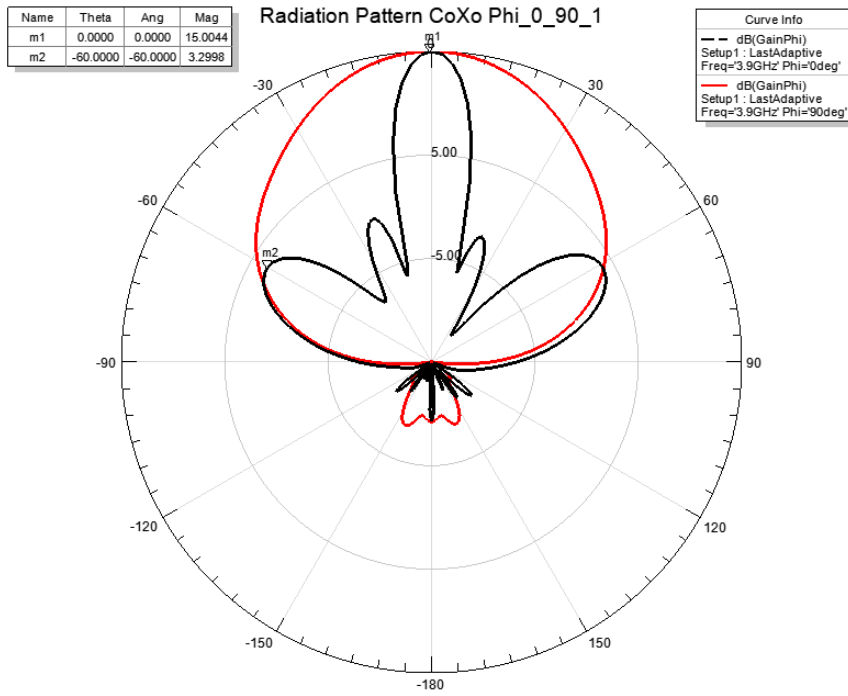


Figure 5.58: Cross- and Co-polar radiation pattern of the four-element linear array

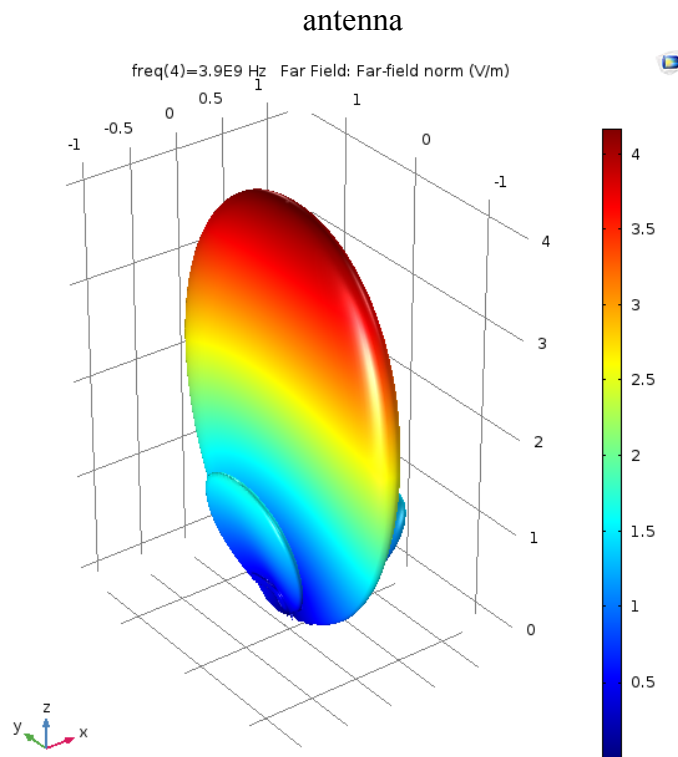


Figure 5.59: 3D radiation pattern of the four-element linear array

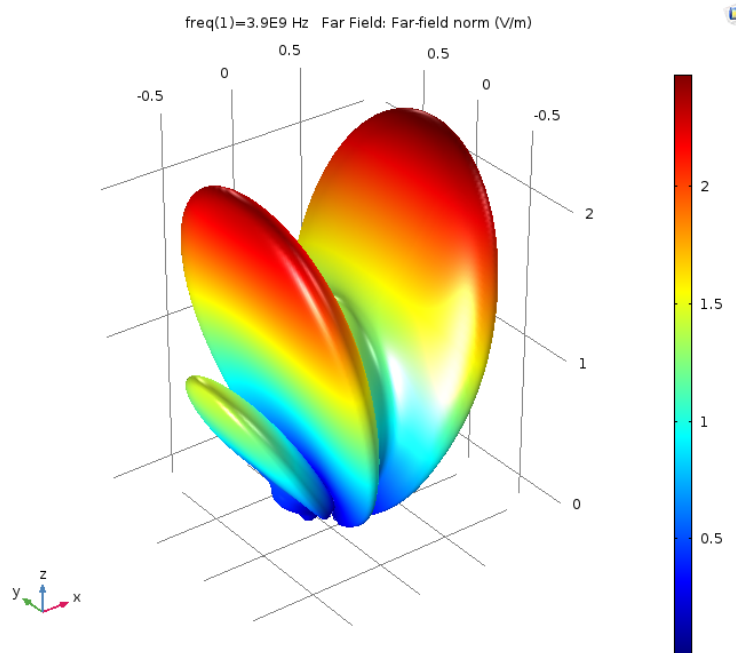


Figure 5.60: 3D radiation pattern of the four-element linear array without vias

By examining the three-dimensional radiation pattern depicted in Figure 5.59, it is observed that the radiation pattern has a very narrow beamwidth in the direction of the array elements. This, in turn, indicates that the proposed feeding method is valid and capable of efficiently excite a dielectric resonator array configuration. Figure 5.60 depicts the radiation pattern in the case if no vias are utilized. It can be seen that the pattern has a null at the boresight. Consequently, severe gain reduction was realized in this particular case. Additional evidence is seen when analyzing the field distribution inside the resonators cavity. As shown in Figure 5.61, the fields inside the cavity are coherent and uniformly distributed among array elements. The mode  $TE_{113}$  is realized for all elements.

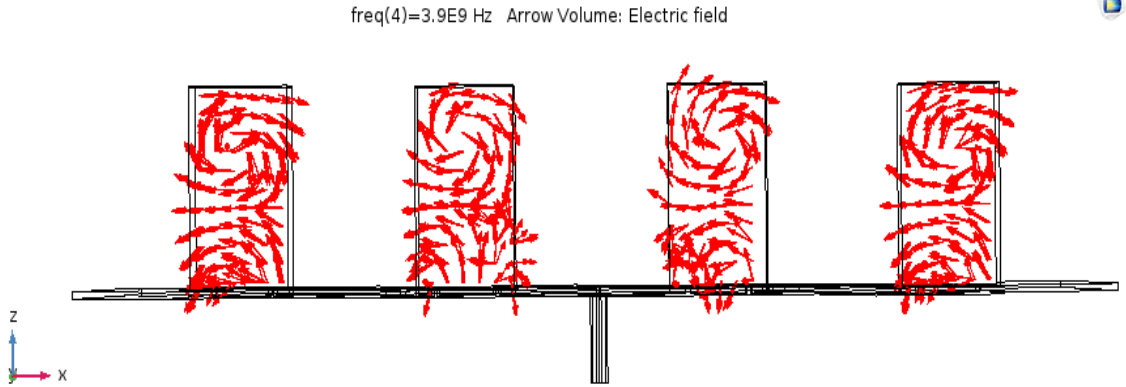


Figure 5.61: Field distribution inside the array structure at the resonance frequency

#### 5.4.4 Field Distribution In the Standing-wave Linear Array

The uniformity of the field distribution among the linear standing-wave dielectric array antennas can be verified by multiplying the radiation pattern of the antenna element by the array factor of four isotropic sources located at the same spacing distance as in the proposed linear array. The array factor of the four isotropic sources, shown in Figure 5.62, can be expressed as following:

$$AF = \frac{\sin\left(N\frac{\Psi}{2}\right)}{N \sin\left(\frac{\Psi}{2}\right)} \quad (5 - 1)$$

where  $\Psi = 2\pi d \cos(\theta)/\lambda_o$ ,  $N$  is number of elements,  $d$  is the element spacing.

On the other hand, the element factor was obtained by simulating the radiation pattern of the antenna element resonating in the same higher-order TE<sub>113</sub> mode, as shown in Figure 5.63. The estimated radiation pattern of the proposed standing-wave is then calculated by the multiplication of the ideal isotropic array factor by the element factor. As depicted in Figure 5.64, the simulated radiation pattern of the array is in

excellent agreement with the estimated one. Thus, it can be claimed that the formation of standing-wave can uniformly excite a dielectric resonator array antenna. It is worth mentioning here that slight discrepancies in the simulated radiation pattern are observed away from the boresight direction. This can be related to the mutual coupling between the array elements since the dielectric resonators are cubic entities while the isotropic sources are nothing but dimensionless point sources. Another reason may relate to the radiations coming from the metallic patches, i.e. the radiations coming from the wide edges of the patches.

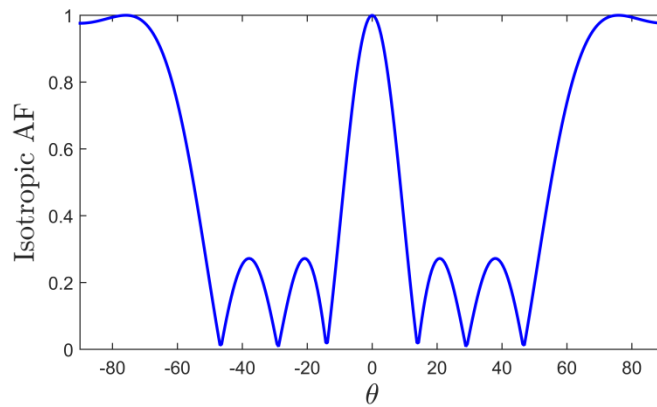


Figure 5.62: Array factor of four equally-spaced isotropic sources

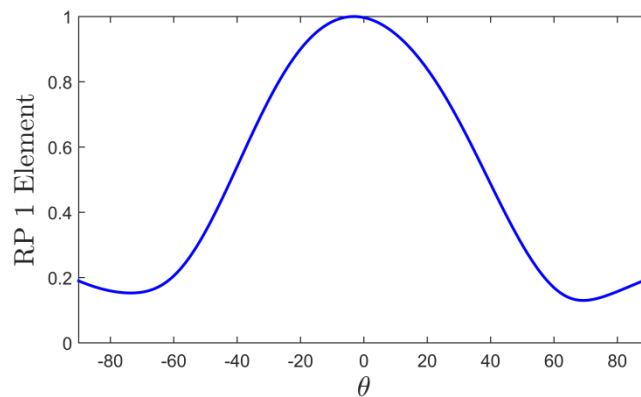


Figure 5.63: Radiation pattern of antenna element (Element factor)

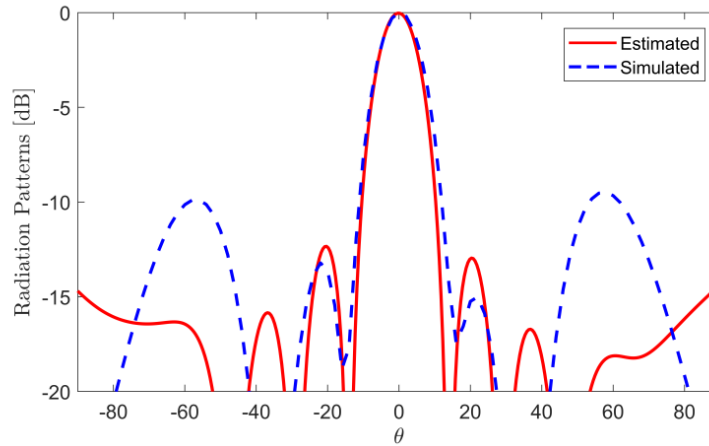


Figure 5.64: Calculated and simulated radiation pattern of 4-element standing-wave dielectric resonator array antenna

The following table summarizes the design parameters of the proposed standing-wave two- and four-element linear array antennas as well as the simulated results.

Table 5.4 Summary of design parameters and performance results of the linear array

Configuration	Dimensions (mm)		$f_o$ (GHz)	Gain (dBi)	Impedance Bandwidth (%)	Radiation Efficiency (%)
Antenna Element	26.2 x 26.2 x 45		3.9	8.8	-----	-----
Two-Element Linear Array	Resonators	26.2x26.2x45.8	3.85	12	4	86.2
	Large Patch	61.5 x 17				
	Small Patches	15 x 17				
Four-Element Linear Array	Resonators	26.2x26.2x45.8	3.9	15	4	81.2
	Large Patches	61.5 x 17				
	Small Patches	15 x 17				
	Vias Radius	4				

### 5.4.5 Summary of the Design Procedure

1. The design process starts by designing a rectangular dielectric resonator antenna that its  $TE_{113}$  mode is realized at the desired operating frequency.
2. Design a microstrip patch so that its length (eventual array elements spacing) corresponds to one and a half waveguide wavelength of that in the dielectric resonator. The operating frequency has to be in consistency with that in Step 1. The optimum patch width can be determined by simulation iterations. Utilize a coaxial probe feeding port at an appropriate location to excite the patch.
3. Add two dielectric resonators (of the same size as in Step 1) on top of the radiating edges of the patch. In order to have the best RF coupling, the overlapping distance  $X_d$  was optimized by simulation.
4. At a distance  $X_g$  from the right and left edges of the main patch, add two more patches of smaller size. Their width has to be consistent with that in Step 2. A number of iterations is needed to find the optimum length. However, the length of these two patches has to be less than the length of the radiating resonators.
5. For potential expansion of array elements, the length of the radiating resonators was defined as a function of the overlapping distance  $X_d$ , the gap between any two patches  $X_g$ , and the length of the smaller patch resides under each resonator. In other words,  $L_r = 2*X_d + 2*X_g + L_{sp}$ . By doing so, the length of the resonators will be slightly modified yet better performance is achieved.
6. To create a four-element array, add two more patches of the same size as in Step 2 at  $X_g$  distance from the radiating edges of the smaller patches designed in Step 4.

7. At the same gap distance  $X_g$  from the outer edges of the patches designed in Step 6, add another two smaller patches of the same size as in Step 4.
  8. At the same locations of the patches in Step 7, add two dielectric resonators so that they reside precisely at the center on top of the patches.
  9. Add a shorting pin to each patch designed in Step 6 to suppress undesired mode.
- The optimum radius and location were found by simulation iterations.



## Chapter 6

### CONCLUSION AND FUTURE PROSPECTS

#### 6.1 Conclusion

The substantial contribution of this dissertation is to prove that the formation of standing-waves inside a dielectric resonator array antenna can be an efficacious feeding mechanism to excite the array structure. Typically, traveling-waves feeding networks used to excite either linear or planar dielectric resonator array antenna consist of numerous quarter-wavelength transmission lines and power dividers which, in turns, lead to high configuration complexity. These power dividers are highly sensitive to the phase change. Additionally, as the operating frequency increases, unfavorable spurious radiations from the feeding network become considerable and passively impact the overall array performance. This dissertation has successfully proposed two different novel dielectric array configurations where a single feeding probe is utilized to excite each array structure.

In the first proposed configuration, low-profile dielectric bridges have been introduced to connect the array elements. The top surface of each bridge is covered by a metallic patch to suppress radiations coming out of the bridges. The array structure is fed using a single coupling aperture resides symmetrically under the center element. When the RF power is coupled to the center element, the waves can be transferred to other array

elements via the dielectric bridges. The waves bounce back and forth inside the array structure forming standing-waves. At the resonant frequency, the interference between these waves becomes constructive; thus the entire structure resonates as a whole. To prove the validity of the concept, two 3-element linear array antennas were first designed and examined by simulation using COMSOL Multiphysics software. The array direction in the first design was chosen to be parallel to the feed line; then it was assumed to be orthogonal in the second one. Due to the field variations inside the center element, the dimensions of the low-profile dielectric bridges are different from one design to another. The results were extensively discussed and demonstrated. Then, the two linear array configurations are combined together to form a planar array with additional four elements being introduced. The proposed 3x3 design provides a realized gain of about 14 dBi at the boresight. The return loss is about -20 dB possessing about 35.7% useful impedance bandwidth. Excellent agreement between the simulation and experimental results is observed.

The second proposed configuration consists of four dielectric resonator antennas forming a linear array. On the top surface of the substrate and between the array elements, there are five metallic patches which are employed to improve exciting the array elements. These patches are slightly extended under the slabs to allow sufficient coupling. Under each dielectric slab, there is one metallic patch reside at the center to further enhance the wave coupling in both directions toward the array elements. The single feeding coaxial probe is attached to the center patch, and its location was optimized to provide excellent impedance matching. The maximum observed gain is 15

dBi at the boresight. The array structure is well matched and the return loss is measured to be -45 dB.

The validity of both designs was observed and demonstrated. One advantageous feature is that the feeding network was extremely simplified to a single port to excite the array structure. For applications at higher frequency bands such as mm-wave applications, these two designs can be easily utilized while maintaining the antenna performance as the microstrip discontinuities and power dividers in the feeding network have been minimized or omitted. Another advantage is that both designs were partially fabricated using 3D printing technology. Therefore, it can be said that the proposed configurations are easy to fabricate since the complexity of designing feeding networks was avoided.

## **6.2 Future prospects**

This dissertation has successfully studied and proposed two novel promising designs for standing-wave dielectric resonator array antennas and provided a proof of the concept for each configuration. Further development of this dissertation can be carried out in several avenues, including but not limited to the following:

1. In certain applications, it is highly required to have arrays producing high gain and pencil-shaped radiation pattern. However, four or nine elements arrays typically produce medium gain. Therefore, it is suggested to increase the number of array elements for further gain enhancement. The dielectric loss factor of the dielectric material strongly impacts the realized gain. Therefore, higher gain can

be observed when utilizing materials with lower dielectric loss tangent such as Quartz and Ceramic.

2. Dielectric resonator antennas are excellent promising candidates to be used at mm-wave applications due to the lack of metallic surfaces. The losses in dielectric array antennas come from the material itself and the feeding network. Therefore, as the proposed design has a simplified feeding network, the losses are limited to the material itself. Therefore, it is suggested to increase the operating frequency to the mm-wave band to fulfill contemporary communication systems requirements and specifications.
3. The first proposed design is based on exciting higher mode inside the elements, i.e.  $TE_{115}$  mode. For certain applications, the size of the array is critical; and compact size is highly preferable. In dielectric resonator antennas, the operating mode can be lowered by reducing the height of the antenna for a given operating frequency. Therefore, a future prospect can be suggested to examine the possibility and validity of applying the same proposed concept on an array operating at lower mode such as  $TE_{113}$  which will result in more compact size.

**Appendix A**

**COMSOL DESIGN PROCEDURE AND RESULTS POST-PROCESSING**

**OF THE PLANAR ARRAY ANTENNA**

The design process can be divided into number of main sections. These sections are module setup, parameters, geometry, definitions, materials, boundary conditions, meshing, and lastly results post-processing. All the design steps in each section will be listed in details.

**I. Module Setup:**

1. Launch COMSOL Multiphysics Software. From the **File** menu, choose **New**. In the **New** window, click **Model Wizard**.
2. In **Model Wizard** window, choose **3D**.
3. From **Select Physics** list, choose **Radio Frequency > Electromagnetic Waves, Frequency Domain (emw)**
4. Click **Add**, and then click **Study**.
5. From **Select Study** list, choose **Preset Studies > Frequency Domain**.
6. Click **Done**.

**II. Parameters**

1. Under **Global Definitions** tab, choose **Parameters**.
2. In the **Settings** window for **Parameters**, enter the following values in the table:

<b>Name</b>	<b>Expression</b>	<b>Value</b>	<b>Description</b>
Thickness	20[mil]	5.08E-4 m	Substrate thickness
L_sub	220[mm]	0.22 m	Substrate length
W_sub	200[mm]	0.2 m	Substrate width
L_line	110[mm]	0.11 m	Feed line length
W_line	1.13[mm]	0.00113 m	Feed line width
L_matching	1.27[mm]	0.00127 m	Matching stub length
W_matching	1.13[mm]	0.00113 m	Matching stub width
L_slot	13.3[mm]	0.0133 m	Coupling slot length
W_slot	11.2[mm]	0.0112 m	Coupling slot width
F0	5.6[GHz]	5.6E9 Hz	Resonant frequency
Lda0	c_const/F0	0.053534 m	Free-space wavelength
H_max	0.2*Lda0	0.010707 m	Maximum mesh element size
Hr1	60.5[mm]	0.0605 m	Resonator 1 height
Lr1	25[mm]	0.025 m	Resonator 1 length
Wr1	25[mm]	0.025 m	Resonator 1 width
Hr2	65[mm]	0.065 m	Resonators 2 height
Lr2	Lr1	0.025 m	Resonators 2 length
Wr2	20[mm]	0.020 m	Resonators 2 width
Hr3	Hr2	0.065 m	Resonators 3 height
Lr3	19.75[mm]	0.01975 m	Resonators 3 length
Wr3	Wr1	0.025 m	Resonators 3 width

Hr4	Hr2	0.065 m	Resonators 4 height
Lr4	Lr3	0.01975 m	Resonators 4 length
Wr4	Wr2	0.020 m	Resonators 4 width
Hvb	8[mm]	0.008 m	Vertical bridge height
Lvb	20[mm]	0.02 m	Vertical bridge length
Wvb	65[mm]	0.065 m	Vertical bridge width
Hhb	2[mm]	0.002 m	Horizontal bridge height
Lhb	30[mm]	0.03 m	Horizontal bridge length
Whb	20[mm]	0.02 m	Horizontal bridge width

### III. Geometry:

- 1) Create a block for the first dielectric resonator (labeled as 1).

#### Block 1 (blk1)

1. On the **Geometry** toolbar, click **Block**.
2. In the **Settings** window for **Block**, type DR1 in the **Label** text field.
3. Under the **Size and Shape** section, type Lr1 in the **Width** text field.
4. Type Wr1 in the **Depth** text field.
5. Type Hr1 in the **Height** text field.
6. In the **Position** section. Choose **Center** from the **Base** list.
7. Type Hr1/2 in the **z** text field.

2) Create a block for the substrate.

### **Block 2 (blk2)**

1. On the **Geometry** toolbar, click **Block**.
2. In the **Settings** window for **Block**, type Substrate in the **Label** text field.
3. Under the **Size and Shape** section, type  $L_{sub}$  in the **Width** text field.
4. Type  $W_{sub}$  in the **Depth** text field.
5. Type Thickness in the **Height** text field.
6. In the **Position** section. Choose **Center** from the **Base** list.
7. Type  $-Thickness/2$  in the **z** text field.

3) Create a block for the microstrip line.

### **Block 3 (blk3)**

1. On the **Geometry** toolbar, click **Block**.
2. In the **Settings** window for **Block**, type Feed Line in the **Label** text field.
3. Under the **Size and Shape** section, type  $W_{line}$  in the **Width** text field.
4. Type  $L_{line}$  in the **Depth** text field.
5. Type Thickness in the **Height** text field.
6. In the **Position** section. Choose **Center** from the **Base** list.
7. Type  $-L_{line}/2$  in the **y** text field.
8. Type  $-Thickness/2$  in the **z** text field.



- 4) Create a block for the matching stub which starts at the end of the feed line in the y-axis.

#### **Block 4 (blk4)**

1. On the **Geometry** toolbar, click **Block**.
2. In the **Settings** window for **Block**, type Matching Stub in the **Label** text field.
3. Under the **Size and Shape** section, type  $W_{\text{matching}}$  in the **Width** text field.
4. Type  $L_{\text{matching}}$  in the **Depth** text field.
5. Type Thickness in the **Height** text field.
6. In the **Position** section. Choose **Center** from the **Base** list.
7. Type  $L_{\text{matching}}/2$  in the **y** text field.
8. Type  $-Thickness/2$  in the **z** text field.

- 5) Create a sphere for the PMLs.

#### **Sphere 1 (sph1)**

1. On the **Geometry** toolbar, click **Sphere**.
2. In the **Settings** window for **Sphere**, type PMLs in the **Label** text field.
3. Under the **Size and Shape** section, type 0.18 in the **Radius** text field.
4. Click **Layers** section. Then enter Layer 1 under the **Layer name** and 0.02 under the **Thickness (m)**.
- 6) Create a block for the second dielectric resonator (labeled as 3 Right).

### **Block 5 (blk5)**

1. On the **Geometry** toolbar, click **Block**.
  2. In the **Settings** window for **Block**, type DR3R in the **Label** text field.
  3. Under the **Size and Shape** section, type Lr3 in the **Width** text field.
  4. Type Wr3 in the **Depth** text field.
  5. Type Hr3 in the **Height** text field.
  6. In the **Position** section. Choose **Center** from the **Base** list.
  7. Type  $(Lr1/2+Lr3/2+Lhb)$  in the **x** text field.
  8. Type  $Hr3/2$  in the **z** text field.
- 7) Create a block for the third dielectric resonator (labeled as 2 Top).

### **Block 6 (blk6)**

1. On the **Geometry** toolbar, click **Block**.
  2. In the **Settings** window for **Block**, type DR2T in the **Label** text field.
  3. Under the **Size and Shape** section, type Lr2 in the **Width** text field.
  4. Type Wr2 in the **Depth** text field.
  5. Type Hr2 in the **Height** text field.
  6. In the **Position** section. Choose **Center** from the **Base** list.
  7. Type  $(Wr1/2+W2/2+Wvb)$  in the **y** text field.
  8. Type  $Hr2/2$  in the **z** text field.
- 8) Create a block for the fourth dielectric resonator (labeled as 3 Left).

### **Block 7 (blk7)**

1. On the **Geometry** toolbar, click **Block**.
  2. In the **Settings** window for **Block**, type DR3L in the **Label** text field.
  3. Under the **Size and Shape** section, type Lr3 in the **Width** text field.
  4. Type Wr3 in the **Depth** text field.
  5. Type Hr3 in the **Height** text field.
  6. In the **Position** section. Choose **Center** from the **Base** list.
  7. Type  $-(Lr1/2+Lr3/2+Lhb)$  in the **x** text field.
  8. Type  $Hr3/2$  in the **z** text field.
- 9) Create a block for the fifth dielectric resonator (labeled as 2 Bottom).

### **Block 8 (blk8)**

1. On the **Geometry** toolbar, click **Block**.
  2. In the **Settings** window for **Block**, type DR2B in the **Label** text field.
  3. Under the **Size and Shape** section, type Lr2 in the **Width** text field.
  4. Type Wr2 in the **Depth** text field.
  5. Type Hr2 in the **Height** text field.
  6. In the **Position** section. Choose **Center** from the **Base** list.
  7. Type  $-(Wr1/2+W2/2+Wvb)$  in the **y** text field.
  8. Type  $Hr2/2$  in the **z** text field.
- 10) Create a block for the horizontal bridge connecting DR1 and DR3R

### **Block 9 (blk9)**

1. On the **Geometry** toolbar, click **Block**.
  2. In the **Settings** window for **Block**, type HB (DR1 and DR3R) in the **Label** text field.
  3. Under the **Size and Shape** section, type Lhb in the **Width** text field.
  4. Type Whb in the **Depth** text field.
  5. Type Hhb in the **Height** text field.
  6. In the **Position** section. Choose **Center** from the **Base** list.
  7. Type  $(Lr1/2+Lhb/2)$  in the **x** text field.
  8. Type  $Hhb/2$  in the **z** text field.
- 11) Create a block for the vertical bridge connecting DR1 and DR2T

### **Block 10 (blk10)**

1. On the **Geometry** toolbar, click **Block**.
2. In the **Settings** window for **Block**, type VB (DR1 and DR2T) in the **Label** text field.
3. Under the **Size and Shape** section, type Lvb in the **Width** text field.
4. Type Wvb in the **Depth** text field.
5. Type Hvb in the **Height** text field.
6. In the **Position** section. Choose **Center** from the **Base** list.
7. Type  $(Wr1/2+Wvb/2)$  in the **y** text field.
8. Type  $Hvb/2$  in the **z** text field.

12) Create a block for the horizontal bridge connecting DR1 and DR3L

**Block 11 (blk11)**

1. On the **Geometry** toolbar, click **Block**.
2. In the **Settings** window for **Block**, type HB (DR1 and DR3L) in the **Label** text field.
3. Under the **Size and Shape** section, type Lhb in the **Width** text field.
4. Type Whb in the **Depth** text field.
5. Type Hhb in the **Height** text field.
6. In the **Position** section. Choose **Center** from the **Base** list.
7. Type  $-(Lr1/2+Lhb/2)$  in the **x** text field.
8. Type  $Hhb/2$  in the **z** text field.

13) Create a block for the vertical bridge connecting DR1 and DR2B

**Block 12 (blk12)**

1. On the **Geometry** toolbar, click **Block**.
2. In the **Settings** window for **Block**, type VB (DR1 and DR2B) in the **Label** text field.
3. Under the **Size and Shape** section, type Lvb in the **Width** text field.
4. Type Wvb in the **Depth** text field.
5. Type Hvb in the **Height** text field.
6. In the **Position** section. Choose **Center** from the **Base** list.

7. Type  $-(W_{r1}/2+W_{vb}/2)$  in the **y** text field.
  8. Type  $H_{vb}/2$  in the **z** text field.
- 14) Create the work plane for the coupling slot which is located between the central resonator (DR1) and the substrate.

### **Work Plane 1 (wp1)**

1. On the **Geometry** toolbar, click **Work Plane**.
2. In the **Settings** window for **Work Plane**, click **Show Work Plane**.

### **Plane Geometry**

Create a rectangle for the coupling slot.

### **Rectangle 1 (r1)**

1. On the **Work Plane** toolbar, click **Primitives** and choose **Rectangle**.
  2. Click the **Zoom Extents** button on the **Graphics** toolbar.
  3. In the Settings window for Rectangle, locate the Size and Shape section.
  4. Type  $L_{\text{slot}}$  in the Width text field.
  5. Type  $W_{\text{slot}}$  in the Height text field.
  6. In the **Position** section. Choose **Center** from the **Base** list.
- 15) Create a block for the sixth dielectric resonator (labeled as 4 Top Right).

### **Block 13 (blk13)**

1. On the **Geometry** toolbar, click **Block**.

2. In the **Settings** window for **Block**, type DR4TR in the **Label** text field.
  3. Under the **Size and Shape** section, type Lr4 in the **Width** text field.
  4. Type Wr4 in the **Depth** text field.
  5. Type Hr4 in the **Height** text field.
  6. In the **Position** section. Choose **Center** from the **Base** list.
  7. Type  $(Lr1/2+Lr4/2+Lhb)$  in the **x** text field.
  8. Type  $(Wr1/2+W4/2+Wvb)$  in the **y** text field.
  9. Type  $Hr4/2$  in the **z** text field.
- 16) Create a block for the seventh dielectric resonator (labeled as 4 Top Left).

#### **Block 14 (blk14)**

1. On the **Geometry** toolbar, click **Block**.
  2. In the **Settings** window for **Block**, type DR4TL in the **Label** text field.
  3. Under the **Size and Shape** section, type Lr4 in the **Width** text field.
  4. Type Wr4 in the **Depth** text field.
  5. Type Hr4 in the **Height** text field.
  6. In the **Position** section. Choose **Center** from the **Base** list.
  7. Type  $-(Lr1/2+Lr4/2+Lhb)$  in the **x** text field.
  8. Type  $(Wr1/2+W4/2+Wvb)$  in the **y** text field.
  9. Type  $Hr4/2$  in the **z** text field.
- 17) Create a block for the eighth dielectric resonator (labeled as 4 Bottom Left).

### Block 15 (blk15)

1. On the **Geometry** toolbar, click **Block**.
  2. In the **Settings** window for **Block**, type DR4BL in the **Label** text field.
  3. Under the **Size and Shape** section, type Lr4 in the **Width** text field.
  4. Type Wr4 in the **Depth** text field.
  5. Type Hr4 in the **Height** text field.
  6. In the **Position** section. Choose **Center** from the **Base** list.
  7. Type  $-(Lr1/2+Lr4/2+Lhb)$  in the **x** text field.
  8. Type  $-(Wr1/2+W4/2+Wvb)$  in the **y** text field.
  9. Type  $Hr4/2$  in the **z** text field.
- 18) Create a block for the ninth dielectric resonator (labeled as 4 Bottom Right).

### Block 16 (blk16)

1. On the **Geometry** toolbar, click **Block**.
2. In the **Settings** window for **Block**, type DR4BR in the **Label** text field.
3. Under the **Size and Shape** section, type Lr4 in the **Width** text field.
4. Type Wr4 in the **Depth** text field.
5. Type Hr4 in the **Height** text field.
6. In the **Position** section. Choose **Center** from the **Base** list.
7. Type  $(Lr1/2+Lr4/2+Lhb)$  in the **x** text field.
8. Type  $-(Wr1/2+W4/2+Wvb)$  in the **y** text field.
9. Type  $Hr4/2$  in the **z** text field.



19) Create a block for the horizontal bridge connecting DR2T and DR4TR.

**Block 17 (blk17)**

1. On the **Geometry** toolbar, click **Block**.
2. In the **Settings** window for **Block**, type HB (DR2T and DR4TR) in the **Label** text field.
3. Under the **Size and Shape** section, type Lhb in the **Width** text field.
4. Type Whb in the **Depth** text field.
5. Type Hhb in the **Height** text field.
6. In the **Position** section. Choose **Center** from the **Base** list.
7. Type  $(Lr1/2+Lhb/2)$  in the **x** text field.
8. Type  $(Wr1/2+Wr2/2+Wvb)$  in the **y** text field.
9. Type  $Hhb/2$  in the **z** text field.

20) Create a block for the horizontal bridge connecting DR2B and DR4BR.

**Block 18 (blk18)**

1. On the **Geometry** toolbar, click **Block**.
2. In the **Settings** window for **Block**, type HB (DR2B and DR4BR) in the **Label** text field.
3. Under the **Size and Shape** section, type Lhb in the **Width** text field.
4. Type Whb in the **Depth** text field.
5. Type Hhb in the **Height** text field.

6. In the **Position** section. Choose **Center** from the **Base** list.
  7. Type  $(Lr1/2+Lhb/2)$  in the **x** text field.
  8. Type  $-(Wr1/2+Wr2/2+Wvb)$  in the **y** text field.
  9. Type  $Hhb/2$  in the **z** text field.
- 21) Create a block for the horizontal bridge connecting DR2T and DR4TL.

**Block 19 (blk19)**

1. On the **Geometry** toolbar, click **Block**.
2. In the **Settings** window for **Block**, type HB (DR2T and DR4TL) in the **Label** text field.
3. Under the **Size and Shape** section, type Lhb in the **Width** text field.
4. Type Whb in the **Depth** text field.
5. Type Hhb in the **Height** text field.
6. In the **Position** section. Choose **Center** from the **Base** list.
7. Type  $-(Lr1/2+Lhb/2)$  in the **x** text field.
8. Type  $(Wr1/2+Wr2/2+Wvb)$  in the **y** text field.
9. Type  $Hhb/2$  in the **z** text field.

- 22) Create a block for the horizontal bridge connecting DR2B and DR4BL.

**Block 20 (blk20)**

1. On the **Geometry** toolbar, click **Block**.

2. In the **Settings** window for **Block**, type HB (DR2B and DR4BL) in the **Label** text field.
3. Under the **Size and Shape** section, type Lhb in the **Width** text field.
4. Type Whb in the **Depth** text field.
5. Type Hhb in the **Height** text field.
6. In the **Position** section. Choose **Center** from the **Base** list.
7. Type  $-(Lr1/2+Lhb/2)$  in the **x** text field.
8. Type  $-(Wr1/2+Wr2/2+Wvb)$  in the **y** text field.
9. Type  $Hhb/2$  in the **z** text field.

23) Create a block for the vertical bridge connecting DR3R and DR4TR.

### **Block 21 (blk21)**

1. On the **Geometry** toolbar, click **Block**.
2. In the **Settings** window for **Block**, type VB (DR3R and DR4TR) in the **Label** text field.
3. Under the **Size and Shape** section, type Lvb in the **Width** text field.
4. Type Wvb in the **Depth** text field.
5. Type Hvb in the **Height** text field.
6. In the **Position** section. Choose **Center** from the **Base** list.
7. Type  $(Lr1/2+Lr3/2+Lhb)$  in the **x** text field.
8. Type  $(Wr1/2+Wvb/2)$  in the **y** text field.
9. Type  $Hvb/2$  in the **z** text field.

24) Create a block for the vertical bridge connecting DR3R and DR4BR.

**Block 22 (blk22)**

1. On the **Geometry** toolbar, click **Block**.
2. In the **Settings** window for **Block**, type VB (DR3R and DR4BR) in the **Label** text field.
3. Under the **Size and Shape** section, type Lvb in the **Width** text field.
4. Type Wvb in the **Depth** text field.
5. Type Hvb in the **Height** text field.
6. In the **Position** section. Choose **Center** from the **Base** list.
7. Type  $(Lr1/2+Lr3/2+Lhb)$  in the **x** text field.
8. Type  $-(Wr1/2+Wvb/2)$  in the **y** text field.
9. Type  $Hvb/2$  in the **z** text field.

25) Create a block for the vertical bridge connecting DR3L and DR4BL.

**Block 23 (blk23)**

1. On the **Geometry** toolbar, click **Block**.
2. In the **Settings** window for **Block**, type VB (DR3L and DR4BL) in the **Label** text field.
3. Under the **Size and Shape** section, type Lvb in the **Width** text field.
4. Type Wvb in the **Depth** text field.
5. Type Hvb in the **Height** text field.

6. In the **Position** section. Choose **Center** from the **Base** list.
  7. Type  $-(Lr1/2+Lr3/2+Lhb)$  in the **x** text field.
  8. Type  $-(Wr1/2+Wvb/2)$  in the **y** text field.
  9. Type  $Hvb/2$  in the **z** text field.
- 26) Create a block for the vertical bridge connecting DR3L and DR4TL.

**Block 24 (blk24)**

1. On the **Geometry** toolbar, click **Block**.
2. In the **Settings** window for **Block**, type VB (DR3L and DR4TL) in the **Label** text field.
3. Under the **Size and Shape** section, type  $Lvb$  in the **Width** text field.
4. Type  $Wvb$  in the **Depth** text field.
5. Type  $Hvb$  in the **Height** text field.
6. In the **Position** section. Choose **Center** from the **Base** list.
7. Type  $-(Lr1/2+Lr3/2+Lhb)$  in the **x** text field.
8. Type  $(Wr1/2+Wvb/2)$  in the **y** text field.
9. Type  $Hvb/2$  in the **z** text field.

Click **Build All Objects** to build the array structure. The Geometry tab should look like Figure A1.

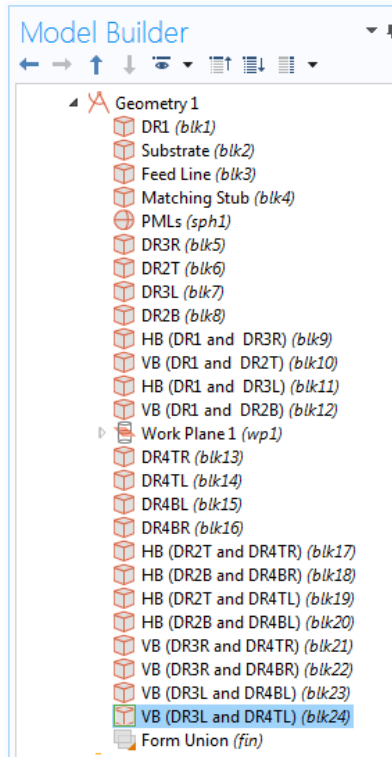


Figure A1: Geometry tab in COMSOL Multiphysics Software

#### IV. Definitions:

- 1) Create a set of selections for the PMLs.

##### Explicit 1

1. On the **Definitions** toolbar, choose **Explicit**.
2. In the **Settings** window for **Explicit**, type PMLs in the **Label** text field.
3. Select Domains 1-4, 22-25 only.

- 2) Create a set of selections for the Substrate.

##### Explicit 2

1. On the **Definitions** toolbar, choose **Explicit**.

2. In the **Settings** window for **Explicit**, type Substrate in the **Label** text field.
  3. Select Domains 6, 20, and 21 only.
- 3) Create a set of selections for the Dielectric Resonators and Bridges.

### **Explicit 3**

1. On the **Definitions** toolbar, choose **Explicit**.
  2. In the **Settings** window for **Explicit**, type Dielectric Resonators and Bridges in the **Label** text field.
  3. Select Domains 7-19 and 26-33 only.
- 4) Create a set of selections for the Feed Line.

### **Explicit 4**

1. On the **Definitions** toolbar, choose **Explicit**.
  2. In the **Settings** window for **Explicit**, type Feed Line in the **Label** text field.
  3. Locate the **Input Entities** section.
  4. Choose **Boundary** from the **Geometric entity level** list.
  5. Select Boundaries 106 and 112 only.
- 5) Create a set of selections for the Ground Plane.

### **Explicit 5**

1. On the **Definitions** toolbar, choose **Explicit**.

2. In the **Settings** window for **Explicit**, type Ground Plane in the **Label** text field.
  3. Locate the **Input Entities** section.
  4. Choose **Boundary** from the **Geometric entity level** list.
  5. Select Boundaries 16, 20, 25, 30, 36, 43, 49, 56, 59, 62, 66, 77, 83, 89, 95, 100, 107-108, 134, 136, 139, 146, 151, 157, 163, 169, 176, and 184 only.
- 6) Create a set of selections for the Scattering Boundaries.

### **Explicit 6**

1. On the **Definitions** toolbar, choose **Explicit**.
  2. In the **Settings** window for **Explicit**, type Scattering Boundaries in the **Label** text field.
  3. Locate the **Input Entities** section.
  4. Choose **Boundary** from the **Geometric entity level** list.
  5. Select Boundaries 5-8, 118-119, 124, and 129 only.
- 7) Create a set of selections for the Far Field Boundaries.

### **Explicit 7**

1. On the **Definitions** toolbar, choose **Explicit**.
2. In the **Settings** window for **Explicit**, type Far Field Boundaries in the **Label** text field.
3. Locate the **Input Entities** section.
4. Choose **Boundary** from the **Geometric entity level** list.



5. Select Boundaries 9-12, 120-121, 125, and 128 only.

8) Create a set of selections for the Metallic Sheets.

### **Explicit 8**

1. On the **Definitions** toolbar, choose **Explicit**.

2. In the **Settings** window for **Explicit**, type Metallic Sheets in the **Label** text field.

3. Locate the **Input Entities** section.

4. Choose **Boundary** from the **Geometric entity level** list.

5. Select Boundaries 21, 26, 51, 60, 69, 96, 101, 141, 147, 153, 159, and 164 only.

9) Create a set of selections for the Far Field Region.

### **Complement 1**

1. On the **Definitions** toolbar, choose **Complement**.

2. In the **Settings** window for **Complement**, type Far Field Region in the **Label** text field.

3. Locate the **Input Entities** section.

4. Type PMLs in the **Selections to invert** text field.

10) Create Perfectly Matched Layer.

### **Perfectly Matched Layer 1 (pml1)**

1. On the **Definitions** toolbar, choose **Perfectly Matched Layer**.

2. Select Domains 1-4 and 22-25 only.
3. In the **Settings** window for **Perfectly Matched Layer**, locate the **Geometry** section.
4. Choose **Spherical** from the **Type** list.

The Definitions tab should look like Figure A2.

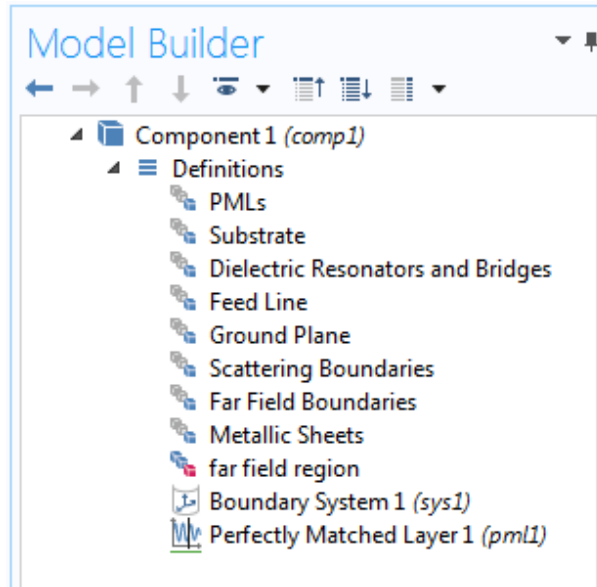


Figure A2: Definitions tab in COMSOL Multiphysics Software

## V. Materials:

Assign the materials properties on the model. Start by assigning air for all domains.

- 1) Add Air material.

### Material 1 (mat1)

1. On the **Home** toolbar, choose **Add Material** to open the **Add Material** window.
2. Go to the **Add Material** window. In the tree, choose **Built-In** > **Air**
3. Click **Add to Component** in the window toolbar.

- 2) Add Substrate material.

**Material 2 (mat2)**

1. In the **Model Builder** window, under **Component 1 (comp1)** right-click **Materials** and choose **Blank Material**.
2. In the **Settings** window for **Material**, type Arlon 25N in the **Label** text field.
3. Locate the **Geometric Entity Selections** section. Choose **Substrate** from the **Selection** list.
4. Locate the **Material Contents** section. Enter the following values:

Property	Name	Value	Unit	Property group
Relative permittivity	epsilon <sub>r</sub>	$3.38*(1-j*0.0015)$	1	Basic
Relative permeability	mu <sub>r</sub>	1	1	Basic
Electrical conductivity	sigma	0	S/m	Basic

- 3) Add Dielectric Resonators and Bridges material.

**Material 3 (mat3)**

1. In the **Model Builder** window, under **Component 1 (comp1)** right-click **Materials** and choose **Blank Material**.
2. In the **Settings** window for **Material**, type PLA in the **Label** text field.
3. Locate the **Geometric Entity Selections** section. Choose **Dielectric Resonators and Bridges** from the **Selection** list.

4. Locate the **Material Contents** section. Enter the following values:

Property	Name	Value	Unit	Property group
Relative permittivity	epsilon <sub>r</sub>	$2.5*(1-j*0.005)$	1	Basic
Relative permeability	mu <sub>r</sub>	1	1	Basic
Electrical conductivity	sigma	0	S/m	Basic

## VI. Boundary Conditions:

Assign the boundary conditions on the array structure.

- 1) Assign the Ground Plane surface.

### Perfect Electric Conductor 2

1. In the **Model Builder** window, go to **Component 1 (comp 1) > Electromagnetic Waves, Frequency Domain (emw)**.
2. Right-click and choose **Perfect Electric Conductor**.
3. In the Settings window for **Perfect Electric Conductor 2**, type Ground Plane in the **Label** text field.
4. In the **Boundary Selection** section, choose **Ground Plane** from the **Selection** list.

- 2) Assign the Metallic Sheets surfaces.

### Perfect Electric Conductor 3

1. In the **Model Builder** window, go to **Component 1 (comp 1) > Electromagnetic Waves, Frequency Domain (emw)**.
  2. Right-click and choose **Perfect Electric Conductor**.
  3. In the Settings window for **Perfect Electric Conductor 3**, type Metallic Sheets in the **Label** text field.
  4. In the **Boundary Selection** section, choose **Metallic Sheets** from the **Selection** list.
- 3) Assign the Feed Line and Matching Stub surfaces.

#### **Perfect Electric Conductor 4**

1. In the **Model Builder** window, go to **Component 1 (comp 1) > Electromagnetic Waves, Frequency Domain (emw)**.
  2. Right-click and choose **Perfect Electric Conductor**.
  3. In the Settings window for **Perfect Electric Conductor 4**, type Feed Line in the **Label** text field.
  4. In **Boundary Selection** section, choose **Feed Line** from the **Selection** list.
- 4) Assign the Feed Port surface.

#### **Lumped Port 1**

1. In the **Model Builder** window, go to **Component 1 (comp 1) > Electromagnetic Waves, Frequency Domain (emw)**.
2. Right-click and choose **Lumped Port**.

3. In the Settings window for **Lumped Port 1**, locate **Boundary Selection** and choose boundary number 105 only
  4. In the **Lumped Port properties** section, choose **Uniform** from the **Type of lumped port** list.
  5. Choose **Cable** from the **Terminal type** list.
  6. Choose **On** from the **Wave excitation at this port** list.
  7. Type 1[V] in the text field of the **Voltage**.
- 5) Assign the Scattering Boundary Conditions.

#### **Scattering Boundary Condition 1**

1. In the **Model Builder** window, go to **Component 1 (comp 1) > Electromagnetic Waves, Frequency Domain (emw)**.
  2. Right-click and choose **Scattering Boundary Condition**.
  3. In the **Boundary Selection** section, choose **Scattering Boundaries** from the **Selection** list.
- 6) Assign the Far Field Region.

#### **Far Field Domain 1**

1. In the **Model Builder** window, go to **Component 1 (comp 1) > Electromagnetic Waves, Frequency Domain (emw)**.
2. Right-click and choose **Far-Field Domain**.

3. In the **Domain Selection** section, choose **Far Field Region** from the **Selection** list.

The Electromagnetic Waves, Frequency Domain (emw) tab should look like Figure A3.

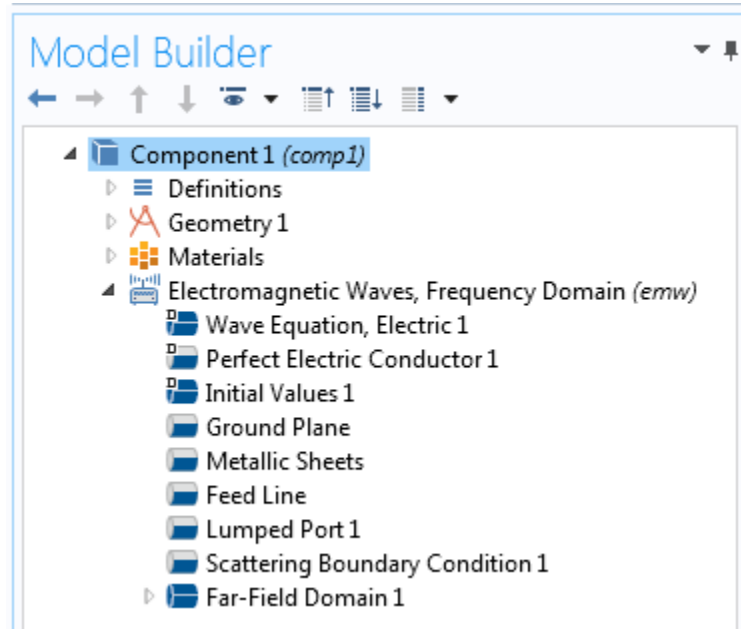


Figure A3: Electromagnetic Waves, Frequency Domain (emw) tab in COMSOL  
Multiphysics Software

## VII. Meshing:

Choose the maximum mesh size in the air domain smaller than 0.2 wavelengths using the parameter **H\_max** that was defined earlier. For other materials, scale the mesh size by the inverse of the square root of the relative permittivity.

- 1) Mesh the Far Field Region.

### Size 1

1. In the **Model Builder** window, under **Component 1 (comp 1)** right-click **Mesh 1** and choose **Size**.
2. In the **Settings** window for **Size 1**, locate the **Geometric Entity Selection** section.
3. Choose **Domain** from the **Geometric entity level** list.
4. Choose **Far Field Region** from the **Selection** list.
5. Locate **Element Size** section, click the **Custom** button.
6. Locate the **Element Size Parameters** section, then select the **Maximum element size** check box.
7. Type  $H_{max}$  in the associated text field.

2) Mesh the Substrate.

## **Size 2**

1. In the **Model Builder** window, under **Component 1 (comp 1)** right-click **Mesh 1** and choose **Size**.
2. In the **Settings** window for **Size 2**, locate the **Geometric Entity Selection** section.
3. Choose **Domain** from the **Geometric entity level** list.
4. Choose **Substrate** from the **Selection** list.
5. Locate **Element Size** section, click the **Custom** button.
6. Locate the **Element Size Parameters** section, then select the **Maximum element size** check box.
7. Type  $H_{max}/\sqrt{3.38}$  in the associated text field.



- 3) Mesh the Dielectric Resonators and Bridges.

### **Size 3**

1. In the **Model Builder** window, under **Component 1 (comp 1)** right-click **Mesh 1** and choose **Size**.
2. In the **Settings** window for **Size 3**, locate the **Geometric Entity Selection** section.
3. Choose **Domain** from the **Geometric entity level** list.
4. Choose **Dielectric Resonators and Bridges** from the **Selection** list.
5. Locate **Element Size** section, click the **Custom** button.
6. Locate the **Element Size Parameters** section, then select the **Maximum element size** check box.
7. Type  $H_{\max}/\sqrt{2.5}$  in the associated text field.

### **Free Tetrahedral 1**

1. In the **Model Builder** window, under **Component 1 (comp 1)** right-click **Mesh 1** and choose **Free Tetrahedral**.
2. In the **Settings** window for **Free Tetrahedral 1**, locate the **Geometric Entity Selection** section.
3. Choose **Domain** from the **Geometric entity level** list.
4. Click **Paste Selection**.
5. In the **Paste Selection** dialog box, type 5-21, 26-33 in the **Selection** text field.
6. Click **OK**.

### **Distribution 1**

1. Right-click **Mesh 1** and choose **Swept**.
2. In the **Model Builder** window, under **Component 1 (comp 1) > Mesh 1** right-click **Swept 1** and choose **Distribution**.
3. In the **Settings** window for **Distribution**, click **Build All**.

The Mesh tab should look like Figure A4.

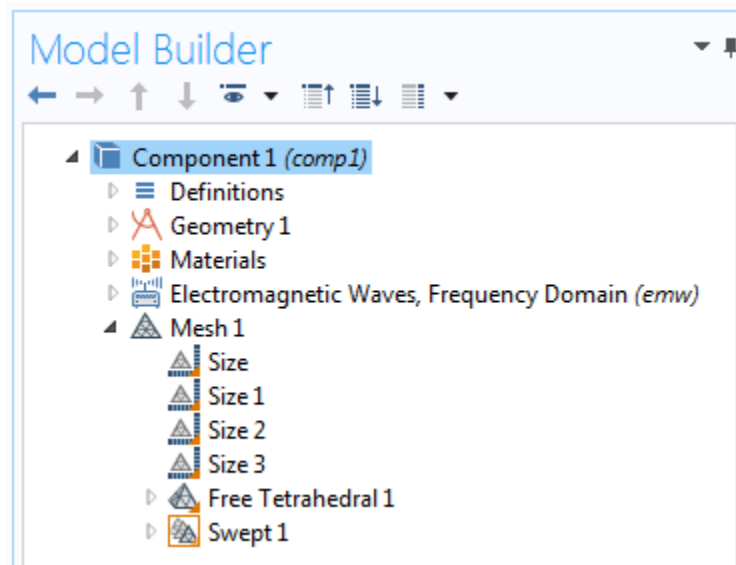


Figure A4: Mesh tab in COMSOL Multiphysics Software

## VIII. Result Post-processing:

To generate the results data, it is required to run the simulation.

### Study 1

#### Step 1: Frequency Domain

1. In the **Settings** window for **Frequency Domain**, locate the **Study Settings** section.
2. In the **Frequencies** text field, type `range(5[GHz],0.1[GHz],7[GHz])`

3. Click **Compute** on the **Home** toolbar.

## **Results**

- 1) Plot the Return Loss response as a function of frequency.

### **S-parameter, S11 dB (emw)**

1. On the **Results** toolbar, locate the **Derived Values**.
2. Right-click and choose **Global Evaluation**.
3. In the **Settings** window for **Global Evaluation**, click **Replace Expression** in the upper-right corner of the **Expression** section.
4. From the menu, choose **Component 1 > Electromagnetic Waves, Frequency Domain > Ports > emw.S11dB – S11**.
5. Click **Evaluate**.
6. In the **Graphics** window, choose **Table 1** and click **Table Graph** to plot the response (Figure 5.39 Simulated curve).

- 2) Plot the Gain response as a function of frequency.

### **Far-field Gain, dBi**

1. On the **Results** toolbar, locate the **Derived Values**.
2. Right-click and choose **Maximum > Surface Maximum**.
3. In the **Settings** window for **Surface Maximum**, choose **Far Field Boundaries** from the **Selection** list.
4. Click **Replace Expression** in the upper-right corner of the **Expression** section.

5. From the menu, choose **Component 1 > Electromagnetic Waves, Frequency Domain > Far field > emw.gainBEfar – Far-Field gain, dBi**.
6. Click **Evaluate**.
7. In the **Graphics** window, choose **Table 2** and click **Table Graph** to plot the response (Figure 5.40 Simulated curve).

3) Plot the 3D Far-field Radiation Pattern.

### **3D Far Field (emw)**

1. On the **Results** toolbar, locate the **3D Far Field (emw)**.
2. Expand it and click **Far Field 1**.
3. In the **Settings** window for **Far Field**, choose **Study1/Solution 1 (sol1)** from the **Data set** list in the **Data** section.
4. Choose the resonant frequency value from the **Parameter value (freq(GHz))**.
5. Click **Replace Expression** in the upper-right corner of the **Expression** section.
6. From the menu, choose **Component 1 > Electromagnetic Waves, Frequency Domain > Far field > emw.normEfar– Far-field norm**.
7. Locate **Evaluation** section, type 360 in both  **$\theta$  resolution** and  **$\phi$  resolution** text field.
8. Click **Evaluate** to depict the 3D far field radiation pattern (Figure 5.32).

4) Plot the 2D Far-field Radiation Patterns.

### **2D Far Field (emw)**

1. On the **Results** toolbar, locate the **2D Far Field (emw)**.
2. Expand it and click **Far Field 1**.
3. In the **Settings** window for **Far Field**, choose **Study1/Solution 1 (sol1)** from the **Data set** list in the **Data** section.
4. Choose the resonant frequency value from the **Parameter value (freq(GHz))**.
5. Click **Replace Expression** in the upper-right corner of the **Expression** section.
6. From the menu, choose **Component 1 > Electromagnetic Waves, Frequency Domain > Far field > emw.normEfar– Far-field norm**.
7. Locate **Evaluation** section, type 360 in the  **$\phi$  resolution** text field.
8. Find the **Normal** subsection, type 1 in the **x** text field.
9. Locate **Legends** section, check the **Show legends** box.
10. Choose **Manual** from the **Legends** list and type Y-Z Plane in the **Legends** text field.
11. Click **Plot** to depict the far field radiations in the y-z plane.
12. To plot the far field radiations in the x-z plane, repeat steps 1 to 7.
13. Then, find the **Reference direction** subsection, type -1 in the **x** text field.
14. Locate the **Normal** subsection, type 1 in the **y** text field.
15. Locate **Legends** section, check the **Show legends** box.
16. Choose **Manual** from the **Legends** list and type X-Z Plane in the **Legends** text field.
17. Click **Plot** to depict the far field radiations in the x-z plane (Figure 5.33).

5) Plot the 3D Field Distribution.

### **3D Arrow Volume 1**

1. On the **Results** toolbar, right-click and choose **3D Plot Group**.
2. Right-click it and choose **Arrow Volume 1**.
3. In the **Settings** window for **Arrow Volume**, choose **Study1/Solution 1 (sol1)** from the **Data set** list in the **Data** section.
4. Choose the resonant frequency value from the **Parameter value (freq(GHz))**.
5. Locate the **Arrow Positioning** section.
6. Type 80 in the **Points** text field for all **x grid points**, **y grid points**, and **z grid points** subsections.
7. Click **Plot** to depict the 3D field distribution inside the array cavity (Figure 5.34).

**Appendix B**

**COMSOL DESIGN PROCEDURE AND RESULTS POST-PROCESSING  
OF THE LINEAR ARRAY ANTENNA**

The design process can be divided into number of main sections. These sections are module setup, parameters, geometry, definitions, materials, boundary conditions, meshing, and lastly results post-processing. All the design steps in each section will be listed in details.

**I. Module Setup:**

1. Launch COMSOL Multiphysics Software. From the **File** menu, choose **New**. In the **New** window, click **Model Wizard**.
2. In **Model Wizard** window, choose **3D**.
3. From **Select Physics** list, choose **Radio Frequency > Electromagnetic Waves, Frequency Domain (emw)**
4. Click **Add**, and then click **Study**.
5. From **Select Study** list, choose **Preset Studies > Frequency Domain**.
6. Click **Done**.

**II. Parameters**

1. Under **Global Definitions** tab, choose **Parameters**.
2. In the **Settings** window for **Parameters**, enter the following values in the table:

<b>Name</b>	<b>Expression</b>	<b>Value</b>	<b>Description</b>
Thickness	62[mil]	0.0015748 m	Substrate thickness
L_sub	400[mm]	0.4 m	Substrate length
W_sub	200[mm]	0.2 m	Substrate width
Lp	61.5[mm]	0.0615 m	Large Patch length
Wp	17[mm]	0.017 m	Large Patch width
Lsp	15[mm]	0.015 m	Small Patch length
F0	3.9[GHz]	3.9E9 Hz	Resonant frequency
Lda0	c_const/F0	0.07687 m	Free-space wavelength
H_max	0.2*Lda0	0.015374 m	Maximum mesh element size
Hr	45.8[mm]	0.0458 m	Resonators height
Lr	26.2[mm]	0.0262 m	Resonators length
Wr	26.2[mm]	0.0262 m	Resonators width
L	20[mm]	0.02 m	SMA Connector height
R	2.124[mm]	0.002124 m	SMA Connector radius
R	0.635[mm]	0.000635 m	Inner Connector radius
Xo	7.6[mm]	0.0076 m	Coaxial Probe offset distance
Xd	4.2[mm]	0.0042 m	Resonator overlapping distance
Xg	1.4[mm]	0.0014 m	Patches Gap size
Xv	22[mm]	0.022 m	Vias offset distance
Rv	4[mm]	0.004 m	Vias radius



### III. Geometry:

- 1) Create a block for the substrate.

#### **Block 1 (blk1)**

1. On the **Geometry** toolbar, click **Block**.
2. In the **Settings** window for **Block**, type Substrate in the **Label** text field.
3. Under the **Size and Shape** section, type L\_sub in the **Width** text field.
4. Type W\_sub in the **Depth** text field.
5. Type Thickness in the **Height** text field.
6. In the **Position** section. Choose **Center** from the **Base** list.
7. Type 0 in the **x**, **y**, and **z** text field.

- 2) Create a block for the central large patch.

#### **Block 2 (blk2)**

1. On the **Geometry** toolbar, click **Block**.
2. In the **Settings** window for **Block**, type Large Patch C in the **Label** text field.
3. Under the **Size and Shape** section, type Lp in the **Width** text field.
4. Type Wp in the **Depth** text field.
5. Type Thickness in the **Height** text field.
6. In the **Position** section. Choose **Center** from the **Base** list.
7. Type 0 in the **x**, **y**, and **z** text field.

- 3) Create a cylinder for the SMA connector.

### **Cylinder 1 (cyl1)**

1. On the **Geometry** toolbar, click **Cylinder**.
2. In the **Settings** window for **Cylinder**, type SMA in the **Label** text field.
3. Under the **Size and Shape** section, type R in the **Radius** text field.
4. Type L in the **Height** text field.
5. In the **Position** section, type X<sub>o</sub> in the **x** text field.
6. Type  $-Thickness/2-L$  in the **z** text field.

- 4) Create a cylinder for the inner connector of the coaxial cable.

### **Cylinder 2 (cyl2)**

1. On the **Geometry** toolbar, click **Cylinder**.
2. In the **Settings** window for **Cylinder**, type Coax Inner in the **Label** text field.
3. Under the **Size and Shape** section, type r in the **Radius** text field.
4. Type L+Thickness in the **Height** text field.
5. In the **Position** section, type X<sub>o</sub> in the **x** text field.
6. Type  $-Thickness/2-L$  in the **z** text field.

- 5) Create a cylinder for the coaxial dielectric filler.

### **Cylinder 3 (cyl3)**

1. On the **Geometry** toolbar, click **Cylinder**.
2. In the **Settings** window for **Cylinder**, type Coax dielectric in the **Label** text field.

3. Under the **Size and Shape** section, type  $R-0.5$  in the **Radius** text field.
  4. Type  $L$  in the **Height** text field.
  5. In the **Position** section, type  $X_0$  in the **x** text field.
  6. Type  $-Thickness/2-L$  in the **z** text field.
- 6) Create a block for the first dielectric resonator.

### **Block 3 (blk3)**

1. On the **Geometry** toolbar, click **Block**.
  2. In the **Settings** window for **Block**, type  $DR1$  in the **Label** text field.
  3. Under the **Size and Shape** section, type  $L_r$  in the **Width** text field.
  4. Type  $W_r$  in the **Depth** text field.
  5. Type  $H_r$  in the **Height** text field.
  6. In the **Position** section. Choose **Center** from the **Base** list.
  7. Type  $(L_p/2+L_r/2-X_d)$  in the **x** text field.
  8. Type  $(H_r/2+Thickness/2)$  in the **z** text field.
- 7) Create a block for the second dielectric resonator.

### **Block 4 (blk4)**

1. On the **Geometry** toolbar, click **Block**.
2. In the **Settings** window for **Block**, type  $DR2$  in the **Label** text field.
3. Under the **Size and Shape** section, type  $L_r$  in the **Width** text field.
4. Type  $W_r$  in the **Depth** text field.

5. Type  $H_r$  in the **Height** text field.
6. In the **Position** section. Choose **Center** from the **Base** list.
7. Type  $(-L_p/2-L_r/2+X_d)$  in the **x** text field.
8. Type  $(H_r/2+Thickness/2)$  in the **z** text field.

8) Create a block for the third dielectric resonator.

### **Block 5 (blk5)**

1. On the **Geometry** toolbar, click **Block**.
2. In the **Settings** window for **Block**, type DR3 in the **Label** text field.
3. Under the **Size and Shape** section, type  $L_r$  in the **Width** text field.
4. Type  $W_r$  in the **Depth** text field.
5. Type  $H_r$  in the **Height** text field.
6. In the **Position** section. Choose **Center** from the **Base** list.
7. Type  $(L_p/2+X_g+L_{sp}+X_g+L_p+X_g+L_{sp}/2)$  in the **x** text field.
8. Type  $(H_r/2+Thickness/2)$  in the **z** text field.

9) Create a block for the fourth dielectric resonator.

### **Block 6 (blk6)**

1. On the **Geometry** toolbar, click **Block**.
2. In the **Settings** window for **Block**, type DR4 in the **Label** text field.
3. Under the **Size and Shape** section, type  $L_r$  in the **Width** text field.
4. Type  $W_r$  in the **Depth** text field.

5. Type Hr in the **Height** text field.
  6. In the **Position** section. Choose **Center** from the **Base** list.
  7. Type  $-(Lp/2+Xg+Lsp+Xg+Lp+Xg+Lsp/2)$  in the **x** text field.
  8. Type  $(Hr/2+Thickness/2)$  in the **z** text field.
- 10) Create a block for the large patch on the right connecting DR1 and DR3.

**Block 7 (blk7)**

1. On the **Geometry** toolbar, click **Block**.
2. In the **Settings** window for **Block**, type Large Patch R (DR1 and DR3) in the **Label** text field.
3. Under the **Size and Shape** section, type Lp in the **Width** text field.
4. Type Wp in the **Depth** text field.
5. Type Thickness in the **Height** text field.
6. In the **Position** section. Choose **Center** from the **Base** list.
7. Type  $(Lp/2+Xg+Lsp+Xg+Lp/2)$  in the **x** text field.

- 11) Create a block for the large patch on the left connecting DR2 and DR4.

**Block 8 (blk8)**

1. On the **Geometry** toolbar, click **Block**.
2. In the **Settings** window for **Block**, type Large Patch L (DR2 and DR4) in the **Label** text field.
3. Under the **Size and Shape** section, type Lp in the **Width** text field.

4. Type  $W_p$  in the **Depth** text field.
5. Type Thickness in the **Height** text field.
6. In the **Position** section. Choose **Center** from the **Base** list.
7. Type  $-(L_p/2+X_g+L_{sp}+X_g+L_p/2)$  in the **x** text field.

12) Create a block for the small patch under DR1.

### **Block 9 (blk9)**

1. On the **Geometry** toolbar, click **Block**.
2. In the **Settings** window for **Block**, type Small Patch DR1 in the **Label** text field.
3. Under the **Size and Shape** section, type  $L_{sp}$  in the **Width** text field.
4. Type  $W_p$  in the **Depth** text field.
5. Type Thickness in the **Height** text field.
6. In the **Position** section. Choose **Center** from the **Base** list.
7. Type  $(L_p/2+X_g+L_{sp}/2)$  in the **x** text field.

13) Create a block for the small patch under DR2.

### **Block 10 (blk10)**

1. On the **Geometry** toolbar, click **Block**.
2. In the **Settings** window for **Block**, type Small Patch DR2 in the **Label** text field.
3. Under the **Size and Shape** section, type  $L_{sp}$  in the **Width** text field.
4. Type  $W_p$  in the **Depth** text field.
5. Type Thickness in the **Height** text field.

6. In the **Position** section. Choose **Center** from the **Base** list.
7. Type  $-(Lp/2+Xg+Lsp/2)$  in the **x** text field.

14) Create a block for the small patch under DR3.

### **Block 11 (blk11)**

1. On the **Geometry** toolbar, click **Block**.
2. In the **Settings** window for **Block**, type Small Patch DR3 in the **Label** text field.
3. Under the **Size and Shape** section, type Lsp in the **Width** text field.
4. Type Wp in the **Depth** text field.
5. Type Thickness in the **Height** text field.
6. In the **Position** section. Choose **Center** from the **Base** list.
7. Type  $(Lp/2+Xg+Lsp+Xg+Lp+Xg+Lsp/2)$  in the **x** text field.

15) Create a block for the small patch under DR4.

### **Block 12 (blk12)**

1. On the **Geometry** toolbar, click **Block**.
2. In the **Settings** window for **Block**, type Small Patch DR4 in the **Label** text field.
3. Under the **Size and Shape** section, type Lsp in the **Width** text field.
4. Type Wp in the **Depth** text field.
5. Type Thickness in the **Height** text field.
6. In the **Position** section. Choose **Center** from the **Base** list.
7. Type  $-(Lp/2+Xg+Lsp+Xg+Lp+Xg+Lsp/2)$  in the **x** text field.

16) Create a cylinder for the shorting via on the right.

#### **Cylinder 4 (cyl4)**

1. On the **Geometry** toolbar, click **Cylinder**.
2. In the **Settings** window for **Cylinder**, type Via R in the **Label** text field.
3. Under the **Size and Shape** section, type Rv in the **Radius** text field.
4. Type Thickness in the **Height** text field.
5. In the **Position** section, type  $(Lp/2+Xg+Lsp+Xg+Lp/2)-Xv$  in the **x** text field.
6. Type  $-Thickness/2$  in the **z** text field.

17) Create a cylinder for the shorting via on the left.

#### **Cylinder 5 (cyl5)**

1. On the **Geometry** toolbar, click **Cylinder**.
2. In the **Settings** window for **Cylinder**, type Via L in the **Label** text field.
3. Under the **Size and Shape** section, type Rv in the **Radius** text field.
4. Type Thickness in the **Height** text field.
5. In the **Position** section, type  $-(Lp/2+Xg+Lsp+Xg+Lp/2)+Xv$  in the **x** text field.
6. Type  $-Thickness/2$  in the **z** text field.

18) Create a sphere for the PMLs.

#### **Sphere 1 (sph1)**



1. On the **Geometry** toolbar, click **Sphere**.
2. In the **Settings** window for **Sphere**, type PMLs in the **Label** text field.
3. Under the **Size and Shape** section, type  $L_{\text{sub}}/60$ [mm] in the **Radius** text field.
4. Click **Layers** section. Then enter Layer 1 under the **Layer name** and  $L_{\text{sub}}/5$  under the **Thickness (mm)**.

Click **Build All Objects** to build the array structure. The Geometry tab should look like Figure B1.

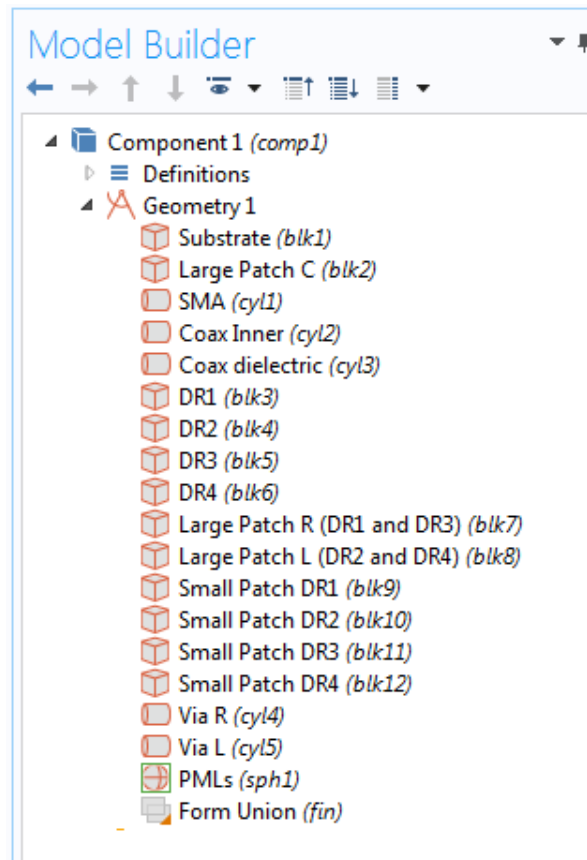


Figure B1: Geometry tab in COMSOL Multiphysics Software

#### IV. Definitions:

- 1) Create a set of selections for the PMLs.

### **Explicit 1**

1. On the **Definitions** toolbar, choose **Explicit**.
2. In the **Settings** window for **Explicit**, type PMLs in the **Label** text field.
3. Select Domains 1-4 and 14-17 only.

- 2) Create a set of selections for the Substrate.

### **Explicit 2**

1. On the **Definitions** toolbar, choose **Explicit**.
2. In the **Settings** window for **Explicit**, type Substrate in the **Label** text field.
3. Select Domains 6, 8-10, 12-13, 23-25, and 27 only.

- 3) Create a set of selections for the Dielectric Resonators.

### **Explicit 3**

1. On the **Definitions** toolbar, choose **Explicit**.
2. In the **Settings** window for **Explicit**, type Dielectric Resonators in the **Label** text field.
3. Select Domains 7, 11, 22, and 26 only.

- 4) Create a set of selections for the Patches and the Ground plane.

### **Explicit 4**

1. On the **Definitions** toolbar, choose **Explicit**.
2. In the **Settings** window for **Explicit**, type Patches and Ground Plane in the **Label** text field.
3. Locate the **Input Entities** section.
4. Choose **Boundary** from the **Geometric entity level** list.
  5. Select Boundaries 15, 25-26, 31-32, 35, 46, 51-52, 57-58, 61, 81, 92, 105, 110-111, 116-117, 120, 131, and 136-137 only.
- 5) Create a set of selections for the coaxial dielectric filler.

#### **Explicit 5**

1. On the **Definitions** toolbar, choose **Explicit**.
2. In the **Settings** window for **Explicit**, type Coax Dielectric Filler in the **Label** text field.
3. Select Domain 19 only.
- 6) Create a set of selections for the shorting vias.

#### **Explicit 6**

1. On the **Definitions** toolbar, choose **Explicit**.
2. In the **Settings** window for **Explicit**, type Shorting Vias in the **Label** text field.
3. Locate the **Input Entities** section.
4. Choose **Boundary** from the **Geometric entity level** list.
5. Select Boundaries 36-41 and 121-126 only.

- 7) Create a set of selections for the conduction surfaces of the coaxial cable.

### **Explicit 7**

1. On the **Definitions** toolbar, choose **Explicit**.
  2. In the **Settings** window for **Explicit**, type Coax Inner Conduction Surfaces in the **Label** text field.
  3. Locate the **Input Entities** section.
  4. Choose **Boundary** from the **Geometric entity level** list.
  5. Select Boundaries 82-83, 86-87, 89-90, and 94-99 only.
- 
- 8) Create a set of selections for the Scattering Boundaries.

### **Explicit 8**

1. On the **Definitions** toolbar, choose **Explicit**.
  2. In the **Settings** window for **Explicit**, type Scattering Boundaries in the **Label** text field.
  3. Locate the **Input Entities** section.
  4. Choose **Boundary** from the **Geometric entity level** list.
  5. Select Boundaries 5-8, 65-66, 71, and 76 only.
- 
- 9) Create a set of selections for the Far Field Boundaries.

### **Explicit 9**

1. On the **Definitions** toolbar, choose **Explicit**.
  2. In the **Settings** window for **Explicit**, type Far Field Boundaries in the **Label** text field.
  3. Locate the **Input Entities** section.
  4. Choose **Boundary** from the **Geometric entity level** list.
  5. Select Boundaries 9-12, 67-68, 72, and 75 only.
- 10) Create a set of selections for the Far Field Region.

### **Complement 1**

1. On the **Definitions** toolbar, choose **Complement**.
  2. In the **Settings** window for **Complement**, type Far Field Region in the **Label** text field.
  3. Locate the **Input Entities** section.
  4. Type PMLs in the **Selections to invert** text field.
- 11) Create Perfectly Matched Layer.

### **Perfectly Matched Layer 1 (pml1)**

1. On the **Definitions** toolbar, choose **Perfectly Matched Layer**.
2. Select Domains 1-4 and 14-17 only.
3. In the **Settings** window for **Perfectly Matched Layer**, locate the **Geometry** section.
4. Choose **Spherical** from the **Type** list.

The Definitions tab should look like Figure B2.

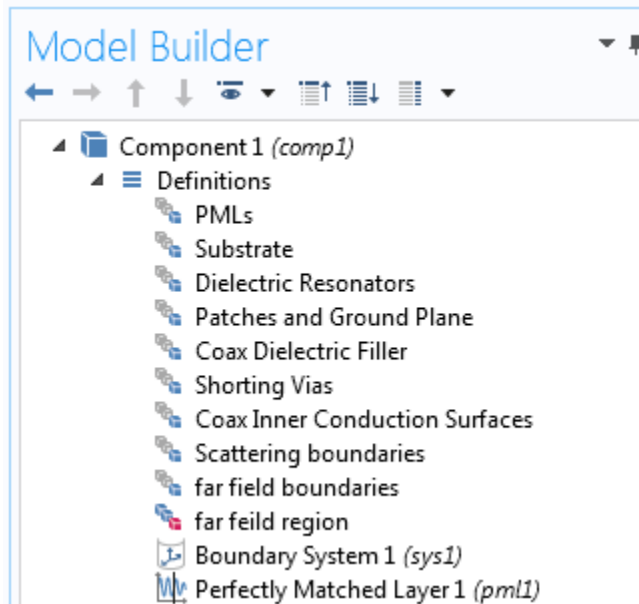


Figure B2: Definitions tab in COMSOL Multiphysics Software

## V. Materials:

Assign the materials properties on the model. Start by assigning air for all domains.

- 1) Add Air material.

### Material 1 (mat1)

1. On the **Home** toolbar, choose **Add Material** to open the **Add Material** window.
2. Go to the **Add Material** window. In the tree, choose **Built-In** > **Air**
3. Click **Add to Component** in the window toolbar.

- 2) Add Substrate material.

### Material 2 (mat2)

1. In the **Model Builder** window, under **Component 1 (comp1)** right-click **Materials** and choose **Blank Material**.
2. In the **Settings** window for **Material**, type Arlon 25N in the **Label** text field.
3. Locate the **Geometric Entity Selections** section. Choose **Substrate** from the **Selection** list.
4. Locate the **Material Contents** section. Enter the following values:

Property	Name	Value	Unit	Property group
Relative permittivity	epsilon <sub>r</sub>	$3.38*(1-j*0.0015)$	1	Basic
Relative permeability	mu <sub>r</sub>	1	1	Basic
Electrical conductivity	sigma	0	S/m	Basic

- 3) Add Dielectric Resonators material.

### **Material 3 (mat3)**

1. In the **Model Builder** window, under **Component 1 (comp1)** right-click **Materials** and choose **Blank Material**.
2. In the **Settings** window for **Material**, type PLA in the **Label** text field.
3. Locate the **Geometric Entity Selections** section. Choose **Dielectric Resonators** from the **Selection** list.
4. Locate the **Material Contents** section. Enter the following values:

Property	Name	Value	Unit	Property group
Relative permittivity	epsilon <sub>r</sub>	$2.5*(1-j*0.005)$	1	Basic

Relative permeability	mur	1	1	Basic
Electrical conductivity	sigma	0	S/m	Basic

- 4) Add Coaxial cable dielectric filler material.

#### **Material 4 (mat4)**

1. In the **Model Builder** window, under **Component 1 (comp1)** right-click **Materials** and choose **Blank Material**.
2. In the **Settings** window for **Material**, type PTEE in the **Label** text field.
3. Locate the **Geometric Entity Selections** section. Choose **Coax Dielectric Filler** from the **Selection** list.
4. Locate the **Material Contents** section. Enter the following values:

Property	Name	Value	Unit	Property group
Relative permittivity	epsilon	2.1	1	Basic
Relative permeability	mur	1	1	Basic
Electrical conductivity	sigma	0	S/m	Basic

#### **VI. Boundary Conditions:**

Assign the boundary conditions on the array structure.

- 1) Assign the Patches and Ground Plane surfaces.

#### **Perfect Electric Conductor 2**



1. In the **Model Builder** window, go to **Component 1 (comp 1) > Electromagnetic Waves, Frequency Domain (emw)**.
2. Right-click and choose **Perfect Electric Conductor**.
3. In the Settings window for **Perfect Electric Conductor 2**, type Patches and Ground Plane in the **Label** text field.
4. In the **Boundary Selection** section, choose **Patches and Ground Plane** from the **Selection** list.

2) Assign the Coaxial inner conduction surfaces.

### **Perfect Electric Conductor 3**

1. In the **Model Builder** window, go to **Component 1 (comp 1) > Electromagnetic Waves, Frequency Domain (emw)**.
2. Right-click and choose **Perfect Electric Conductor**.
3. In the Settings window for **Perfect Electric Conductor 3**, type Coax Inner Conduction Surfaces in the **Label** text field.
4. In the **Boundary Selection** section, choose **Coax Inner Conduction Surfaces** from the **Selection** list.

3) Assign the Shorting Vias surfaces.

### **Perfect Electric Conductor 4**

1. In the **Model Builder** window, go to **Component 1 (comp 1) > Electromagnetic Waves, Frequency Domain (emw)**.

2. Right-click and choose **Perfect Electric Conductor**.
  3. In the Settings window for **Perfect Electric Conductor 4**, type Shorting Vias in the **Label** text field.
  4. In **Boundary Selection** section, choose **Shorting Vias** from the **Selection** list.
- 4) Assign the Feed Port surface.

### **Lumped Port 1**

1. In the **Model Builder** window, go to **Component 1 (comp 1) > Electromagnetic Waves, Frequency Domain (emw)**.
  2. Right-click and choose **Lumped Port**.
  3. In the Settings window for **Lumped Port 1**, locate **Boundary Selection** and choose boundary number 84 only
  4. In the **Lumped Port properties** section, choose **Coaxial** from the **Type of lumped port** list.
  5. Choose **Cable** from the **Terminal type** list.
  6. Choose **On** from the **Wave excitation at this port** list.
  7. Type 1[V] in the text field of the **Voltage**.
- 5) Assign the Scattering Boundary Conditions.

### **Scattering Boundary Condition 1**

1. In the **Model Builder** window, go to **Component 1 (comp 1) > Electromagnetic Waves, Frequency Domain (emw)**.

2. Right-click and choose **Scattering Boundary Condition**.
  3. In the **Boundary Selection** section, choose **Scattering Boundaries** from the **Selection** list.
- 6) Assign the Far Field Region.

### Far Field Domain 1

1. In the **Model Builder** window, go to **Component 1 (comp 1) > Electromagnetic Waves, Frequency Domain (emw)**.
2. Right-click and choose **Far-Field Domain**.
3. In **Domain Selection** section, choose **Far Field Region** from the **Selection** list.

The Electromagnetic Waves, Frequency Domain (emw) tab should look like Figure B3.

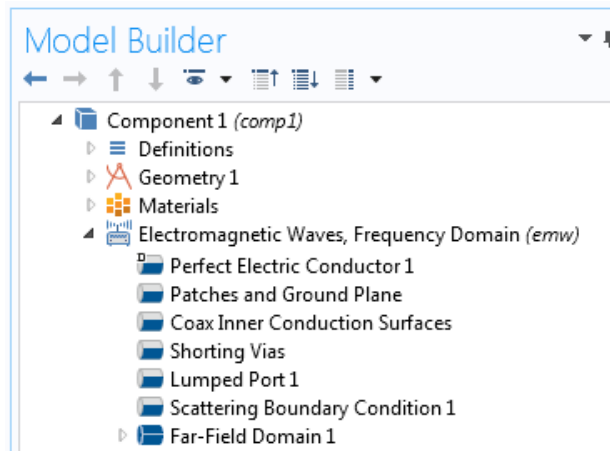


Figure B3: Electromagnetic Waves, Frequency Domain (emw) tab in COMSOL

Multiphysics Software

## VII. Meshing:

Choose the maximum mesh size in the air domain smaller than 0.2 wavelengths using the parameter **H\_max** that was defined earlier. For other materials, scale the mesh size by the inverse of the square root of the relative permittivity.

1) Mesh the Far Field Region.

### **Size 1**

1. In the **Model Builder** window, under **Component 1 (comp 1)** right-click **Mesh 1** and choose **Size**.
2. In the **Settings** window for **Size 1**, locate the **Geometric Entity Selection** section.
3. Choose **Domain** from the **Geometric entity level** list.
4. Choose **Far Field Region** from the **Selection** list.
5. Locate **Element Size** section, click the **Custom** button.
6. Locate the **Element Size Parameters** section, and then select the **Maximum element size** check box.
7. Type H\_max in the associated text field.

2) Mesh the Substrate.

### **Size 2**

1. In the **Model Builder** window, under **Component 1 (comp 1)** right-click **Mesh 1** and choose **Size**.
2. In the **Settings** window for **Size 2**, locate the **Geometric Entity Selection** section.
3. Choose **Domain** from the **Geometric entity level** list.
4. Choose **Substrate** from the **Selection** list.

5. Locate **Element Size** section, click the **Custom** button.
6. Locate the **Element Size Parameters** section, then select the **Maximum element size** check box.
7. Type  $H_{\max}/\sqrt{3.38}$  in the associated text field.

3) Mesh the Dielectric Resonators.

### **Size 3**

1. In the **Model Builder** window, under **Component 1 (comp 1)** right-click **Mesh 1** and choose **Size**.
2. In the **Settings** window for **Size 3**, locate the **Geometric Entity Selection** section.
3. Choose **Domain** from the **Geometric entity level** list.
4. Choose **Dielectric Resonators** from the **Selection** list.
5. Locate **Element Size** section, click the **Custom** button.
6. Locate the **Element Size Parameters** section, and then select the **Maximum element size** check box.
7. Type  $H_{\max}/\sqrt{2.5}$  in the associated text field.

4) Mesh the Coaxial Dielectric Filler.

### **Size 4**

1. In the **Model Builder** window, under **Component 1 (comp 1)** right-click **Mesh 1** and choose **Size**.
2. In the **Settings** window for **Size 4**, locate the **Geometric Entity Selection** section.

3. Choose **Domain** from the **Geometric entity level** list.
4. Choose **Coax Dielectric Filler** from the **Selection** list.
5. Locate **Element Size** section, click the **Custom** button.
6. Locate the **Element Size Parameters** section, and then select the **Maximum element size** check box.
7. Type  $H_{\max}/\sqrt{2.1}$  in the associated text field.

### **Free Tetrahedral 1**

1. In the **Model Builder** window, under **Component 1 (comp 1)** right-click **Mesh 1** and choose **Free Tetrahedral**.
2. In the **Settings** window for **Free Tetrahedral 1**, locate the **Geometric Entity Selection** section.
3. Choose **Domain** from the **Geometric entity level** list.
4. Click **Paste Selection**.
5. In the **Paste Selection** dialog box, type 5-21, 26-33 in the **Selection** text field.
6. Click **OK**.

### **Distribution 1**

1. Right-click **Mesh 1** and choose **Swept**.
2. In the **Model Builder** window, under **Component 1 (comp 1) > Mesh 1** right-click **Swept 1** and choose **Distribution**.
3. In the **Settings** window for **Distribution**, click **Build All**.

The Mesh tab should look like Figure B4.

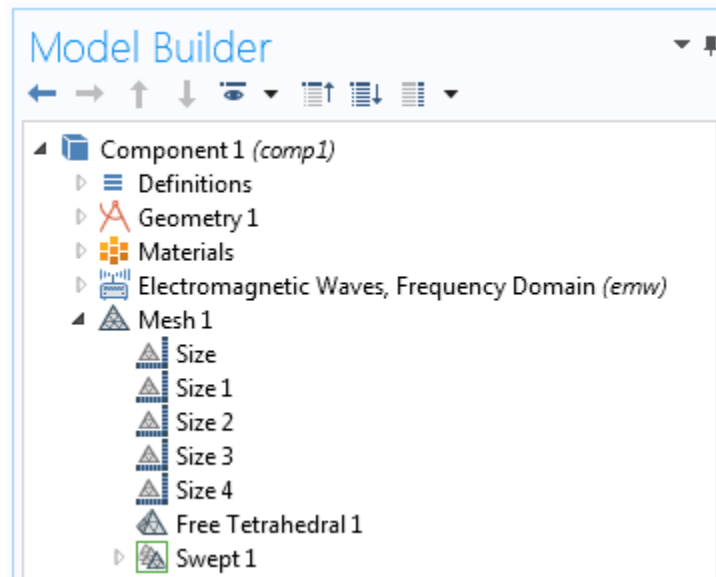


Figure B4: Mesh tab in COMSOL Multiphysics Software

## VIII. Result Post-processing:

To generate the results data, it is required to run the simulation.

### Study 1

#### Step 1: Frequency Domain

1. In the **Settings** window for **Frequency Domain**, locate the **Study Settings** section.
2. In the **Frequencies** text field, type `range(3.5[GHz],0.05[GHz],4.5[GHz])`
3. Click **Compute** on the **Home** toolbar.

### Results

- 1) Plot the Return Loss response as a function of frequency.

### **S-parameter, S11 dB (emw)**

1. On the **Results** toolbar, locate the **Derived Values**.
2. Right-click and choose **Global Evaluation**.
3. In the **Settings** window for **Global Evaluation**, click **Replace Expression** in the upper-right corner of the **Expression** section.
4. From the menu, choose **Component 1 > Electromagnetic Waves, Frequency Domain > Ports > emw.S11dB – S11**.
5. Click **Evaluate**.
6. In the **Graphics** window, choose **Table 1** and click **Table Graph** to plot the response (Figure 5.56).

- 2) Plot the Gain response as a function of frequency.

### **Far-field Gain, dBi**

1. On the **Results** toolbar, locate the **Derived Values**.
2. Right-click and choose **Maximum > Surface Maximum**.
3. In the **Settings** window for **Surface Maximum**, choose **Far Field Boundaries** from the **Selection** list.
4. Click **Replace Expression** in the upper-right corner of the **Expression** section.
5. From the menu, choose **Component 1 > Electromagnetic Waves, Frequency Domain > Far field > emw.gainDBEfar – Far-Field gain, dBi**.
6. Click **Evaluate**.



7. In the **Graphics** window, choose **Table 2** and click **Table Graph** to plot the response (Figure 5.57).

3) Plot the 3D Far-field Radiation Pattern.

### **3D Far Field (emw)**

1. On the **Results** toolbar, locate the **3D Far Field (emw)**.
2. Expand it and click **Far Field 1**.
3. In the **Settings** window for **Far Field**, choose **Study1/Solution 1 (sol1)** from the **Data set** list in the **Data** section.
4. Choose the resonant frequency value from the **Parameter value (freq(GHz))**.
5. Click **Replace Expression** in the upper-right corner of the **Expression** section.
6. From the menu, choose **Component 1 > Electromagnetic Waves, Frequency Domain > Far field > emw.normEfar– Far-field norm**.
7. Locate **Evaluation** section, type 360 in both  **$\theta$  resolution** and  **$\phi$  resolution** text field.
8. Click **Evaluate** to depict the 3D far field radiation pattern (Figure 5.59).

4) Plot the 2D Far-field Radiation Patterns.

### **2D Far Field (emw)**

1. On the **Results** toolbar, locate the **2D Far Field (emw)**.
2. Expand it and click **Far Field 1**.

3. In the **Settings** window for **Far Field**, choose **Study1/Solution 1 (sol1)** from the **Data set** list in the **Data** section.
  4. Choose the resonant frequency value from the **Parameter value (freq(GHz))**.
  5. Click **Replace Expression** in the upper-right corner of the **Expression** section.
  6. From the menu, choose **Component 1 > Electromagnetic Waves, Frequency Domain > Far field > emw.normdBefar– Far-field norm, dB**.
  7. Locate **Evaluation** section, type 360 in the  **$\phi$  resolution** text field.
  8. Find the **Normal** subsection, type 1 in the **x** text field.
  9. Locate **Legends** section, check the **Show legends** box.
  10. Choose **Manual** from the **Legends** list and type Y-Z Plane in the **Legends** text field.
  11. Click **Plot** to depict the far field radiations in the y-z plane.
  12. To plot the far field radiations in the x-z plane, repeat steps 1 to 7.
  13. Then, find the **Reference direction** subsection, type -1 in the **x** text field.
  14. Locate the **Normal** subsection, type 1 in the **y** text field.
  15. Locate **Legends** section, check the **Show legends** box.
  16. Choose **Manual** from the **Legends** list and type X-Z Plane in the **Legends** text field.
  17. Click **Plot** to depict the far field radiations in the x-z plane (Figure 5.58).
- 5) Plot the 3D Field Distribution.

### **3D Arrow Volume 1**

1. On the **Results** toolbar, right-click and choose **3D Plot Group**.
2. Right-click it and choose **Arrow Volume 1**.
3. In the **Settings** window for **Arrow Volume**, choose **Study1/Solution 1 (sol1)** from the **Data set** list in the **Data** section.
4. Choose the resonant frequency value from the **Parameter value (freq(GHz))**.
5. Locate the **Arrow Positioning** section.
6. Type 80 in the **Points** text field for all **x**, **y**, and **z grid points** subsections.
7. Click **Plot** to depict the 3D field distribution inside the array cavity (Figure 5.61).

## REFERENCES

- [1] J.A. Fleming, "Researches in Radiotelegraphy" Royal Institution Lecture, in "Wireless telegraphy" ed. E. Eastwood, Applied Science pub, London, 1909.
- [2] "IEEE Standard Definitions of Terms for Antennas," IEEE Std 145-2013 (Revision of IEEE Std 145-1993), pp. 1–92, 2014.
- [3] J. Kraus, "Antennas since Hertz and Marconi," IEEE Transactions on Antennas and Propagation, vol. 33, no. 2, pp. 131–137, 1985.
- [4] C. A. Balanis, "Antenna Theory: A Review," Proceedings of the IEEE, vol. 80, no. 1, pp. 7–23, 1992.
- [5] S. Keyrouz and D. Caratelli, "Dielectric Resonator Antennas: Basic Concepts, Design Guidelines, and Recent Developments at Millimeter-Wave Frequencies," International Journal of Antennas and Propagation, vol. 2016, pp. 1–20, 2016.
- [6] A. Petosa, Dielectric Resonator Antenna Handbook. Boston, USA: Artech House, 2007.
- [7] M. Mrnka and Z. Raida, "Gain improvement of higher order mode dielectric resonator antenna by thin air gap," 2016 International Conference on Broadband Communications for Next Generation Networks and Multimedia Applications (CoBCom), pp. 1–3, 2016.
- [8] S. Fakhte, H. Oraizi, and L. Matekovits, "High Gain Rectangular Dielectric Resonator Antenna Using Uniaxial Material at Fundamental Mode," IEEE Transactions on Antennas and Propagation, vol. 65, no. 1, pp. 342–347, 2017.
- [9] Nasimuddin and K. Esselle, "Antennas with dielectric resonators and surface mounted short horns for high gain and large bandwidth," IET Microwaves, Antennas & Propagation, vol. 1, no. 3, pp. 723–728, 2007.
- [10] T. A. Denidni, Y. Coulibaly, and H. Boutayeb, "Hybrid Dielectric Resonator Antenna With Circular Mushroom-Like Structure for Gain Improvement," IEEE Transactions on Antennas and Propagation, vol. 57, no. 4, pp. 1043–1049, 2009.
- [11] P. Bhartia, R. S. Tomar, and K. V. S. Rao, Millimeter-Wave Microstrip and Printed Circuit Antennas. Boston, USA: Artech House, 1991.
- [12] D. Kajfez and P. Guillon, Dielectric Resonators. Dedham, USA: Artech House, 1986.

- [13] S. Long, M. Mcallister, and L. Shen, "The resonant cylindrical dielectric cavity antenna," *IEEE Transactions on Antennas and Propagation*, vol. 31, no. 3, pp. 406–412, 1983.
- [14] M. Mcallister, S. Long, and G. Conway, "Rectangular dielectric resonator antenna," *Electronics Letters*, vol. 19, no. 6, pp. 218–219, 1983.
- [15] M. Mcallister and S. Long, "Resonant hemispherical dielectric antenna," *Electronics Letters*, vol. 20, no. 16, pp. 657–659, 1984.
- [16] A. Petosa and A. Ittipiboon, "Dielectric Resonator Antennas: A Historical Review and the Current State of the Art," *IEEE Antennas and Propagation Magazine*, vol. 52, no. 5, pp. 91–116, 2010.
- [17] K. M. Luk and K. W. Leung, *Dielectric Resonator Antennas*. Baldock, England: Research Studies Press, 2003.
- [18] Z. Ying and P.-S. Kildal, "Improvements of dipole, helix, spiral, microstrip patch and aperture antennas with ground planes by using corrugated soft surfaces," *IEE Proceedings - Microwaves, Antennas and Propagation*, vol. 143, no. 3, pp. 244–248, 1996.
- [19] M. S. Ibrahim, "A dielectric resonator antenna over corrugated ground plane with metallic and nonmetallic metamaterial superstrates," *2017 11th European Conference on Antennas and Propagation (EUCAP)*, pp. 3031–3033, 2017.
- [20] K. Leung, Z. Chen, K. Luk, and E. Yung, "Aperture coupled dielectric resonator antenna with a thick ground plane," *IEEE Transactions on Antennas and Propagation*, vol. 46, no. 8, pp. 1242–1243, 1998.
- [21] R. Kranenburg and S. Long, "Microstrip transmission line excitation of dielectric resonator antennas," *Electronics Letters*, vol. 24, no. 18, pp. 1156–1157, 1988.
- [22] K.-W. Leung, K.-M. Luk, K. Y. A. Lai, and D. Lin, "Theory and Experiment of an Aperture-Coupled Hemispherical Dielectric Resonator Antenna," *IEEE Transactions on Antennas and Propagation*, vol. 43, no. 11, pp. 1192–1198, 1995.
- [23] A. Kishk, "Dielectric resonator antenna, a candidate for radar applications," *Proceedings of the 2003 IEEE Radar Conference (Cat. No. 03CH37474)*, pp. 258–264, 2003.
- [24] S. Caizzone, W. Elmarissi, G. Buchner, and M. Sgammini, "Compact 6+1 antenna array for robust GNSS applications," *2016 International Conference on Localization and GNSS (ICL-GNSS)*, pp. 1–4, 2016.
- [25] W. Huang and A. Kishk, "Compact dielectric resonator antenna for microwave breast cancer detection," *IET Microwaves, Antennas & Propagation*, vol. 3, no. 4, pp. 638–644, 2009.

- [26] M. S. Iqbal and K. P. Esselle, "A compact wideband dielectric resonator antenna for on-body applications," 2014 IEEE MTT-S International Microwave Workshop Series on RF and Wireless Technologies for Biomedical and Healthcare Applications (IMWS-Bio2014), 2014.
- [27] E. A. J. Marcatili, "Dielectric Rectangular Waveguide and Directional Coupler for Integrated Optics," *Bell System Technical Journal*, vol. 48, no. 7, pp. 2071–2102, 1969.
- [28] S. Maity and B. Gupta, "Closed Form Expressions to Find Radiation Patterns of Rectangular Dielectric Resonator Antennas for Various Modes," *IEEE Transactions on Antennas and Propagation*, vol. 62, no. 12, pp. 6524–6527, 2014.
- [29] R. K. Mongia and A. Ittipiboon, "Theoretical and experimental investigations on rectangular dielectric resonator antennas," *IEEE Transactions on Antennas and Propagation*, vol. 45, no. 9, pp. 1348–1356, 1997.
- [30] J. V. Bladel, "On the Resonances of a Dielectric Resonator of Very High Permittivity," *IEEE Transactions on Microwave Theory and Techniques*, vol. 23, no. 2, pp. 199–208, 1975.
- [31] J. V. Bladel, "The Excitation of Dielectric Resonators of Very High Permittivity," *IEEE Transactions on Microwave Theory and Techniques*, vol. 23, no. 2, pp. 208–217, 1975.
- [32] C. A. Balanis, *Advanced Engineering Electromagnetics*. New York, USA: Wiley, 1989.
- [33] X. S. Fang and K. W. Leung, "Designs of Single-, Dual-, Wide-Band Rectangular Dielectric Resonator Antennas," *IEEE Transactions on Antennas and Propagation*, vol. 59, no. 6, pp. 2409–2414, 2011.
- [34] K. W. Leung, E. H. Lim, and X. S. Fang, "Dielectric Resonator Antennas: From the Basic to the Aesthetic," *Proceedings of the IEEE*, vol. 100, no. 7, pp. 2181–2193, 2012.
- [35] R. L. Haupt and Y. Rahmat-Samii, "Antenna Array Developments: A Perspective on the Past, Present and Future," *IEEE Antennas and Propagation Magazine*, vol. 57, no. 1, pp. 86–96, 2015.
- [36] S. G. Brown, British Patent No. 14449, 1899.
- [37] G. Marconi, "On Methods Whereby the Radiation of Electric Waves May be Mainly Confined to Certain Directions, and Whereby the Receptivity of a Receiver May be Restricted to Electric Waves Emanating from Certain Directions," *Proceedings of the Royal Society A: Mathematical, Physical and Engineering Sciences*, vol. 77, no. 518, pp. 413–421, 1906.

- [38] F. Braun, "Electrical oscillations and wireless telegraphy," Nobel Lecture, Dec. 11, 1909
- [39] F. Adcock, "Improvement in Means for Determining the Direction of a Distant Source of Electro-magnetic Radiation," UK Patent 130,490, Aug. 7, 1919.
- [40] H. Unz, "Linear Arrays with arbitrarily distributed elements," IRE Transactions on Antennas and Propagation, vol. 8, no. 2, pp. 222–223, 1960.
- [41] D. King, R. Packard, and R. Thomas, "Unequally-spaced, broad-band antenna arrays," IRE Transactions on Antennas and Propagation, vol. 8, no. 4, pp. 380–384, 1960.
- [42] W. Stutzman, "Shaped-beam synthesis of nonuniformly spaced linear arrays," IEEE Transactions on Antennas and Propagation, vol. 20, no. 4, pp. 499–501, 1972.
- [43] C. L. Dolph, "A Current Distribution for Broadside Arrays Which Optimizes the Relationship between Beam Width and Side-Lobe Level," Proceedings of the IRE, vol. 34, no. 6, pp. 335–348, 1946.
- [44] H. J. Riblet, "Discussion of Dolph's paper," Proceedings of the IRE, vol. 35, pp. 489–492, 1947.
- [45] R. H. Duhamel, "Optimum Patterns for Endfire Arrays," Proceedings of the IRE, vol. 41, no. 5, pp. 652–659, 1953.
- [46] A. Tennant, M. Dawoud, and A. Anderson, "Array pattern nulling by element position perturbations using a genetic algorithm," Electronics Letters, vol. 30, no. 3, pp. 174–176, 1994.
- [47] W. L. Stutzman and G. A. Thiele, Antenna Theory and Design. New York, USA: Wiley, 2013.
- [48] C. A. Balanis, Antenna Theory: Analysis and Design. New York, USA: John Wiley & Sons, Inc., 2005.
- [49] M. Birand and R. Gelsthorpe, "Experimental millimetric array using dielectric radiators fed by means of dielectric waveguide," Electronics Letters, vol. 17, no. 18, pp. 633–635, 1981.
- [50] A. Petosa, R. Mongia, A. Ittipiboon, and J. Wight, "Investigation of various feed structures for linear arrays of dielectric resonator antennas," IEEE Antennas and Propagation Society International Symposium. 1995 Digest, vol. 4, pp. 1982–1985, 1995.
- [51] C. S. Lee, M. Ezzat, and S. Jeong, "Single-layer dual microstrip-array antenna," 2014 IEEE Antennas and Propagation Society International Symposium (APSURSI), pp. 1067–1068, 2014.

- [52] S. Chakraborty and U. Mukherjee, "Comparative study of micro strip patch line feed and coaxial feed antenna design using genetic algorithms," 2011 2nd International Conference on Computer and Communication Technology (ICCCT-2011), pp. 203–208, 2011.
- [53] P. Hall and C. Hall, "Coplanar corporate feed effects in microstrip patch array design," *IEE Proceedings H Microwaves, Antennas and Propagation*, vol. 135, no. 3, pp. 180–186, 1988.
- [54] E. Levine, G. Malamud, S. Shtrikman, and D. Treves, "A study of microstrip array antennas with the feed network," *IEEE Transactions on Antennas and Propagation*, vol. 37, no. 4, pp. 426–434, 1989.
- [55] A. Lakshmanan and C. S. Lee, "A Standing-Wave Microstrip Array Antenna," *IEEE Transactions on Antennas and Propagation*, vol. 59, no. 12, pp. 4858–4861, 2011.
- [56] Z. Wu, L. E. Davis, and G. Drossos, "Cylindrical dielectric resonator antenna arrays," 11th International Conference on Antennas and Propagation (ICAP 2001), 2001.
- [57] A. Petosa, J. Wight, R. Mongia, and A. Ittipiboon, "Design of microstrip-fed series array of dielectric resonator antennas," *Electronics Letters*, vol. 31, no. 16, pp. 1306–1307, Mar. 1995.
- [58] A. Behloul, N. Sahnoune, I. Messaoudene, and A. Benghalia, "Rectangular dielectric resonator antenna array for 5.8 GHz WLAN applications," *Proceedings of 2014 Mediterranean Microwave Symposium (MMS2014)*, 2014.
- [59] M. G. Turcan, M.-V. Moni, and G. Banciu, "Studies of aperture-coupled rectangular dielectric resonator antenna arrays," 2016 International Conference on Communications (COMM), 2016.
- [60] G. Loos and Y. Antar, "Investigation of a novel aperture-coupled dielectric resonator antenna subarray," *Proceedings of IEEE Antennas and Propagation Society International Symposium and URSI National Radio Science Meeting*, vol. 3, pp. 1510–1513, 1994.
- [61] Y. Zhang, A. A. Kishk, A. B. Yakovlev, and A. W. Glisson, "Analysis and Experimental Study of Wideband Dielectric Resonator Antenna Arrays for Waveguide-Based Spatial Power Combining," 2007 IEEE/MTT-S International Microwave Symposium, 2007.
- [62] Y. Z. Y. Zhang and A. Kishk, "Analysis of dielectric resonator antenna arrays with supporting perforated rods," 2nd European Conference on Antennas and Propagation (EuCAP 2007), 2007.
- [63] M. Haneishi and B. Wu, "Array antenna composed of circularly polarized dielectric resonator antennas," *IEEE Antennas and Propagation Society International*



Symposium. 1999 Digest. Held in conjunction with: USNC/URSI National Radio Science Meeting (Cat. No.99CH37010), vol. 1, pp. 252–255, 1999.

- [64] A. Buerkle, K. F. Brakora, and K. Sarabandi, “Fabrication of a DRA Array Using Ceramic Stereolithography,” *IEEE Antennas and Wireless Propagation Letters*, vol. 5, pp. 479–482, 2006.

